The Virtues of Passive Damping for Feedback Controlled Flexible Structures

by

Richard Gueler

S.B. Aeronautics and Astronautics
Massachusetts Institute of Technology
(1988)

Submitted to the Department of Aeronautics and Astronautics
in partial fulfillment of the requirements for the degree of

Masters of Science in Aeronautics and Astronautics

at the

MASSACHUSETTS INSTITUTE OF TECHNOLOGY

June 1991

Author_____
Department of Aeronautics and Astronautics
May 16, 1991

Certified by_____
Prof. Andreas H. von Flotow
Associate Professor
Thesis Supervisor

Accepted by_____
Prof. Harold Y. Wachman
Chairman, Departmental Graduate Committee

The Virtues of Passive Damping for Feedback Controlled Flexible Structures

by

Richard Gueler

Submitted to the Department of Aeronautics and Astronautics
on May 16, 1991, in partial fulfillment of the
requirements for the degree of
Masters of Science in Aeronautics and Astronautics

Abstract

One key design variable that has largely been neglected in control-structure design is passive structural damping. Passive damping improves nominal performance by eliminating degrading structural vibrations resulting in improved control characteristics and lowered required effort. A great advantage of added passive damping in SISO controlled structures is the improved stability and performance robustness characteristics given plant uncertainties. Theoretical formulations verifying the improved stability robustness characteristics on simple controlled structures are derived based on phase margin, gain margin and root locus properties of the structures. Numerical studies performed on more complicated systems verify the improved design characteristics for passively damped controlled structures. The theory is expanded to include MIMO controlled structures where the robustness properties of these systems are greatly affected by uncertainties in plant directions. Numerical studies verify the improved performance and robustness characteristics of passively damped MIMO controlled structures.

Thesis Supervisor: Prof. Andreas H. von Flotow
Title: Associate Professor

Acknowledgments

I am grateful to Professor Andreas von Flotow who through his kindness and generosity advised this thesis. He helped me continue through the tough times and always provided encouragement. I also would like to thank Dr. Mathieu Mercadal for proof reading my thesis.

Foremost, I am grateful to my parents, Abe and Laura Gueler who were always there in my time of need to provide love and kindness. Through their encouragement, I was able to survive my years at M.I.T.

Contents

Chapter 1

Introduction

1.1 Background and Motivation

With the development of high performing space systems, the interaction among the engineering disciples and subsystems is becoming increasingly important. This is particularly true in the fields of structural and control system design. The need for larger and higher performing spacecraft is continually increasing. But due to high cost of placing these craft into orbit, the need for light systems is equally important. This may result in extremely flexible structures which causes control-structure interaction. Thus methodologies to control flexible structures and design of structures for control are of great importance. Incorporating the two disciplines will allow for improved performance, mass reduction, and improved reliability.

Traditionally, the structure and control system of a spacecraft are design separately. First the structural engineer attempts to develop a minimum mass design based on environmental conditions and performance requirements. With the structural design complete, the control engineer attempts to develop a control system based on performance requirements such as command following and disturbance rejection capabilities. Past methodologies avoid the problem of control-structure interaction by limiting the control bandwidth far below the structural modes of vibration. This prevents large structural vibrations which can degrade performance and cause instability. To meet the requirement of future missions, control of flexible structures

with closed loop bandwidths within the natural frequency is essential to maintain low weight and high performance requirements. Such systems include large space based antennas, space telescopes, and solar arrays which are extremely flexible, yet require precision pointing.

The overlap of control bandwidth with structural modes of vibration presents several challenges to the designer, since accurate modeling of the structure is essential in the control design. Furthermore, future system will make use of multi-input-multi-output design further complicating the design procedure because of the interaction between inputs and outputs. New structural design methodologies need to incorporate control and system objectives. One such method involves computing the optimal stiffness and mass distribution for good control [5, 10, 14, 15, 16, 17, 18, 23, 25, 26]. This methodology uses constrained non-linear optimization to simultaneously derive a structural and control design that minimizes a performance variable and/or mass given system constraints. Advanced MIMO control design techniques such as LQG, H_2, and H_∞ are used to derive appropriate control design [7, 8, 19, 22]. These methods use plant inversion techniques based on modeled dynamics to derive appropriate control laws. This makes them very sensitive to model uncertainties which can degrade performance and cause instability. Robust control methods such as μ synthesis and H_∞ control design exist, but are highly complex and overly conservative [6, 12, 22].

While several methodologies have shown progress towards improving the control of flexible structures, one important structural parameter that has been largely neglected is passive structural damping. Only recently, have passive damping techniques received attention in improving the characteristics of controlled structures [1, 9, 11, 21, 24, 31]. Passive damping provides a fail safe method for the removal of structural vibrational energy . This reduces the need for active control to remove these vibrations, thus providing better rigid body control and disturbance rejection of the system [9]. The reduced control effort can bring about weight reductions as a result of smaller actuators and power sources [11]. Other advantages of passive damping are that it requires no power, is often less expensive than active control systems, and can not drive the structure unstable [1].

One key advantage of increasing the amount of passive damping in a structure is the improved robustness characteristics [28, 31, 12]. The addition of passive damping pulls the plant poles deeper into the left hand plane. This allows more room for the system root locus to avoid the right hand plane, thus improving the stability robustness properties. Von Flotow et al. [31] pointed out that for high bandwidth control of flexible structures, pole-zero cancellation is necessary. Uncertainty in the modeled dynamics can cause a pole-zero flip which cause the root locus to enter the right hand plane resulting in an unstable system. The degree of damping to prevent this is based on the pole-zero separation as a result of the uncertainty and the bandwidth of the controller. While much research is currently talking place in the area of robust control design, very little work is place on how to design structures so that they are inherently robust. Robust plant design by modifying stiffness and mass properties of structures is difficult. Passive damping adds a new dimension to the design process allowing for robust structural dynamics.

While passive damping is very beneficial, active control is necessary for good performance such as for command following or shape control. Thus an active/passive damping mix is desirable. Passive damping is used for stability robustness and active control is used for performance.

The Passive and Active Control of Space Structures (PACOSS) study [24] has demonstrated the benefits of passive damping on controlled flexible structures such as improving performance, reducing weight, and reducing system complexity. Dynamic and control testing was performed on a large flexible structure (Dynamic Test Article (DTA)). The goal of the control system was to provide active vibration suppression of disturbances on the structure. An active and active/passive mix were examined. Results of the study were as follows.

1. Reduce complexity:
   Nine actuators needed for active control as opposed to two actuators for the active/passive mix.

2. Reduced control effort:
   Maximum torque required reduced from 1371 $N \cdot m$ to 167 $N \cdot m$.

3. Improved Reliability.

4. Improved Performance:
   A factor of 230 improvement in settling time as a result of a slew maneuver.
5. Reduced Weight:
   Mass reduction of 140 *lbs* ($\sim$ 2% of total weight).

The passive damping levels added to the structure were about 5% of critical at the modes of concern. McLoughlin [21] pointed out similar advantages for passively damped controlled structures.

This thesis will explore the advantages of increasing the amount of passive damping on feedback controlled flexible structures with particular attention placed on the stability and performance robustness characteristics. While previous studies have shown improvements in performance and robustness through the addition of passive damping, these issues have never been directly address. Expansion of the idea of robust structural design using passive damping to MIMO have never been addressed. Derivation of required passive damping levels for robust structural design would provide the structural designer with useful information to improve the system design. Though the examination of simple examples, theoretical limits in stability of the control structure are determined as a function of passive damping. Design studies are then used to verify these derivations and provide further evidence in the advantages of passive damping for SISO and MIMO controlled structures. This thesis promotes the principle of robust structural design through the addition of passive damping techniques to improve performance and robustness of controlled flexible structures.

1.2 Thesis Outline

Chapter 2

The virtues of passive damping on controlled structures using theoretical methods are examined. Both performance and robustness properties of simple structures are investigated. Effects of passive damping for structural vibration suppression are examined. Three methods for determining the required amount of damping given pole/zero uncertainty are examined. The first method determines the amount of passive damping needed for robust control based on the shape of the root locus plot

of a controlled structure. The second method looks at open loop phase uncertainty and derives a required amount of passive damping to achieve a desired phase margin. The third method examines the stability properties of a simple structure with PD control where an allowable pole/zero uncertainty given passive damping is derived. Uncertainty in the plant directions of a simple two degree of freedom structure is also examined to show the benefits of passive damping for MIMO control.

Chapter 3

The necessary structural modeling techniques and control design techniques for examining the virtues of passive damping are discussed in chapter 3. State space models of the structure in modal space are derived. Passive damping is added as a percentage of critical. H_2 optimal control design techniques are discussed.

Chapter 4

Simple SISO examples are used to numerically examine the virtues of passive damping of flexible structures. The first structure examined is a two mass system connected by a spring. Control of the position of one mass is achieved by applying an appropriate force on the other mass. Both unrobust and robust control techniques are used to derive the necessary control law for good disturbance rejection. Performance and robustness improvements are examined for increased passive damping. A similar study is performed on a four disk system connected by flexible springs. The system has noncollocated actuator and sensor. Benefits of passive damping for high and low bandwidth control are examined.

Chapter 5

In this chapter, passive damping effects are examined on MIMO systems. Two systems are examined. The first system is the four disk system with two noncollocated actuators and sensors. The second system is a nine disk system connected by flexible springs with two actuator and sensors. Performance and robustness characteristics are computed as a function of passive damping.

Chapter 6

A summary of the results from chapter 4 is presented and comparison to the

theoretical derivations in chapter 2 is made. Suggestions for future research in the area of passive damping for use in the control of flexible structures are made.

Chapter 2

Passive Damping in Controlled Structures

Design trends in large spacecraft have resulted in the need for precision control of flexible structures. To meet future weight requirements, space structures will be extremely flexible making them very susceptible to environmental and onboard disturbances. Through the use of passive damping techniques, reduction of structural disturbance excitation is achieved, allowing for more precise control. To eliminate unwanted dynamics of the structure, plant inversion techniques must be used in the control design. Thus an accurate representation of the structure is needed to design the controller. For high bandwidth control of lightly damped structures, uncertainty in the structure model results in unrobust systems. As von Flotow indicated [31], small amounts of passive damping in the structure can greatly improve the stability robustness properties of the system, thus bringing about the idea of structural design for robustness. In this chapter, performance and robustness benefits of passively damped controlled structures are theoretically examined. Simple examples are used to provide evidence of the advantages of increasing passive damping in controlled structures.

2.1 Nominal Performance Benefits

With control system performance requirements being pushed upward while at the same time spacecraft are built lighter and more flexible, the interaction between the control system and structure dynamics has become increasingly important. The limit of the closed-loop bandwidth is based on the structural flexibility as well as sensor and actuator dynamics. The objective for most controlled structures is to achieve good rigid body control with little structural vibration. If not correctly dealt with, these structural vibrations can result in poor performance or even instability. Passive damping techniques provides a simple method to eliminate structural vibrational energy, thus improving design objectives and allowing for higher bandwidth control.

In order to achieve high bandwidth control, high controller gains are necessary. Control dynamics are added to provide active damping and good steady state tracking as well as filtering of unwanted dynamics or noise. Hughes et al. [13] and Spanos [30] found that for structures with stable rigid body control and collocated sensors and actuators, the flexible dynamics of the structure would not destabilize the system. While this is obvious since there is no dynamic link between the sensor and actuator, control maneuvers add vibrational energy to the structure. This results in vibrations that can be undesirable, especially for structures used for precision pointing such as solar arrays or antennas. Thus passive damping is useful to eliminate vibrations caused by rigid body control and disturbances on the structure.

Lets consider a single degree of freedom structure consisting of a point mass connected to a fixed body by a spring and a damper as shown in figure 2-1. The equation of motion of the system is

$$m\ddot{x}(t) + c\dot{x}(t) + kx(t) = f(t) \tag{2.1}$$

where $f(t)$ is the disturbance force on the mass and $x(t)$ is the displacement from the unforced location. The values m, c, and k are the mass, damping constant, and stiffness respectively. Given a unit impulse disturbance at $t = 0$, the resulting

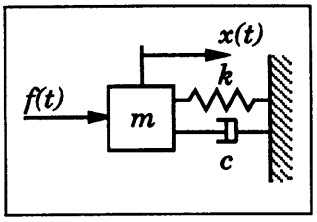

Figure 2-1: Single Degree of Freedom Spring/Mass/Damper System.

vibrations are described by an exponentially decaying sinusoid

$$x(t) = \frac{1}{m}\frac{1}{\omega_n\sqrt{1-\zeta^2}}e^{-\zeta\omega_n t}\sin\left(\omega_n\sqrt{1-\zeta^2}t\right) \tag{2.2}$$

where ω_n is the natural frequency of the system and ζ is the damping ratio.

$$\omega_n = \sqrt{\frac{k}{m}} \quad \zeta = \frac{c}{2\sqrt{km}} \tag{2.3}$$

The impulse response is shown in figure 2-2. Note that the rate of decay of the sinusoid is inversely proportional to the damping ratio. Undamped structures experience no decay in vibration. The maximum overshoot of the disturbance response occurs when the time derivative of the response is zero.

$$\frac{dx}{dt} = -\zeta\omega_n e^{-\zeta\omega_n t}\sin\left(\omega_n\sqrt{1-\zeta^2}t\right) + \omega_n\sqrt{1-\zeta^2}e^{-\zeta\omega_n t}\cos\left(\omega_n\sqrt{1-\zeta^2}t\right) = 0 \tag{2.4}$$

For lightly damped system ($\zeta \approx 0$), the derivative of the displacement is zero at the following times.

$$\omega_n\sqrt{1-\zeta^2}t \approx \frac{\pi}{2}, \frac{3\pi}{2}, \frac{5\pi}{2}\cdots \tag{2.5}$$

The maximum overshoot occurs in the first time period.

$$x_{max} = x(\pi/2\omega_n) = \frac{1}{\omega_n\sqrt{1-\zeta^2}}e^{-\zeta\frac{\pi}{2}} \tag{2.6}$$

Note that the maximum overshoot is inversely proportional to the damping ratio.

Thus passive damping provides a simple and fail-safe method of reducing struc-

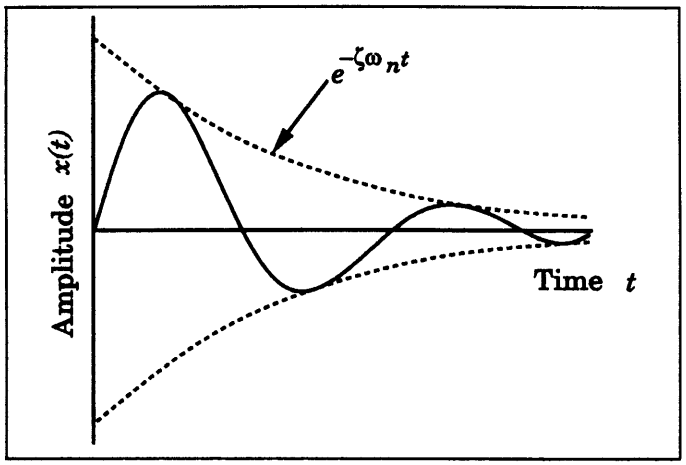

Figure 2-2: Impulse Response of Spring/Mass/Damper System.

tural vibrations as a result of disturbances. This simple example shows how the settling time and overshoot given an impulse disturbance are reduced by increasing passive damping. In high bandwidth maneuvers of a spacecraft, structural vibrations are excited. To maintain precise control of the structure, either passive or active techniques are needed to reduce these vibrations. An advantage of passive damping in controlled structures thus results from the reduction in effort required by the controller to provide vibration suppression.

2.2 Robustness Benefits

2.2.1 Gain Stabilization

One method to robustly control a flexible structure is to assure that the open loop gains of the system are below some uncertainty bound in the frequency domain. By observing the singular values of the open loop system $T(s)$ and applying stability robustness bounds such as the small gain theorem, the advantages of passive damping on controlled structures are evident. Since the open loop gain at structural resonance is inversely proportional to damping, large gains are observed for lightly damped structures. While active control techniques can be used to minimize structural ex-

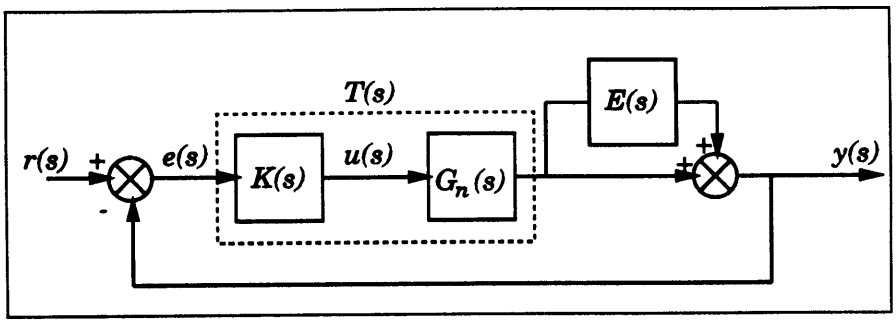

Figure 2-3: Closed-Loop System with Multiplicative Error.

citation at resonance, an accurate representation of the structure is needed in the control system design. The addition of passive damping provides a simple method to reduce the gains at resonance, allowing for robust control of a flexible structure.

Consider a modeled structure $G_n(s)$ with feedback compensation $K(s)$ as shown in figure 2-3. The open loop system is given by $T(s) = G_n(s)K(s)$. For good command following and disturbance rejection, high loop gain is necessary within its bandwidth ω_{cl}. Thus the singular values of the open loop system must be much greater than one across the bandwidth of the system.

$$\sigma_{min}[T(j\omega)] \gg 1 \quad \forall\, \omega < \omega_{cl} \tag{2.7}$$

The uncertainty in the structure is modeled as a multiplicative error given by $E(s)$. The actual dynamics of the structure $G_a(s)$ are then given by the following equation.

$$G_a(s) = [I + E(s)]G_n(s) \tag{2.8}$$

If it is assumed that the plant is square, i.e. the number of actuators equals the number of sensors, then the multiplicative error is as follows.

$$E(s) = [G_a(s) - G_n(s)]G_n^{-1}(s) \tag{2.9}$$

Though the use of the small gain theorem, Athans [3] found that a sufficient

condition for stability robustness is given by the following inequality.

$$\sigma_{max}[E(j\omega)] < \sigma_{min}[I + T^{-1}(j\omega)] \quad \forall\, \omega \tag{2.10}$$

Applying the condition for good performance given by equation 2.7, and some basic facts about singular values given in appendix A.1, the singular values of the uncertainty must be less than one within the closed-loop bandwidth of the system.

$$\sigma_{max}[E(j\omega)] < 1 \quad \forall\, \omega < \omega_{cl} \tag{2.11}$$

Substituting in equation 2.9 into the inequality and applying the properties of singular values given in appendix A.1, a sufficient condition for stability robustness is given by the following inequality.

$$\frac{\Delta\sigma}{\sigma_{min}[G_n(j\omega)]} = \frac{\sigma_{max}[G_a(j\omega)] - \sigma_{max}[G_n(j\omega)]}{\sigma_{min}[G_n(j\omega)]} < 1 \quad \forall\, \omega < \omega_{cl} \tag{2.12}$$

This inequality indicates that the peak singular values of the actual plant dynamics are extremely important to the stability robustness properties of the system. The height of these peaks are determined by the amounts of passive damping in the structure.

Consider a plant with one eigenvalue with a nominal natural frequency of ω_n and an actual natural frequency ω_a. The plots of the singular values are shown in figure 2-4. For low frequencies, the nominal and actual plant should match well. The greatest difference in singular values $\Delta\sigma$ is at resonance, as the figure shows. The peak values of the singular values are inversely proportional to damping. Thus passive damping provides a simple method to make the overall system more robust.

Even though this example is extremely conservative in nature, it does provide insight to the benefits of passive damping on the stability robustness properties of controlled structures. What ever techniques are used to filter out the plant dynamics for high bandwidth control, it must include the uncertainty in the modeled dynamics to ensure the system is robustly stable. The more passive damping in the structure, the less effective the filtering needs to be across the uncertainty region of the plant

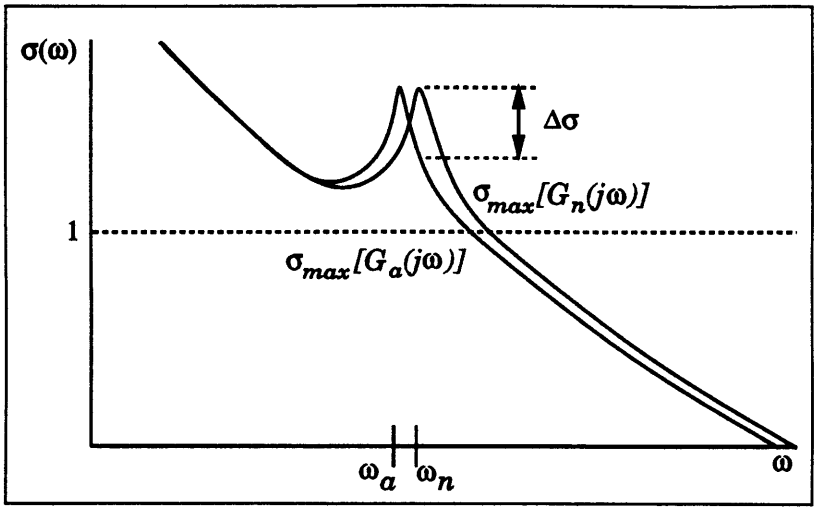

Figure 2-4: Singular Values of Nominal and Actual Plant.

dynamics.

2.2.2 Phase Stabilization

Robust Pole-Zero Cancellation

In order to achieve high bandwidth control of a flexible structure, the unwanted dynamics within the control bandwidth of the plant must be canceled out. This is accomplished by notch filtering the control signals at the structural natural frequencies, resulting in perfect cancellation of plant poles by compensator zeros. Thus an accurate model of the structure is needed to determine its poles for the design of the compensator. For undamped systems, uncertainty in the plant pole location can result in instability in the closed-loop system.

Figure 2-5 shows the root locus of the system with plant poles below and above the compensator zero as a result of uncertainty in modeled plant dynamics. If it is assumed that there is a phase lag of -90^o due to all other dynamics of the loop, the departure angle of the root locus is 180^o as a result of an uncertainty with the plant pole above the compensator zero. But if the uncertainty results in the plant pole being below the compensator zero, the departure angle of the root locus is 0^o

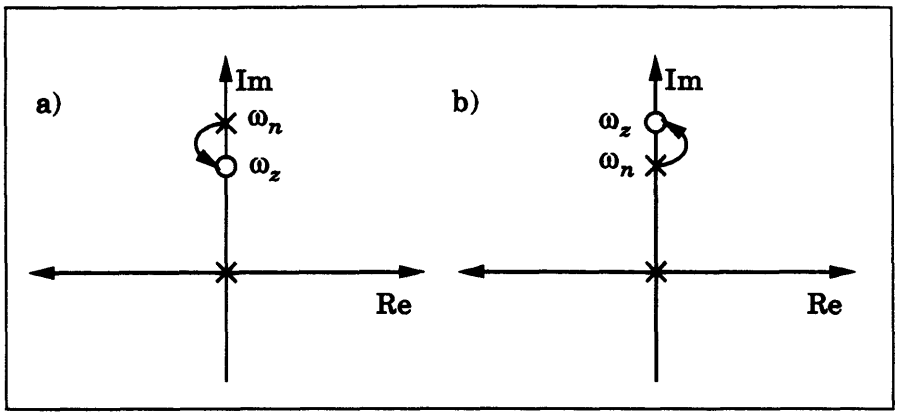

Figure 2-5: Departure Angles of Root Locus of a Single Oscillatory System as a Result in Uncertainty in Pole Location.

resulting in an unstable system. The plant poles migrate to the zero in semicircles. By placing a little damping in the structure, the plant poles are shifted to the left resulting in a system where the plant poles can migrate to the compensator zeros in a stable manner. The degree to which the poles migrate to the right hand side is based on the pole-zero separation resulting from uncertainty in the plant model. If it is assumed that the poles migrate to the zeros in semicircles, the amount of passive damping to assure stability robustness is given by the following

$$\zeta = \frac{|\omega_z - \omega_n|}{\omega_z + \omega_n} \tag{2.13}$$

where ω_z is the zero natural frequency and ω_n is the pole natural frequency. This amount of passive damping will assure that the root locus will not cross the imaginary axis.

Phase Properties of Passively Damped SISO Plants

In the following example, the amount of passive damping for the control of a simple system with one oscillatory mode is considered. In order to achieve a desired close-loop bandwidth including the structural natural frequency, pole-zero cancellation is needed to filter out resonances of the plant. This calculation is a first order approximation of

the amount of damping needed to achieve high bandwidth control. The derivations are based on findings reported by von Flotow and Vos [31].

The plant under consideration contains a single oscillatory mode represented by the following transfer function

$$G(s) = \frac{1}{s^2 + 2\zeta\omega_n s + \omega_n^2} \tag{2.14}$$

where ω_n is its natural frequency and ζ is the amount of passive damping. For this system, the phase angle $\theta(\omega)$ at any frequency is given by the following.

$$\theta(\omega) = -\tan^{-1}\frac{2\zeta\omega_n\omega}{\omega_n^2 - \omega^2} \tag{2.15}$$

It can be shown that at resonance ($\omega_n = \omega$), the change in phase angle with respect to frequency is given by

$$\frac{d\theta}{d\omega} = \frac{-1}{\zeta\omega_n} \tag{2.16}$$

which says that the phase change at resonance is sharp for low damping (see Figure 2-6). If the uncertainty in the eigenfrequency is given by $\delta\omega = \omega_n - \omega_{actual}$, then a first order approximation in the uncertainty in phase angle near resonance is given by the following.

$$\delta\theta = \frac{-\delta\omega}{\zeta\omega_n} \tag{2.17}$$

Thus the uncertainty in phase of the plant given an uncertainty in natural frequency is inversely proportional to the damping. Von Flotow defined a permissible amount of modal damping as a result of uncertainty in eigenfrequency as

$$\zeta > \frac{\delta\omega}{\omega_n} \tag{2.18}$$

where it is assumed that the desired phase margin is $\delta\theta = 1\ rad(\sim 60^(o))$.

In order achieve precision control of a plant, the plant dynamics within the control bandwidth must be filtered by canceling plant poles with compensator zeros. By observing the phase excursion given by the plant uncertainty, the effects of non-

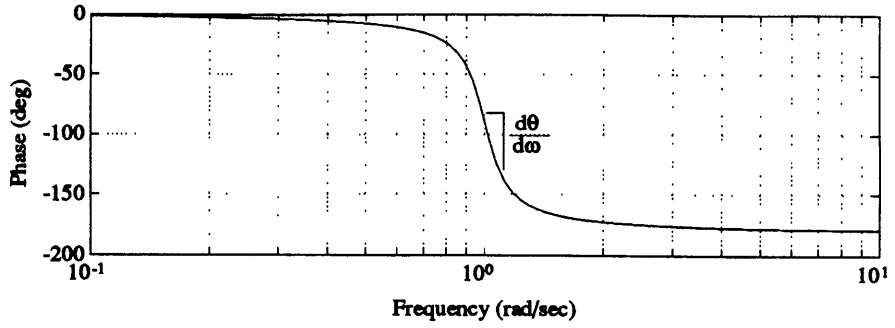

Figure 2-6: Bode Plot Illustrating Phase Change at Resonance.

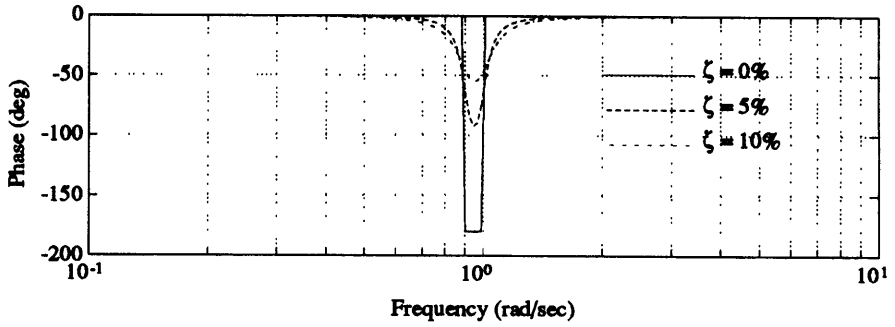

Figure 2-7: Bode Plot Illustrating Phase Excursion for Different Amounts of Passive Damping.

perfect pole-zero cancellation on closed-loop stability can be determined. Figure 2-7 shows the phase excursion as a result of the actual plant natural frequency being less than the modeled frequency ($\omega_{actual} < \omega_n$) which introduces a local phase lag. Given an undamped structure with nonperfect pole-zero cancellation, the phase excursion is 180°, thus impossible to stabilize. The introduction of damping reduces this phase excursion.

Given a phase margin of $\delta\theta_m$, which is the amount of phase needed to drive the system to instability, the permissible amount of uncertainty in the plant natural frequency is given by

$$\delta\omega \leq \delta\theta_m \zeta\omega_n \tag{2.19}$$

Thus it is sufficient to say that the amount of damping needed given a pole-zero

mismatch of $\delta\omega$ and a desired phase margin of $\delta\theta_m$ is

$$\zeta \geq \frac{1}{\delta\theta_m}\frac{\delta\omega}{\omega_n} \tag{2.20}$$

This is a low order example of the virtues of passive damping in the robust control of a structure. A quantitative amount of passive damping required for robust stability is determined based on modeling uncertainty in the structural natural frequencies. In application to real systems, the deeper the closed-loop poles can be pushed into the left hand plane, the less sensitive they need to be to model uncertainties. Passive damping provides a simple and safe way to push the plant poles into the left hand plane, thus improving the stability robustness properties of the system.

2.2.3 Simple Structure with PD Control

Hughes [13] and Spanos [30] found that high bandwidth control of a structure with noncollocated sensors and actuators is impossible with zero passive damping. The high gains at resonance destabilize the system, thus open-loop bandwidth must be well below the first structural mode as to not excite the system. A conservative approach in the control design dictates that open-loop bandwidth should be one order of magnitude below the first structural mode of lightly damped structures to prevent structural excitation. In order to achieve high bandwidth control, notch filtering at structural resonance is needed to prevent structural excitation. The degree of filtering is highly dependent on the amount of passive damping and structural uncertainty.

The following example examines the benefits of passive damping on a simple structure with PD control. The example is based on findings reported by Spanos [30]. Stability bounds are determined based on structural configurations indicating performance limits.

Lets consider a structure with one rigid body mode and one flexible mode at frequency ω_n. The transfer function representing the structure is given by

$$\frac{y(s)}{u(s)} = \frac{1}{Js^2} + \frac{\phi_{in}\phi_{jn}}{s^2 + 2\zeta\omega_n s + \omega_n^2} = \frac{\alpha_n s^2 + 2\zeta\omega_n s + \omega_n^2}{Js^2(s^2 + 2\zeta\omega_n s + w_n^2)} \tag{2.21}$$

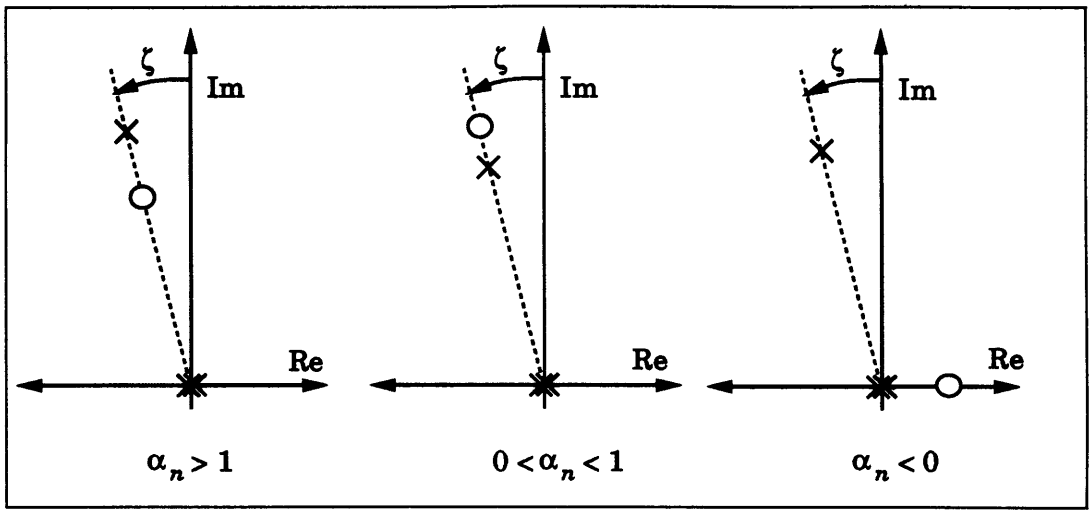

Figure 2-8: Pole-Zero Patterns for Different Values of α_n.

where $y(s)$ is the measured position of the structure and $u(s)$ is the control effort applied to the structure. The inertia of the structure is given by J and the amount of modal damping is ζ. The term α_n represents the modal participation coefficient of the mode defined as

$$\alpha_n = 1 + J\phi_{in}\phi_{jn} \tag{2.22}$$

where ϕ is the eigenvector of a given mode normalized to unit mass. The modal participation coefficient reflects the mass participation in a given mode. The resulting structure has alternating pole-zero patterns as shown in figure 2-8. Three types of modes are represented by the system based on the value of α_n.

appendage mode: Resulting from collocated sensors and actuators where $\alpha_n > 1$.

in-the-loop minimum phase mode: Resulting from noncollocated sensors and actuators with a minimum phase plant where $0 < \alpha_n < 1$.

in-the-loop nonminimum phase mode: Resulting from noncollocated sensors and actuators with a nonminimum phase plant where $\alpha_n < 0$.

Note that a rigid body system is indicated by $\alpha_n = 1$ when the flexible modes are canceled by the zeros.

If the mode is minimum phase and lightly damped, it can be shown that α_n is also the ratio between square of the pole and zero frequency

$$\alpha_n = \frac{\omega_n^2}{\omega_z^2} \tag{2.23}$$

where ω_z is the zero frequency. Thus a relationship between the modal participation coefficient and plant pole-zero separation is established.

$$\frac{\omega_z - \omega_n}{\omega_n} = \frac{1}{\sqrt{\alpha_n}} - 1 \tag{2.24}$$

This is significant since the separation between poles and zeros is inversely proportional to the mass participation in the mode defined by α_n.

With the plant model defined, a PD controller is coupled to the system as shown in figure 2-9. The controller consists of two gains; K_p which amplifies the position error and K_d which amplifies the time derivative of position (velocity). The inertia term (J) was removed by absorbing it into the two gains. To achieve a closed-loop bandwidth of ω_{cl} for the rigid body plant, the controller gains must be as follows,

$$K_p = (\sqrt{4\zeta_{cl}^4 + 4\zeta_{cl}^2 + 2} - 2\zeta_{cl}^2 - 1)w_{cl}^2 \tag{2.25}$$

$$K_d = 2\zeta_{cl}\sqrt{K_p} \tag{2.26}$$

where ζ_{cl} is the desired closed-loop damping ratio. For most systems, it is desirable to have a closed-loop damping ratio of $\zeta_{cl} = 1/\sqrt{2}$. The characteristic equation of the closed-loop system is then given by the following fourth order equation.

$$s^4 + (K_d\alpha_n + 2\zeta\omega_n)s^3 + (2\zeta\omega_n K_d + \alpha_n K_p + \omega_n^2)s^2 + (2\zeta\omega_n K_p + K_d\omega_n^2)s + (K_p\omega_n^2) = 0 \tag{2.27}$$

By using the Routh stability criterion, the stability conditions for the closed-loop

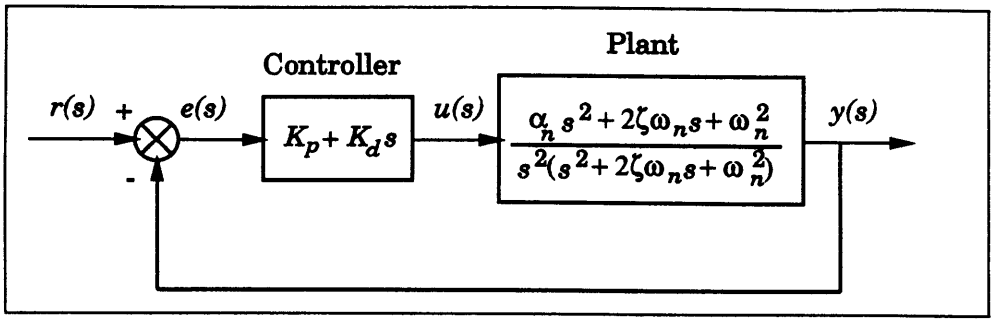

Figure 2-9: Single Mode Structure with PD Controller.

system are given by the following three equations.

$$0 < K_d\alpha_n + 2\zeta\omega_n \tag{2.28}$$

$$0 < K_pK_d\alpha_n^2 + (2\zeta K_p + 2\zeta K_d^2 + K_d\omega_n)\omega_n\alpha_n + (4\zeta^2\omega_n K_d + 2\zeta\omega_n^2 - 2\zeta K_p - K_d\omega_n)\omega_n \tag{2.29}$$

$$0 < 2\zeta K_p^2 K_d\alpha_n^2 + (4\zeta^2 K_p^2 + 4\zeta^2 K_p K_d^2 + 2\zeta\omega_n K_d^3 + K_d^2\omega_n^2)\omega_n\alpha_n + (8\zeta^3\omega_n K_p K_d + 4\zeta^2\omega_n^2 K_d^2 - 4\zeta^2 K_p^2 + 2\zeta\omega_n^3 K_d - 4\zeta\omega_n K_p K_d - K_d^2 w_n^2)\omega_n \tag{2.30}$$

For a given closed-loop bandwidth ω_{cl} and damping ratio ζ_{cl} as well as a structural natural frequency ω_n and modal damping ζ, conditions on the modal participation coefficient α_n can be determined to maintain stability. The dominant governing equation for stability based on the Routh stability criterion is given by equation 2.30. By observing the necessary modal participation coefficient for stability at various frequencies as well as amounts of modal damping, the benefits of passive damping on the controlled structure are evident (see figure 2-10). The regions above the lines define structural designs with PD control which are stable.

As figure 2-10 shows, for structures with collocated sensors and actuators ($\alpha_n > 1$), the closed-loop system is always stable. But for noncollocated system, instability can occur when the closed-loop bandwidth is within a tenth of the first natural frequency ($\omega_n/\omega_{cl} = 1/10$), especially for lightly damped systems. For undamped structures,

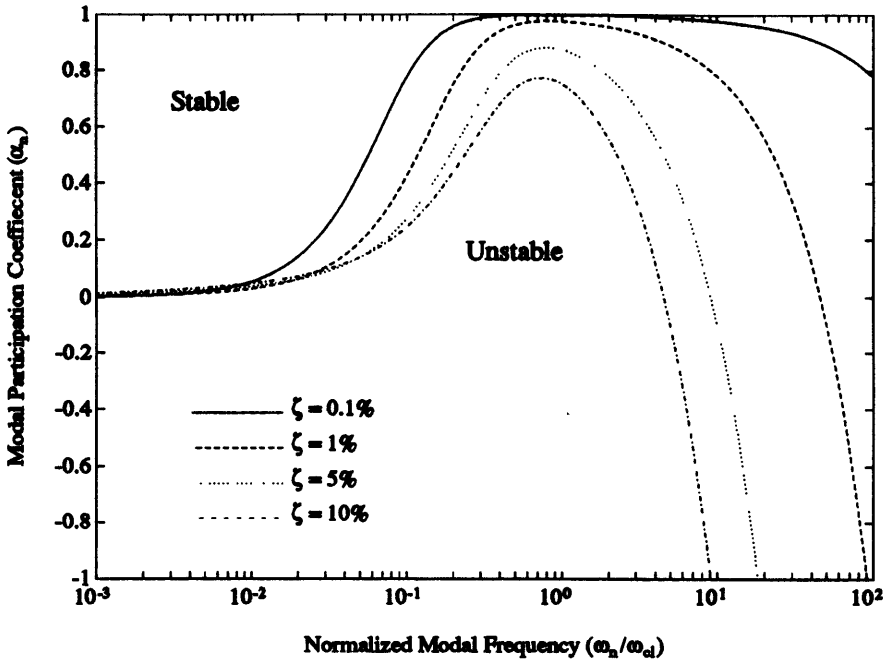

Figure 2-10: Stability Bounds of One Mode Structure with PD Control for Various Levels of Modal Damping.

α_n must be greater than one for all frequencies. Nonminimum phase plants ($\alpha < 0$) cannot be stabilized with PD control. As damping increases, the minimum allowable amount of α_n decreases and the maximum allowable closed-loop bandwidth increases.

Root locus plots for the single mode structure using PD control with $\alpha_n = 0.8$ and $\omega_n = \omega_{cl} = 1$ are shown in figure 2-11. Notice that the poles migrate to the zeros in semicircles similar to the results shown in section 2.2.2. The compensator zero is used to draw the rigid body poles into the left hand plane. Furthermore, the flexible body poles depart to the right as they migrate towards the plant zeros. Thus undamped systems can not be stabilized. Passive damping pushes the flexible body root locus into the left hand plane allowing for stable control of the structure. The amount of damping needed to stabilize the system is dependent on the size of the semicircle resulting from the root locus of the flexible body pole migration to the plant zero. The size of the semicircle is based on the plant pole-zero separation and the bandwidth of the structure. Larger pole-zero separation and higher bandwidth systems result in larger semicircles.

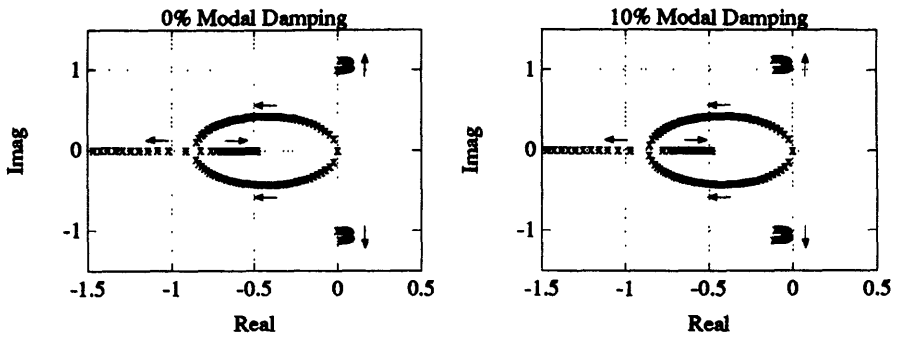

Figure 2-11: Root Locus Plots of One Mode Structure with PD Control.

By using the results obtained in figure 2-10 and applying equation 2.24, a relationship can be established between the maximum allowable plant pole-zero separation and modal damping for control within the structural bandwidth as shown in figure 2-12. The figure shows an inverse linear proportionality between modal damping needed to stabilize a controlled structure and pole-zero separation. These results show good comparison to the assumptions in section 2.2.2 where the amount of damping needed to assure stability given pole-zero uncertainty was based on the size of the semicircles made by the root locus resulting from plant poles migrating to zeros. Furthermore, it indicates that less damping is required than that assumed by von Flotow's linear approximation using equation 2.18.

Given a simple structure consisting of one mode with PD control, the importance of passive damping to the performance and stability of the control structure are made evident. The closed-loop bandwidth is dependent on both the plant pole-zero separation and amount of structural damping. An implicit relationship between maximum pole-zero separation and modal damping to achieve stable control within the structural bandwidth is established.

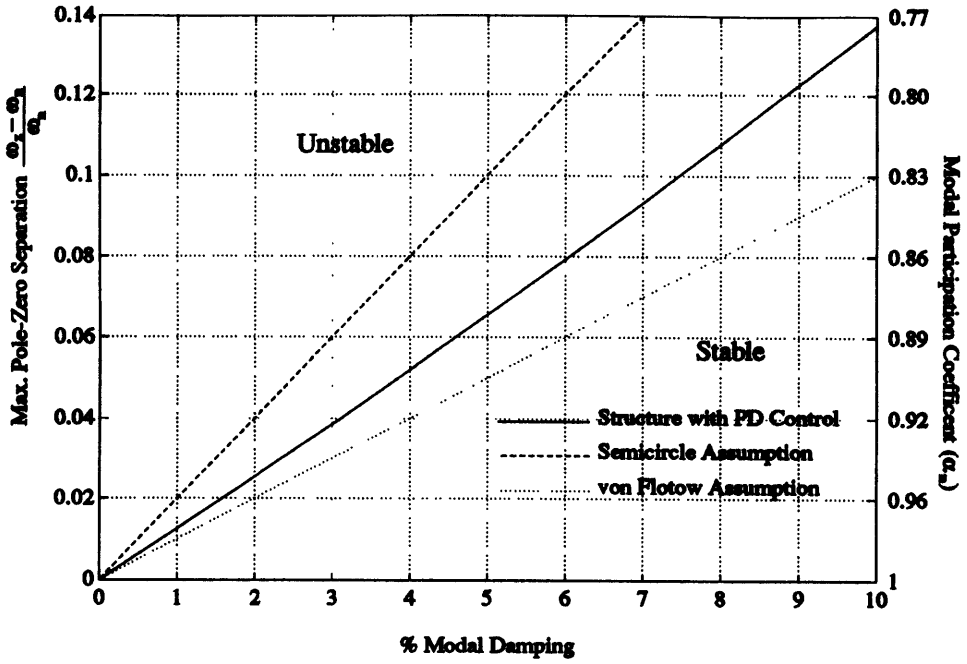

Figure 2-12: Maximum Allowable Plant Pole-Zero Separation to Maintain Stability of One Mode Structure with PD Control.

2.2.4 Directional Properties of Passively Damped MIMO Plants

A major source of model uncertainty lies in the directional information about the plant. Small changes in plant variables can result in dramatic differences in the directional information of a plant which can cause instability. The addition of passive damping to a MIMO plant reduces the uncertainty in directional information of the plant. The directional information of a plant describes how the inputs and outputs of the system interact. MIMO control techniques take advantage of the interactions and coupling between the plant inputs and outputs to improve the control characteristics of the system.

Plant zeros are dependent on plant directions in comparison to plant poles which are based on modal frequencies. In optimal control design, plant inversion techniques are used to develop high performance controllers. This results in cancellation of plant transmission zeros by compensator poles and replacing them with more desirable dy-

namics (see [3]). Thus accuracy of plant directions with respect to model uncertainty is extremely important in the design of MIMO optimal controllers.

Lets consider a n degree of freedom structural model defined by the following matrix differential equation

$$M\ddot{x}(t) + C\dot{x}(t) + Kx(t) = u(t) \tag{2.31}$$

where M is the mass matrix, C is the damping matrix, K is the stiffness matrix, and $u(t)$ in the applied accelerations. The eigensystem of the plant is defined by the eigenvalues Λ and eigenvectors Φ.

$$K\Phi = M\Phi\Lambda \tag{2.32}$$

The eigenvectors are normalized about the mass matrix $\Phi^T M\Phi = I$. By transforming the differential equation to modal coordinates, the matrix equation is converted into n uncoupled differential equations.

$$\ddot{\eta}(t) + 2Z\Lambda^{1/2}\dot{\eta}(t) + \Lambda\eta(t) = \Phi^T u(t) \tag{2.33}$$

The vector $\eta(t)$ are the states of the structure in modal coordinates given by the transformation $x(t) = \Phi\eta(t)$. The diagonal elements of Z represent the amount of modal damping at each mode as a ratio of critical. The scalar transfer function with relation to actual outputs is derived.

$$\frac{x_j(s)}{u_i(s)} = \sum_{r=1}^{n} \frac{\Phi_{jn}\Phi_{ni}}{s^2 + 2\zeta_n\omega_n s + \omega_n^2} \tag{2.34}$$

Notice that the poles of the plant are given by the denominator of the transfer functions which are the same for all input to output relationships. Thus there is no change in the directionality of the plant near pole frequencies. Directional changes are based on the numerator of the transfer function which also defines the plant zero locations. Thus uncertainty in the plant zeros indicates uncertainty in the plant directions.

Lets consider a two degree of freedom system. The resulting transfer function is given by the following equation.

$$\frac{x_j(s)}{u_i(s)} = \frac{(\Phi_{j1}\Phi_{1i} + \Phi_{j2}\Phi_{2i})s^2 + 2(\Phi_{j1}\Phi_{1i}\zeta_2\omega_2 + \Phi_{j2}\Phi_{2i}\zeta_1\omega_1)s + (\Phi_{j1}\Phi_{1i}\omega_2^2 + \Phi_{j2}\Phi_{2i}\omega_1^2)}{(s^2 + 2\zeta_1\omega_1 s + \omega_1^2)(s^2 + 2\zeta_2\omega_2 s + \omega_2^2)} \tag{2.35}$$

Notice that the plant eigenvectors play no part in the denominator of the transfer function, thus they do not affect the poles of the plant. Furthermore, the denominator is the same for all input to output mappings.

The directional information of the plant is a measure of the interaction of the inputs and outputs of the system. For a two input two output system with equal modal damping ($\zeta_1 = \zeta_2 = \zeta$), one such indicator of plant directions is the ratio of the output states given equal inputs. The ratio of the output states given only the input $u_1(s)$ is

$$\frac{x_1(s)}{x_2(s)} = \frac{a_1 s^2 + 2\zeta a_2 s + a_3}{b_1 s^2 + 2\zeta b_2 s + b_3} \tag{2.36}$$

where

$$\begin{aligned} a_1 &= \Phi_{11}\Phi_{11} + \Phi_{12}\Phi_{21} & b_1 &= \Phi_{21}\Phi_{11} + \Phi_{22}\Phi_{21} \\ a_2 &= \Phi_{11}\Phi_{11}\omega_2 + \Phi_{12}\Phi_{21}\omega_1 & b_2 &= \Phi_{21}\Phi_{11}\omega_2 + \Phi_{22}\Phi_{21}\omega_1 \\ a_3 &= \Phi_{11}\Phi_{11}\omega_2^2 + \Phi_{12}\Phi_{21}\omega_1^2 & b_3 &= \Phi_{21}\Phi_{11}\omega_2^2 + \Phi_{22}\Phi_{21}\omega_1^2 \end{aligned} \tag{2.37}$$

Notice that plant poles play no part in the ratio of the outputs, thus not affecting plant directions.

Since the Laplace transform is a representation of the system in frequency space ($s = j\omega$), the frequency behavior of the plant output ratios is the following complex function.

$$\frac{x_1(j\omega)}{x_2(j\omega)} = \frac{(a_3 - a_1\omega^2) + 2\zeta a_2\omega j}{(b_3 - b_1\omega^2) + 2\zeta b_2\omega j} \tag{2.38}$$

The ratio of the magnitudes of the outputs is then

$$\left|\frac{x_1(\omega)}{x_2(\omega)}\right| = \frac{|x_1(\omega)|}{|x_2(\omega)|} = \sqrt{\frac{(a_3 - a_1\omega^2)^2 + 4\zeta^2 a_2\omega^2}{(b_3 - b_1\omega^2)^2 + 4\zeta^2 b_2\omega^2}} \tag{2.39}$$

and the phase difference between the two outputs is then

$$\theta(\omega) = \angle\frac{x_1(\omega)}{x_2(\omega)} = \angle x_1(\omega) - \angle x_2(\omega) \tag{2.40}$$

$$\theta(\omega) = \tan^{-1}\frac{2\zeta a_2\omega}{a_3 - a_1\omega^2} - \tan^{-1}\frac{2\zeta b_2\omega}{b_3 - b_1\omega^2} \tag{2.41}$$

The change in phase difference θ with respect to frequency ω is then given by

$$\frac{d\theta}{d\omega} = 2\zeta\left[\frac{a_2a_3 + a_1a_2\omega^2}{(a_3 - a_1\omega^2)^2 + 4\zeta^2a_2\omega^2} - \frac{b_2b_3 + b_1b_2\omega^2}{(b_3 - b_1\omega^2)^2 + 4\zeta^2b_2\omega^2}\right] \tag{2.42}$$

The frequency where the phase change is critical is at the location of the plant zeros ($\omega_{z1} = \sqrt{a_3/a_1}$ and $\omega_{z2} = \sqrt{b_3/b_1}$). For small damping values, $d\theta/d\omega$ at the zero frequencies is

$$\left.\frac{d\theta}{d\omega}\right|_{\omega_{z1}} \approx \frac{a_1}{\zeta a_2} \qquad \left.\frac{d\theta}{d\omega}\right|_{\omega_{z2}} \approx \frac{b_1}{\zeta b_2} \tag{2.43}$$

If the uncertainty in the zero location is given by $\delta\omega_{z1} = \omega_{z1} - \omega_{z1,actual}$, then a first order approximation of the uncertainty in phase difference between the two outputs is given by the following.

$$\delta\theta = \delta\omega_{z1}\frac{a_1}{\zeta a_2} \tag{2.44}$$

Thus the uncertainty in the phase difference between the outputs of the plant at the plant zero locations is inversely proportional to damping. These results are similar to the change in phase angle with respect to frequency for SISO systems (see equation 2.16). Similar equations can be derived for output ratios as a result of inputs into the second channel and for ratios of inputs while measuring only one output. This idea can be extended for higher order MIMO systems.

The importance of damping to the change in phase difference with respect to frequency is easily shown in the following example. Consider a two mass system connected by a spring and a damper as shown in figure 2-13. Position of the two masses are measured and force is also applied to the two masses. The plant transfer

function is given by

$$G(s) = \frac{x(s)}{u(s)} = \frac{1}{s^2[m_1 m_2 s^2 + (m_1 + m_2)cs + (m_1 + m_2)k]} \begin{bmatrix} m_2 s^2 + cs + k & cs + k \\ cs + k & m_1 s^2 + cs + k \end{bmatrix} \tag{2.45}$$

where two zeros exist on the diagonal terms and one zero on the off-diagonal terms. The system contains one rigid body mode and one flexible mode at

$$\omega_n = \sqrt{\frac{(m_1 + m_2)k}{m_1 m_2}} \tag{2.46}$$

The amount of modal damping is given by

$$\zeta = \frac{c}{2}\sqrt{\frac{m_1 + m_2}{m_1 m_2 k}} \tag{2.47}$$

The change in phase difference between the first and second output given inputs into the first channel at the frequency of the location of the zero is given by

$$\left.\frac{d\theta}{d\omega}\right|_{w=\sqrt{k/m}} = \frac{m_2}{c} \tag{2.48}$$

Notice the inverse proportionality of the function with respect to the amount of passive damping in the plant. A plot of the phase difference for various amounts of passive damping and $m_1 = m_2 = 1$ and $k = 1$ is shown in figure 2-14. As damping increases, the change in phase difference with respect to frequency decreases. Notice the 180° jump in phase difference for undamped structures.

This indicates that the uncertainty in direction through the plant is reduced by the addition of passive damping to a structure. For undamped systems, the degree of uncertainty in the relative phase difference between the two outputs due to an uncertainty in zero location is 180 degrees. This may cause the system to go unstable if one tries to control the plant near the frequency of the zero. For the given two mass system, the addition of just 1% modal damping to plant results in a drop in phase difference from 180 degrees to 15 degrees given a 10% uncertainty in the zero

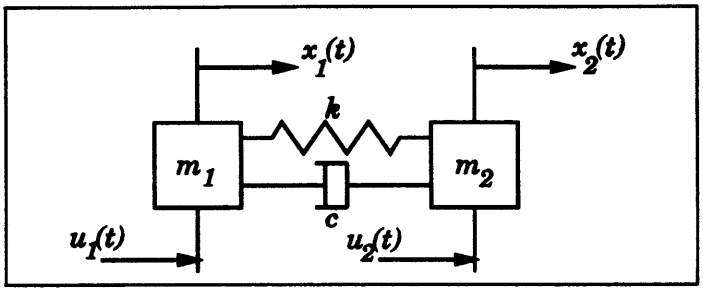

Figure 2-13: Two Mass Spring Damper MIMO Plant.

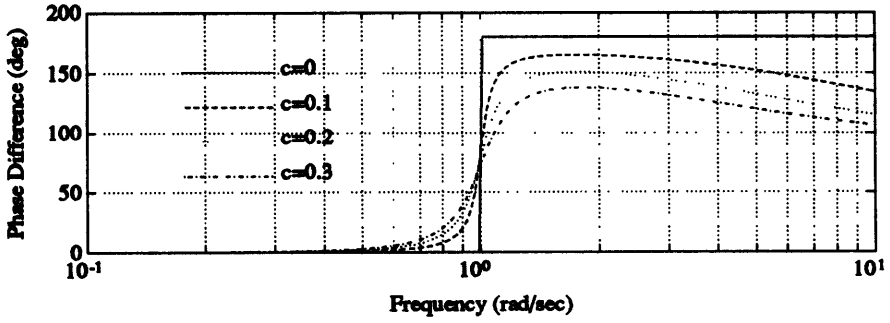

Figure 2-14: Phase Difference for Various Amounts of Passive Damping on Two Mass Spring Damper MIMO Plant.

location.

Chapter 3

Model and Controller Derivation

This chapter discusses the mathematical necessities for derivation of the structural model and computation of the control law to examine the virtues of passive damping on controlled structures. The structure is represented by the stiffness and mass matrix derived from a lumped parameter model. The structural model is then transformed to modal space to add damping as a ratio of the structural natural frequencies. With the structural model defined, a model based compensator is used to derive a control design. H_2 optimal control design is used due to the ease of computation and physical understanding of performance measure being minimized. H_2 optimal control design minimizes the H_2 norm of a weighted system which represents the total spectral power as a result of white noise inputs. H_2 control design allows for a general control design framework similar to that of Linear Quadratic Gaussian control design involving the solution of two Riccati equations. Computation of the H_2 norm is accomplished by solving a Lyapunov equation based on the closed-loop state matrices.

3.1 Development of Structural Model

The type of structures under investigation are linear structures with control effort and external disturbances affecting the system. The equations of motion for a structure

are given by the following matrix differential equation of motion

$$M\ddot{q}(t) + C\dot{q}(t) + Kq(t) = F_e u(t) + F_d \xi(t) \tag{3.1}$$

where M is the mass matrix, C is the damping matrix, and K is the stiffness matrix. Each of these matrices are of dimensions $n \times n$ where n is the number of degrees of freedom of the structure. The vector $q(t)$ is the amplitude of motion of the structure. The matrix F_e is a $n \times p_e$ applied load distribution matrix which relates the control effort vector $u(t)$ to the structural system. Similarly, the matrix F_d is a $n \times p_d$ disturbance load distribution matrix which relates the disturbance load vector $\xi(t)$ to the structural system. Lumped parameter models are used to derive the system matrices as a function of structural design variables.

For many structures, especially lightly damped systems, a modal space representation of the plant is desirable since damping can be added as a ratio of the structural natural frequencies (ζ_i) which can be computed experimentally.

Given an undamped structure defined by the mass and stiffness matrix, the eigensystem of the plant is defined as

$$K\Phi = M\Phi\Lambda \tag{3.2}$$

where Λ is a diagonal eigenvalue matrix and Φ is the eigenvector matrix of the plant. The diagonal elements of Λ are the square of the natural frequencies of the structure ($\lambda_i = \omega_i^2$). The eigenvectors are normalized about the mass matrix to one.

$$\Phi^T M \Phi = I \tag{3.3}$$

By transforming the plant states from physical space $q(t)$ to modal space $\eta(t)$,

$$q(t) = \Phi\eta(t) \tag{3.4}$$

the following modal space equations of motion for the structure are derived.

$$\ddot{\eta}(t) + \Lambda\eta(t) = \Phi^T M^{-1} F_e u(t) + \Phi^T M^{-1} F_d \xi(t) \tag{3.5}$$

Modal damping is introduced into the system

$$C = \begin{bmatrix} 2\zeta_1\omega_1 & & \\ & \ddots & \\ & & 2\zeta_n\omega_n \end{bmatrix} \tag{3.6}$$

where ζ_i is the damping ratio at frequency ω_i. For many cases, equal damping ratio is assumed across frequencies ($C = 2\zeta\Lambda^{\frac{1}{2}}$). Thus the damped modal space equations of motion are as follows.

$$\ddot{\eta}(t) + 2\zeta\Lambda^{\frac{1}{2}}\dot{\eta}(t) + \Lambda\eta(t) = \Phi^T M^{-1} F_e u(t) + \Phi^T M^{-1} F_d \xi(t) \tag{3.7}$$

The state space representation of the plant in modal coordinates is similar to the one in physical coordinates.

$$\dot{x}(t) = A_p x(t) + B_p u(t) + B_d w(t) \tag{3.8}$$

$$y(t) = C_p x(t) \tag{3.9}$$

The state vector $x(t)$ is made up of the modal displacements and velocities.

$$x(t) = \begin{bmatrix} \eta(t) \\ \dot{\eta}(t) \end{bmatrix} \tag{3.10}$$

The state matrices are as follows.

$$A_p = \begin{bmatrix} 0 & I \\ -\Lambda & -2\zeta\Lambda^{1/2} \end{bmatrix} \quad B_p = \begin{bmatrix} 0 \\ \Phi^T M^{-1} F_e \end{bmatrix} \quad B_d = \begin{bmatrix} 0 \\ \Phi^T M^{-1} F_d \end{bmatrix} \tag{3.11}$$

$$C_p = \tilde{C}_p \begin{bmatrix} \Phi & 0 \\ 0 & \Phi \end{bmatrix} x(t) \tag{3.12}$$

The output state matrix C_p transforms the measured state to physical space where $\tilde{C}_p$ is the physical output state matrix.

3.2 H_2 Optimal Control Design

3.2.1 Computation of H_2 Norm

The H_2 norm of a closed-loop system is a measure of its total spectral power as a result of white noise inputs. This makes the H_2 norm an ideal performance measure. Furthermore, the H_2 norm is easy to compute given the closed-loop state space representation of the system, involving the solution to a Lyapunov equation.

The H_2 norm of a system defined by the transfer function $G(s)$ is as follows

$$\|G\|_{H_2} \equiv \left\{ \frac{1}{2\pi} \int_{-\infty}^{\infty} \text{trace} \left[G^H(j\omega) G(j\omega) \right] \, d\omega \right\}^{\frac{1}{2}} \tag{3.13}$$

where the transfer function $G(s) = C(sI - A)^{-1}B$ is the loop under investigation. Through the use of Parseval's theorem, the H_2 is also the following time based integral [22, page 14].

$$\|G\|_{H_2} \equiv \left\{ \int_{0}^{\infty} \text{trace} \left[G^T(t) G(t) \right] \, dt \right\}^{\frac{1}{2}} \tag{3.14}$$

The function $G(t)$ is the inverse Laplace transform of $G(s)$, which is the response due to impulses applied at the inputs of the system. Thus minimizing the H_2 norm also minimizes the impulse response of the system.

Given a system transfer function $G(s)$, the solution of the H_2 norm is conveniently obtained by the following equation [7, pages 831–846].

$$\|G\|_{H_2} = \sqrt{\text{trace} \left[B^T L_o B \right]} = \sqrt{\text{trace} \left[C L_c C^T \right]} \tag{3.15}$$

The matrices L_o and L_c are the observability and controllability gramians respectively.

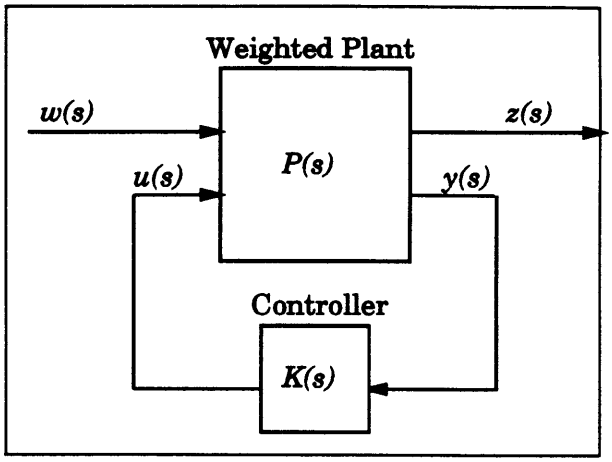

Figure 3-1: Linear Fractional Transformation of System

They are evaluated by solving the following Lyapunov equations.

$$A^T L_o + L_o A + C^T C = 0 \tag{3.16}$$

$$A L_c + L_c A^T + B B^T = 0 \tag{3.17}$$

Thus by applying the associative state space matrices under consideration, the H_2 norm can easily be computed. For a solution to the H_2 norm to exist, the state matrix A must be negative definite, i.e. the system is stable. Furthermore, the H_2 norm can not be computed with any feedforward terms ($D = 0$).

One advantage of using the H_2 norm as the control cost is that several loops can be studied at the same time, and weights can easily be placed on critical values. Furthermore, weights in the frequency domain can easily be augmented into the plant, thus allowing for loop shaping in the design. To better represent the system under investigation, a linear fractional transformation is used such as in figure 3-1.

The inputs into the plant $w(s)$ can represent disturbances, sensor noise, command signals, etc. Similarly, the outputs from the plant $z(s)$ can represent state values, effort, state errors, etc. The measured signals are given by $y(s)$ and the control effort by $u(s)$. The plant is defined by the state function where $P(s)$ is the associative

transfer function.

$$\left[\begin{array}{c} \dot{x}(t) \\ z(t) \\ y(t) \end{array}\right] = \left[\begin{array}{c|cc} A_p & B_1 & B_2 \\ \hline C_1 & D_{11} & D_{12} \\ C_2 & D_{21} & D_{22} \end{array}\right] \left[\begin{array}{c} x(t) \\ w(t) \\ u(t) \end{array}\right] \tag{3.18}$$

The compensator is given by the following transfer function.

$$K(s) = C_k(sI - A_k)^{-1}B_k \tag{3.19}$$

For a solution to the H_2 norm to exist, no feedforward terms can exist ($D_{11} = 0$). Furthermore, it is assumed the no measurements of the effort are taken directly ($D_{22} = 0$). The intention of H_2 optimal control design is to minimize the H_2 norm of the loop $G(s) = z(s)/w(s)$ where its state matrices are as follows.

$$A = \left[\begin{array}{cc} A_p & B_2C_k \\ B_kC_2 & A_k \end{array}\right] \quad B = \left[\begin{array}{c} B_1 \\ B_kD_{21} \end{array}\right] \quad C = \left[\begin{array}{cc} C_1 & D_{12}C_k \end{array}\right] \tag{3.20}$$

A common representation of the plant $P(s)$ is to have disturbance and sensor noise as inputs and plant states and effort as outputs as shown in figure 3-2 where W_d is the weighting on disturbances, W_s is the weighting on sensor noises, W_e is the weighting on the effort, and W_p is the weighting on the plant states. For this example, the transfer function $P(s)$ is defined as

$$P(s) := \left[\begin{array}{c|cc} A_p & \left[\begin{array}{cc} B_dW_d & 0 \end{array}\right] & B_p \\ \hline \left[\begin{array}{c} 0 \\ W_p \end{array}\right] & \left[\begin{array}{cc} 0 & 0 \\ 0 & 0 \end{array}\right] & \left[\begin{array}{c} W_e \\ 0 \end{array}\right] \\ C_p & \left[\begin{array}{cc} 0 & W_s \end{array}\right] & 0 \end{array}\right] \tag{3.21}$$

A compensator that minimizes the H_2 norm of the weighted closed-loop system $z(s)/w(s)$ can be computed directly using a simple algorithm involving solution of two Riccati equations.

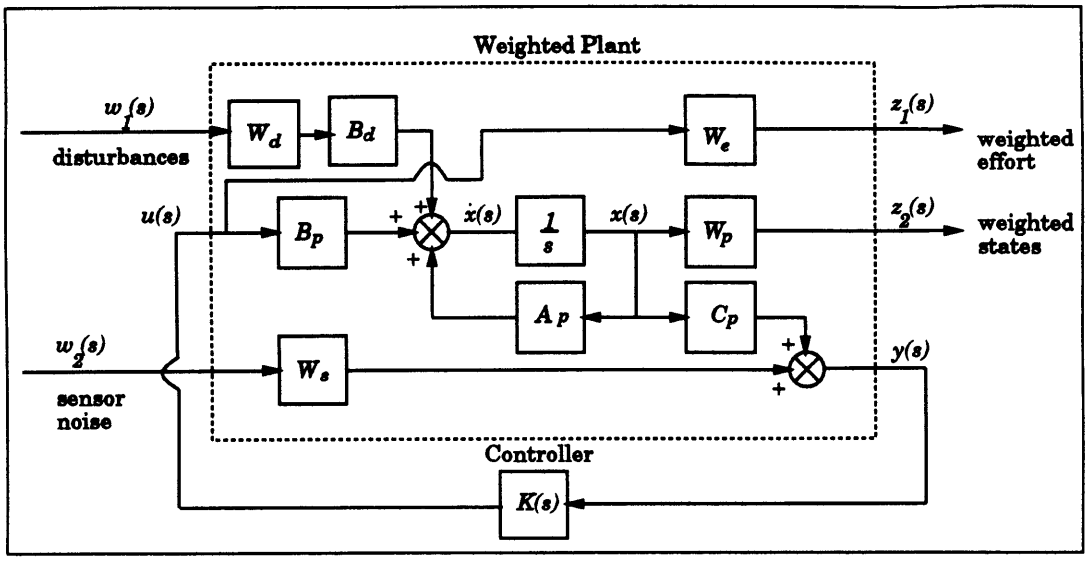

Figure 3-2: Example Block Diagram of a Closed-Loop System

3.2.2 Computation of Controller

H_2 optimal control design allows for a general framework to design a control system. The H_2 optimal control design algorithm computes the optimal controller $K(s)$ that minimizes the H_2 norm of the loop $z(s)/w(s)$ defined by the weighted plant $P(s)$.

$$P(s) := \left[\begin{array}{c|cc} A_p & B_1 & B_2 \\ \hline C_1 & D_{11} & D_{12} \\ C_2 & D_{21} & D_{22} \end{array}\right] \tag{3.22}$$

The compensator uses the model based compensator framework as shown in figure 3-3. The design technique essentially uses optimal Kalman filter design to compute the necessary filter gains H for good state estimation and Linear Quadratic Regulator design to compute the necessary control gains G for good performance. The control and filter gains G and H are computed to minimize the H_2 norm of the closed-loop system. The optimal compensator $K(s)$ is given by the following state space equation.

$$\dot{\hat{x}}(t) = [A_p - HC_2 - B_2G + HD_{22}G]\hat{x}(t) + Hy(t) \tag{3.23}$$

$$u(t) = -G\hat{x}(t) \tag{3.24}$$

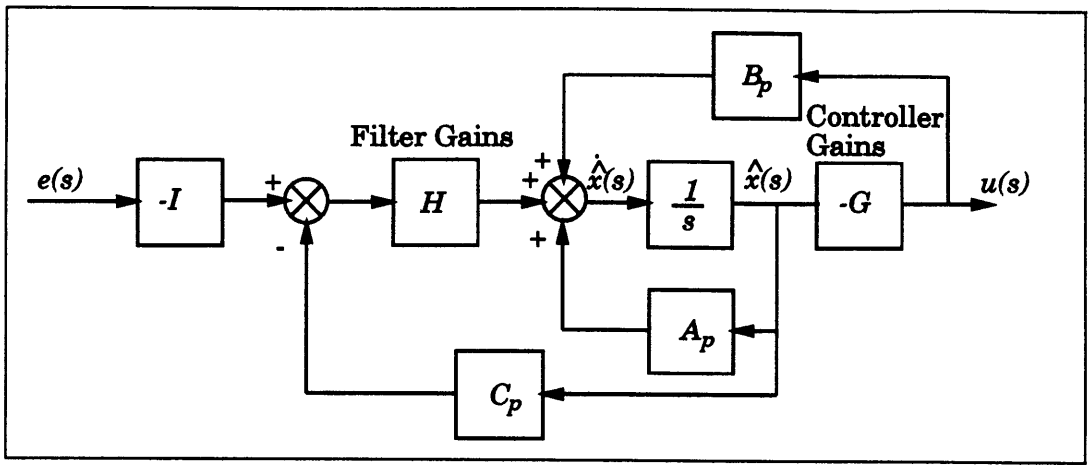

Figure 3-3: Model Based Compensator

In order for the plant to be well posed, no feed forward terms can exist ($D_{11} = 0$). Furthermore, D_{12} and D_{21}^T must have full column rank.

The following matrix transformation relates the LQG weights and the plant variables in the H_2 design.

$$\begin{bmatrix} Q & N_c \\ N_c^T & R \end{bmatrix} = \begin{bmatrix} C_1^T C_1 & C_1^T D_{12} \\ D_{12}^T C_1 & D_{12}^T D_{12} \end{bmatrix} \tag{3.25}$$

$$\begin{bmatrix} \Xi & N_f \\ N_f^T & \Theta \end{bmatrix} = \begin{bmatrix} B_1 B_1^T & B_1 D_{21}^T \\ D_{21} B_1^T & I \end{bmatrix} \tag{3.26}$$

The matrices N_c and N_f are correlation matrices between sensor noises and disturbances.

The computation of the optimal filter gains and controller gains that minimize the H_2 norm of $z(s)/w(s)$ involves the solution of two Riccati equations. The filter gains H are given by

$$H = (\Sigma C_2^T + N_f)\Theta^{-1} \tag{3.27}$$

such that Σ is a symmetric positive semidefinite matrix that satisfies the following

algebraic Ricatti equation (ARE).

$$\Sigma A_p^T + A_p \Sigma - (C_2 \Sigma + N_f^T)^T \Theta^{-1} (C_2 \Sigma + N_f^T) + \Xi = 0 \tag{3.28}$$

The controller gains G are given by

$$G = R^{-1}(B_2^T M + N_c^T) \tag{3.29}$$

such that M is a symmetric positive semidefinite matrix that satisfies the following ARE.

$$A_p^T M + M A_p - (B_2^T M + N_c^T)^T R^{-1} (B_2^T M + N_c^T) + Q = 0 \tag{3.30}$$

The computation of the H_2 compensator is simple given the plant defined by $P(s)$. It allows for a very general framework where the H_2 norm of an loop defined by $z(s)/w(s)$ can be minimized. This design methodology is an expansion of the LQR design method, thus many of its properties can be exploited. With the H_2 optimal compensator, the H_2 norm of the closed-loop system is computed by solving the Lyapunov equations discussed in section 3.2.1.

Chapter 4

SISO Design Studies

In this chapter, numerical studies are performed on simple SISO controlled flexible structures to verify the effectiveness of increasing passive damping to improve performance and robustness characteristics. Comparisons to the theoretical derivations from chapter 2 are made to validate the assumptions. Passive damping levels below 10% of critical are examined because it is easily obtainable without much added mass and complexity. Anderson et al. [1] showed that 6% average modal damping was achieved with about 15% added structural mass or about 10% of total mass for application to the MIT Interferometer Testbed. All examples make use of H_2 optimal control design to derive the necessary control law. Performance variables such as the H_2 norm, settling time, and control effort variance are examined for various amounts of passive damping. Robustness characteristics are computed based on uncertainty in a specific design variable. Stability and good performance bounds are derived for various amounts of damping. Good performance robustness is based on a no more that $\pm 5\%$ change in the nominal H_2 norm as a result of the uncertainty.

4.1 Two Mass System Example

The first system under investigation is a modally damped two mass system connected by a spring as shown in figure 4-1. The system has uncollocated sensors and actuators. This is a benchmark problem for the control of flexible structures originally proposed

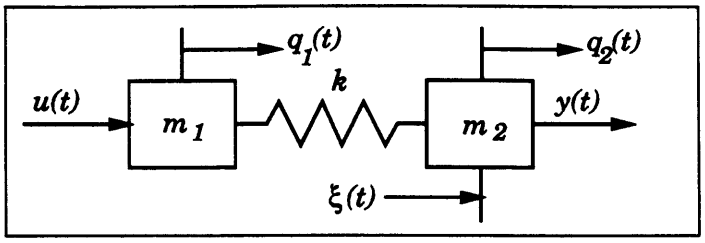

Figure 4-1: Two Mass System.

by Wie et al. [32]. It is the simplest of flexible structures containing one flexible mode. The objective of the control system is to reject disturbances on the second mass by applying forces on the first mass. A large uncertainty is assumed in the stiffness of the structure, resulting in uncertainty in the plant-pole locations. The performance and stability properties of the system as a result of trading off damping for stiffness are investigated. H_2 optimal control techniques are applied to develop a stabilizing controller.

4.1.1 Derivation of Structural Model

The two mass structure is modeled as two lumped masses of mass m connected by a flexible spring with a stiffness of k. The control force $u(t)$ acts on the first mass and position $y(t)$ of the second mass is measured. The equations of motion of the undamped system are given by the following matrix equations

$$M\ddot{q}(t) + Kq(t) = F_e u(t) + F_d \xi(t) \tag{4.1}$$

where the matrices are as follows.

$$M = \begin{bmatrix} m_1 & 0 \\ 0 & m_2 \end{bmatrix} \quad K = \begin{bmatrix} k & -k \\ -k & k \end{bmatrix} \tag{4.2}$$

$$F_e = \begin{bmatrix} 1 \\ 0 \end{bmatrix} \quad F_d = \begin{bmatrix} 0 \\ 1 \end{bmatrix} \tag{4.3}$$

The lumped masses under consideration are equal ($m_1 = m_2 = m$). In order to add modal damping to the system, it is transformed to a modal space. The eigensystem of the plant is given by

$$K\Phi = M\Phi\Lambda \quad \text{where} \quad \Phi^T M\Phi = I \tag{4.4}$$

where Λ is the eigenvalue matrix and Φ is the eigenvector matrix.

$$\Lambda = \begin{bmatrix} 0 & 0 \\ 0 & \frac{2k}{m} \end{bmatrix} \quad \Phi = \frac{1}{\sqrt{2m}} \begin{bmatrix} 1 & 1 \\ 1 & -1 \end{bmatrix} \tag{4.5}$$

The system consists of one rigid body mode and one mode with a natural frequency at $\omega_n = \sqrt{2k/m}$. The transformation $q(t) = \Phi\eta(t)$ is used to convert the plant from physical space to modal space where $\eta(t)$ is the modal displacement. The modal states are then used to derive the modal state space equations.

$$x(t) = \begin{bmatrix} \eta(t) \\ \dot{\eta}(t) \end{bmatrix} \tag{4.6}$$

The resulting modal state space equation of motion are as follows.

$$\dot{x}(t) = A_p x(t) + B_p u(t) + B_d \xi(t) \tag{4.7}$$

$$y(t) = C_p x(t) + \theta(t) \tag{4.8}$$

where the state matrices are

$$A_p = \begin{bmatrix} 0 & I \\ -\Lambda & -2\zeta\Lambda^{\frac{1}{2}} \end{bmatrix} \quad B_p = \begin{bmatrix} 0 \\ \Phi^T M^{-1} F_e \end{bmatrix} \quad B_d = \begin{bmatrix} 0 \\ \Phi^T M^{-1} F_d \end{bmatrix} \tag{4.9}$$

$$C_p = \begin{bmatrix} 0 & 1 & 0 & 0 \end{bmatrix} \begin{bmatrix} \Phi & 0 \\ 0 & \Phi \end{bmatrix} \tag{4.10}$$

The measurements of the system are given by $y(t)$, control effort by $u(t)$, sensor noise by $\theta(t)$, and disturbances by $\xi(t)$. Modal damping is defined by the damping ratio ζ.

In this design example, the effects on stability and performance robustness of the system are investigated as a result of presumed trade-offs between stiffness and modal damping. It is assumed that the addition of passive damping will require sacrifice in stiffness to maintain a constant mass.

$$\frac{\Delta k}{k_o} = \alpha\zeta \tag{4.11}$$

This penalizes larger values of damping. The drop in stiffness for increased damping is proportional to α as shown above where k_o is the nominal stiffness of the undamped plant.

$$k = k_o - \Delta k = k_o(1 - \alpha\zeta) \tag{4.12}$$

In this design example, the nominal system is given by

$$\begin{aligned} m_1 = m_2 &= 1\ kg \\ k_0 &= 1\ N/m \\ \zeta &= 0\ N\cdot s/m \end{aligned}$$

The plant has a natural frequency of $\omega_n = \sqrt{2}\ rad/sec$. The migrations of plant poles for increasing ζ and various values of α are shown in figure 4-2. No zeros are present in the undamped plant. The two poles at the origin result from the rigid body mode and the two off the origin are the result of the vibrational mode.

4.1.2 Unrobust H_2 Optimal Control Example

System Description

The first example investigates the advantages of passive damping on the two mass system with active vibration suppression. The system makes use of H_2 optimal control design to derive the necessary control law. Robustness issues are ignored in the

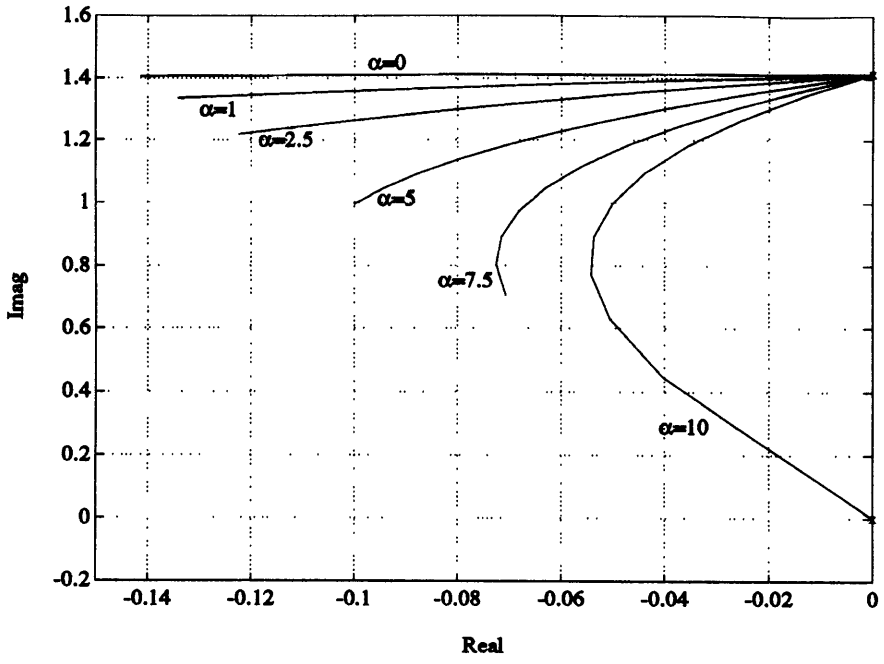

Figure 4-2: Migration of Plant Poles of Nominal Two Mass System for Increasing ζ and Various α.

control design. The intention is to develop a control system that can suppress within 15 seconds an impulse disturbance on the second mass by applying a force on the first mass. Changes in performance and stability levels as a result of increased modal damping are investigated. Uncertainty is assumed in the stiffness of the plant. Trade-offs between stiffness and damping are studied.

The system framework under investigation is shown in figure 3-2. Inputs to the system are disturbances $w_1(t)$ and sensor noises $w_2(t)$. It is assumed that sensor noises are small compared to disturbances allowing for good estimation. Outputs from the system are weighted effort $z_1(t)$ and weighted physical plant states $z_2(t)$. H_2 optimal control design as discussed in section 3.2.2 is used to compute the control design that minimizes the H_2 norm of $z(s)/w(s)$. The weights of the system are as follows.

$$W_d = 1$$

$$W_e = 1$$

$$W_s = 0.001$$

$$W_p = \begin{bmatrix} 0 & & & \\ & 1 & & \\ & & 0 & \\ & & & 1 \end{bmatrix} \begin{bmatrix} \Phi & 0 \\ 0 & \Phi \end{bmatrix}$$

Since it is only desired to eliminate disturbances on the second mass, weighting terms on the first mass states are set to zero. The plant state weighting matrix is multiplied by the plant eigenvectors to properly weight the physical states. The resulting weighted plant state representation is given by the following state equation.

$$\begin{bmatrix} \dot{x}(t) \\ z_1(t) \\ z_2(t) \\ y(t) \end{bmatrix} = \left[\begin{array}{c|ccc} A_p & B_d W_d & 0 & B_p \\ \hline 0 & 0 & 0 & W_e \\ W_p & 0 & 0 & 0 \\ C_p & 0 & W_s & 0 \end{array}\right] \begin{bmatrix} x(t) \\ w_1(t) \\ w_2(t) \\ u(t) \end{bmatrix} \tag{4.13}$$

Given the system framework and weighting, the two Riccati equation problem described in section 3.2.2 is used to compute the optimal H_2 compensator. The resulting compensator is of the same order as the plant. The computational framework for the investigation of the virtues of passive damping is simple. First the plant model is computed with modal damping values ζ. The stiffness to damping stiffness/damping trade-off ratio α is used to compute the plant stiffness. With the plant model computed, the weighted system is formed and the H_2 optimal control design algorithm is used to derive the optimal compensator. The engineering software package MATLAB was used to perform investigation. The package has control system design tools such as H_2 control design built in. Once the H_2 compensator is computed, the closed-loop system is formed and performance and stability levels are computed. For this investigation, performance measures included the H_2 norm and settling time as well as maximum deflection due to an impulse disturbance on the second mass. Control effort measured was based on the effort variance due to zero mean white noise disturbances. The variance is the deviation of effort from its mean value given the disturbances. See section A.2 for computation of effort variance.

Uncertainty was assumed in stiffness k. Upper and lower stability bounds of stiffness for increased damping were computed. Computations were performed for various trade-off ratios α. For the particular case of $\alpha = 1$, robust performance properties were computed. Changes in performance levels such as the H_2 norm and settling time were computed for various level of modal damping and uncertainties in stiffness.

Results

Results of the investigation using H_2 optimal control on the two mass system gave clear indication that passive damping greatly improves the stability robustness properties without much effect on nominal performance. Furthermore, vast improvements in performance robustness were obtained for increased damping.

The performance measure which the control design optimized was the H_2 norm between the weighted plant inputs and outputs. Figure 4-3 shows the changes in the H_2 norm for increased damping. The H_2 norm was normalized by dividing it by the H_2 norm of the undamped case. For small amounts of damping, performance levels remain relatively unchanged. But for increased damping, the performance levels are based on the trade-off ratio α. For low values of α (little stiffness lost in adding passive damping), damping improved performance due to the added passive vibration suppression, thus reducing the need for active vibration suppression. About a 20% improvement was achieved for 20% modal damping and $\alpha = 0$.

For high values of α, nominal closed-loop performance degraded for increased damping, but robustness continues to increase. This is due to the large drop in stiffness resulting from the high stiffness to damping trade-off ratio. This softens the link between the masses, decreasing its natural frequency and controllability. But for α less than 2.5, the H_2 norm of the closed-loop system did not degrade significantly.

Figure 4-4 shows the normalized variance of the effort as a result of white noise disturbances. For up to 4% modal damping, effort is decreased slightly for all values of α. Up to a 20% drop in effort is experienced for values of α less than 2.5. This is due to the fact that passive damping dissipates some of the vibrational energy, thus

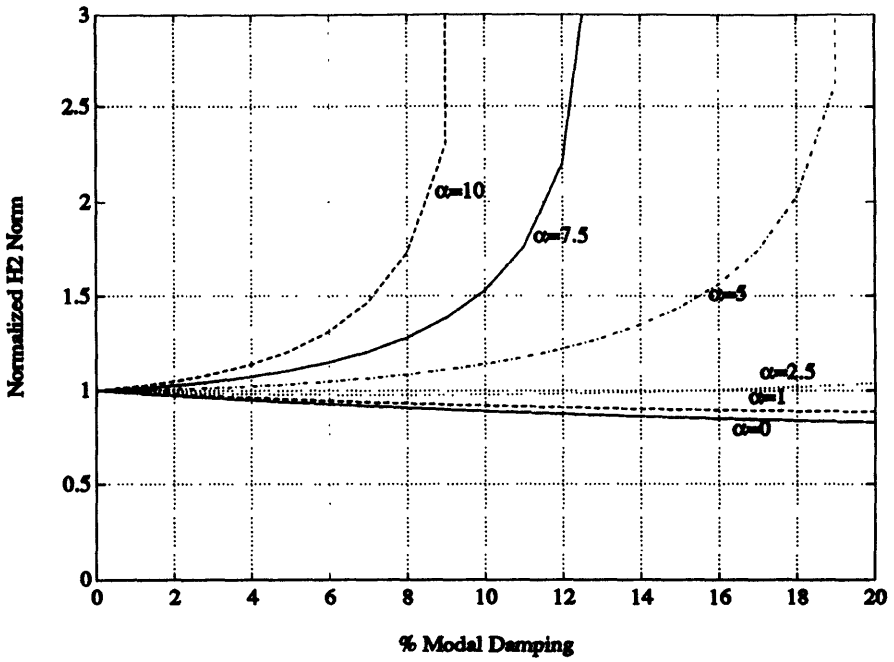

Figure 4-3: Normalized H_2 Norm of Nominal System for Increasing ζ and Various Levels of α.

reducing the effort of active vibration suppression. Obviously for high stiffness to damping trade-off ratios, the great drop in stiffness results in more effort needed to provide vibration suppression due to its high flexibility.

While the past two figures show changes in nominal performance levels for various values of modal damping, they are not realistic performance measures. Performance issues such as settling time and maximum deflection due to real disturbances provide a better understanding of actual performance issues. Figure 4-5 and 4-6 show the changes in settling time and maximum deflection given an impulse disturbance on the second mass. Again, all values are normalized by dividing them by the nominal value with no modal damping. These results are similar to that with the H_2 norm. For low damping, the settling time is not greatly affected. For low values of α and high damping, settling time drops off significantly. An almost 40% drop in settling time occurs with 20% modal damping with $\alpha = 0$. Again, high values of α show increased settling time due to the great trade-off in stiffness for damping. Similar results are experienced for the maximum deflection of the second mass.

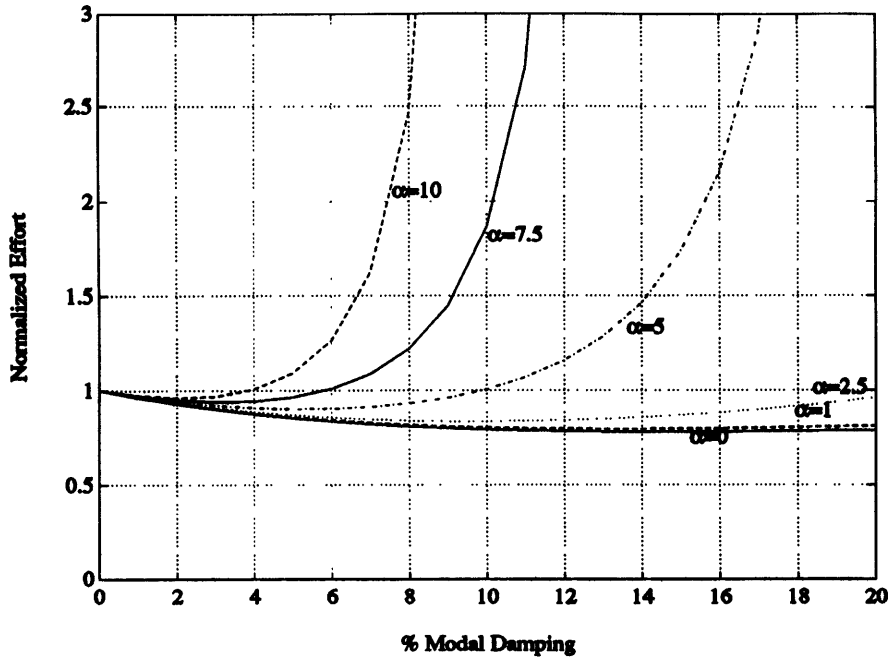

Figure 4-4: Normalized Effort Variance of Nominal System for Increasing ζ and Various Levels of α.

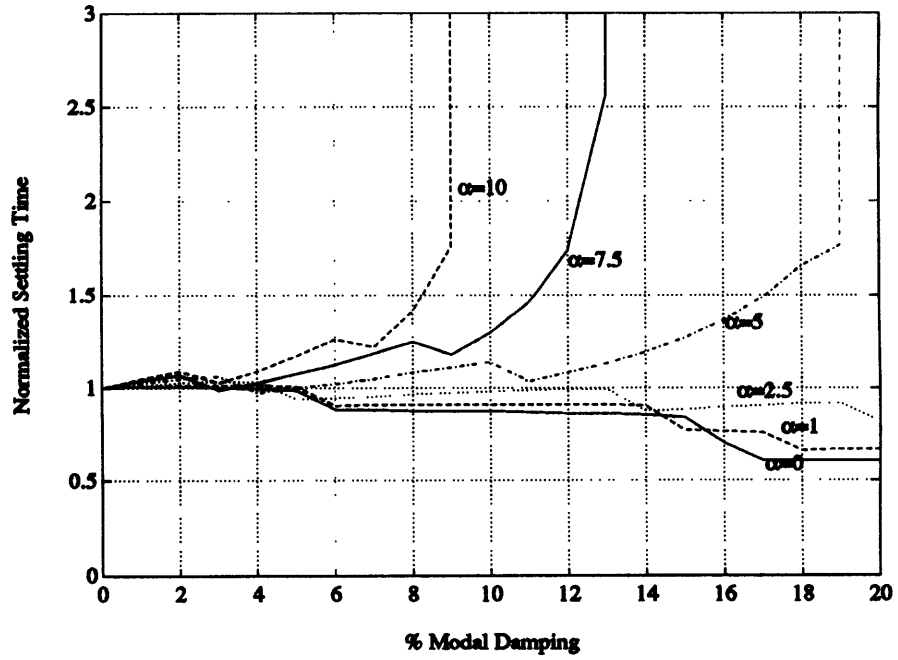

Figure 4-5: Normalized Settling Time of Nominal System for Increasing ζ and Various Levels of α.

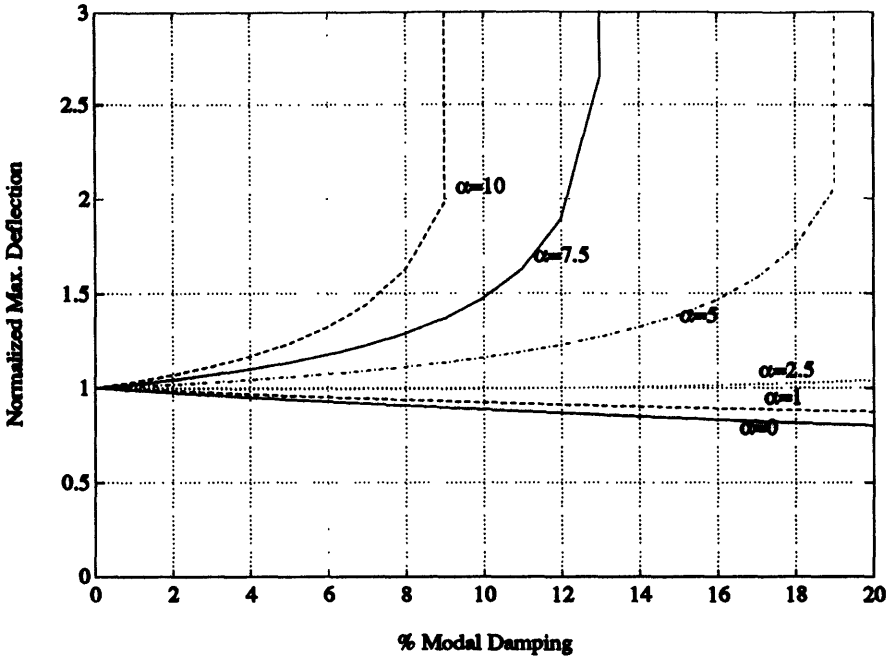

Figure 4-6: Normalized Maximum Deflection of Nominal System for Increasing ζ and Various Levels of α.

Even though passive damping did improve performance characteristics of the closed-loop system, not much improvement was gained. Thus why use passive damping if active damping can provide a good job? The next two figures show the main advantage of passive damping in a system using unrobust control design methods. Figures 4-7 and 4-8 show the upper and lower bounds in stiffness needed for the closed-loop system to remain stable. For the nominal system with no modal damping, there was no downward stability margin. But as modal damping increased, so did the stability margins. At about 8% modal damping, about an 8% lower margin in stiffness was acceptable for the system to remain robustly stable. For low values of α, the change in the lower stiffness bound changed linearly with modal damping at a rate of 1.1. This agrees with the results in chapter 2 where a linear relation between plant pole uncertainty and modal damping was observed.

On the upper stiffness bounds, even greater stability robustness properties were experienced for increased damping. With 10% modal damping, all the systems experienced infinite upward stability margins. With $\alpha = 0$, only 6% modal damping was

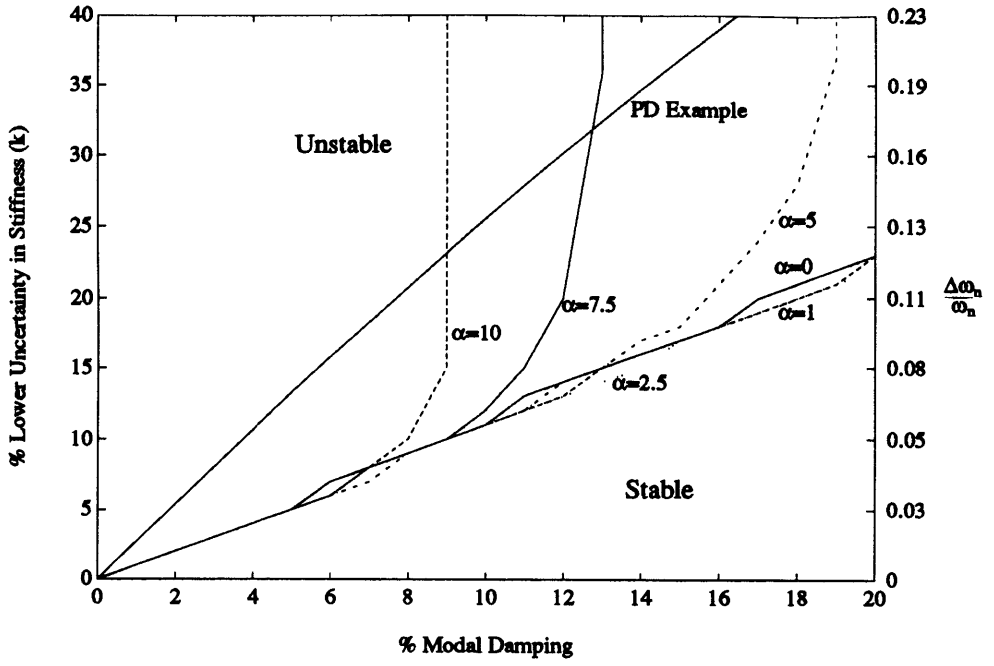

Figure 4-7: Lower Stiffness Bound for Stability for Increasing ζ and Various Levels of α.

needed to achieve infinite upper stiffness uncertainty.

These results provide clear evidence that increased passive damping on controlled structures results in some improvement in nominal performance characteristics, but greatly improves the stability robustness characteristics. With zero damping, no downward stiffness uncertainty was allowed for stability. The addition of damping greatly improved the stability robustness characteristics of the system.

In comparison to the results found in section 2.2.3. About 2.5 times more passive damping was needed to robustly stabilize the two mass system as compared to the single mode structure with PD control. This system used a higher order optimal compensator design based on the modeled system, thus more sensitive to modeled uncertainties. Still, a linear relationship between modeled uncertainty and passive damping was observed for $\alpha < 2.5$,

$$0.6\zeta \approx \frac{\Delta\omega_n}{\omega_n} \tag{4.14}$$

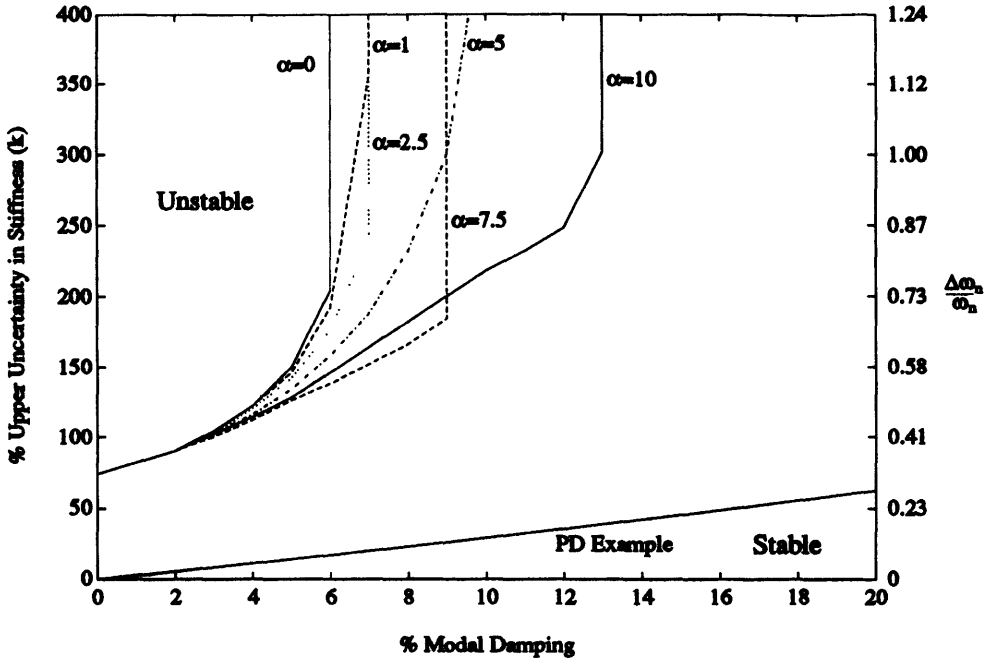

Figure 4-8: Upper Stiffness Bound for Stability for Increasing ζ and Various Levels of α.

where $\Delta\omega_n$ is the uncertainty in natural frequency.

The next examples show the performance robustness characteristics for various amounts of modal damping for the specific case of $\alpha = 1$. Figure 4-9 shows the values of the H_2 norm given a percent uncertainty in stiffness k and various amounts of modal damping ζ. For zero damping, there is no downward performance robustness due the fact the system goes unstable. But as damping increases, not only does the H_2 norm drops down slightly, but it maintains a broader performance level given the uncertainty in stiffness. With 16% modal damping, the H_2 norm remains relatively unchanged for even 15% downward stiffness uncertainty. This is a vast improvement over the case with zero modal damping.

Performance robustness improvements are also achieved using real performance levels such as settling time due to an impulse disturbance on the second mass as shown in figure 4-10. Even though settling time is not well maintained for low damping, it does provide a more robust system in comparison to the undamped case. High levels of damping provide significant maintainability in performance given uncertainty in

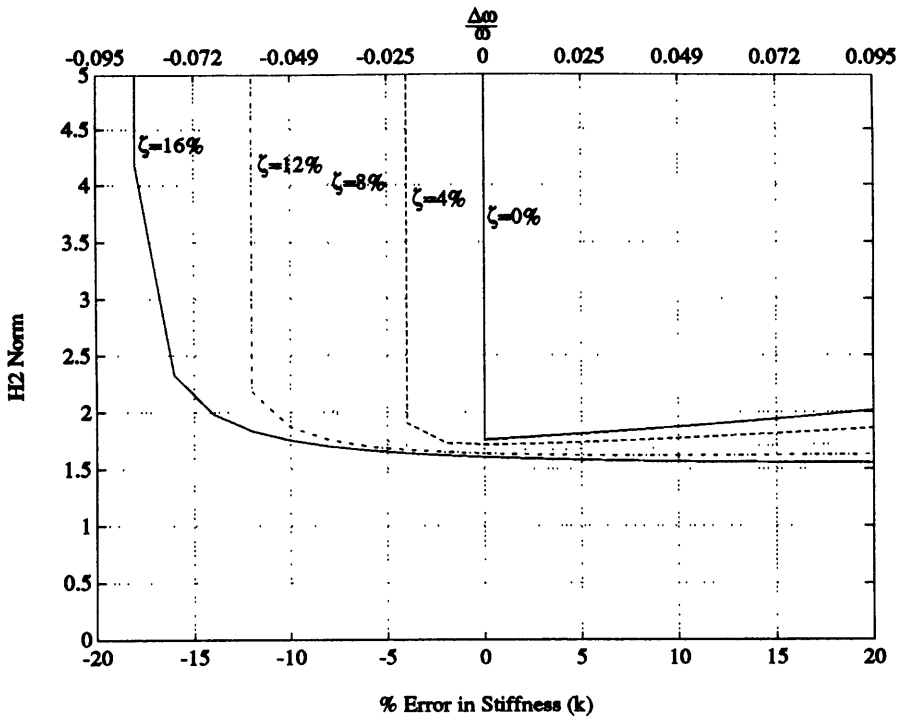

Figure 4-9: H_2 Norm Given an Error in Stiffness k ($\alpha = 1$).

stiffness, especially for upward stiffness uncertainty.

Figure 4-11 shows the motion of H_2 compensator poles and zeros as well as plant poles for increasing damping in the design model for $\alpha = 1$. For zero modal damping, compensator zero cancellation of plant poles is not achieved for the given weighted plant. But as damping increases, the compensator zeros move closer to the poles, providing better plant inversion resulting in improved performance. Thus passive damping improves stability and performance robustness characteristics of the plant allowing for improved plant inversion by the compensator, thus permitting higher bandwidth control.

The results presented show that the addition of passive damping to a simple structure improves the design of a controlled structure. Passive damping provides a method to easily dissipate vibrational energy which can cause the system to go unstable. Furthermore, by pushing the plant poles away from the imaginary axis, maintainability of stability and performance levels is improved given plant model uncertainty. With the increase in damping, also came a decrease in control effort resulting in systems with lower power requirement, smaller actuators, and less complexity than cases without

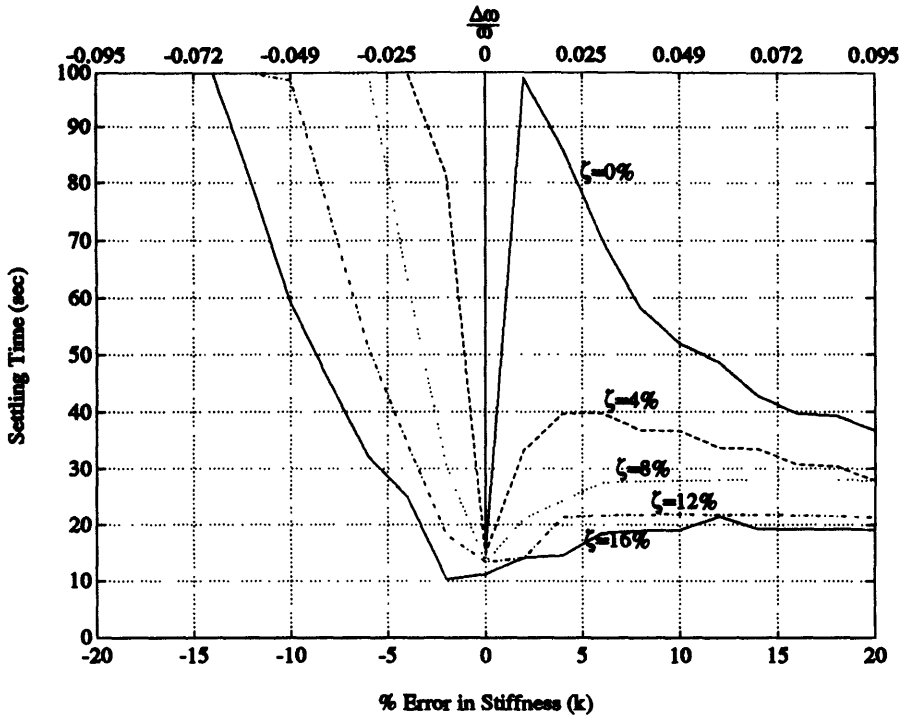

Figure 4-10: Settling Time Given an Error in Stiffness k ($\alpha = 1$).

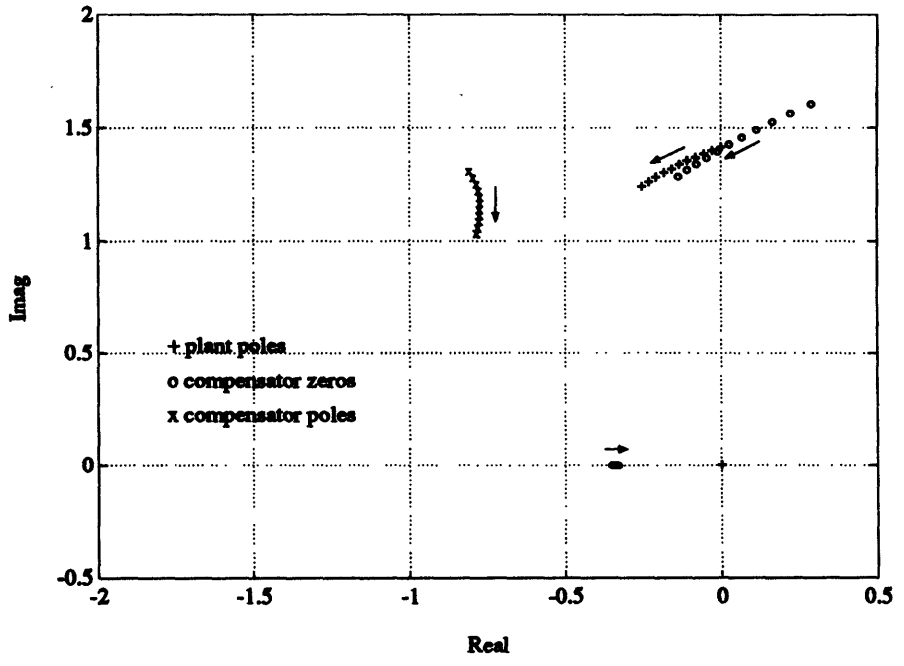

Figure 4-11: Migration of Plant Poles as well as Compensator Poles and Zeros for Increasing Damping ($\alpha = 1$).

passive damping.

4.1.3 Robust H_2 Optimal Control Example

The previous example examined the virtues of passive damping on unrobust control design. It clearly indicated that the addition of passive damping greatly enhances the stability robustness as well as the performance properties of the system. Furthermore, it improves the performance robustness properties of the system. This investigation examines the advantages of adding passive damping to uncertain systems with robust control design. Even with robust design techniques, passive damping is still advantageous since it helps in the reduction of control effort, improves on the robustness characteristics achieved, and allows higher robust performance.

Robust H_2 optimal control design is used to derive a controller for the two mass system. No direct methods exist for the computation of the robust controller. Instead, constrained non-linear optimization is used to determine the optimal control design variables to minimize the H_2 norm of the system. Constraints are placed such that the perturbed system as a result of the addition of the uncertainty is stable. Two cases are examined with $+100\%$ & -50% uncertainty and $\pm 10\%$ uncertainty in the plant stiffness. Trade-off studies between stiffness and modal damping are performed.

System Description

The system under investigation is similar to that in the previous section, except that sensor noise is completely ignored. The system framework is shown in figure 4-12. The controller used in this example is a third order compensator where the polynomial coefficients a_i were design variables.

$$K(s) = \frac{a_1(s+a_2)(s^2+a_3s+a_4)}{(s+a_5)(s^2+a_6s+a_7)} \tag{4.15}$$

The nonlinear optimization routine computes the optimal values of a_i such that it minimizes the H_2 norm of $z(s)/w(s)$ given the constraints that the perturbed system due to uncertainties in stiffness remains stable. To ensure the closed-loop system

settles in a reasonable amount of time, constraints are also placed on the closed-loop poles such that they are to the left of -0.15. This assures a settling time of about 20 seconds given impulse disturbances. The optimization objective is as follows

$$\min_{a_i} \left\| \frac{z(s)}{w(s)} \right\|_{H_2} \tag{4.16}$$

such that

$$\Re\{\lambda_i[A_{cl}(k)]\} < -0.15 \tag{4.17}$$

$$\Re\{\lambda_i[A_{cl}(k + \Delta k_1)]\} < 0 \tag{4.18}$$

$$\Re\{\lambda_i[A_{cl}(k - \Delta k_2)]\} < 0 \tag{4.19}$$

The upper bound on stiffness is given by Δk_1 and the lower bound by Δk_2. The weighting terms and uncertainty used in the example are as follows.

$$\begin{aligned}
W_d &= 1 \\
W_e &= 1 \\
W_p &= \begin{bmatrix} 0 & & & \\ & 1 & & \\ & & 0 & \\ & & & 1 \end{bmatrix} \begin{bmatrix} \Phi & 0 \\ 0 & \Phi \end{bmatrix} \\
\Delta k_1 &= 2k \\
\Delta k_2 &= 0.5k
\end{aligned}$$

The resulting weighted plant state representation is given by the following equation.

$$\begin{bmatrix} \dot{x}(t) \\ z_1(t) \\ z_2(t) \\ y(t) \end{bmatrix} = \left[\begin{array}{c|cc} A_p & B_d W_d & B_p \\ \hline 0 & 0 & W_e \\ W_p & 0 & 0 \\ C_p & 0 & 0 \end{array}\right] \begin{bmatrix} x(t) \\ w(t) \\ u(t) \end{bmatrix} \tag{4.20}$$

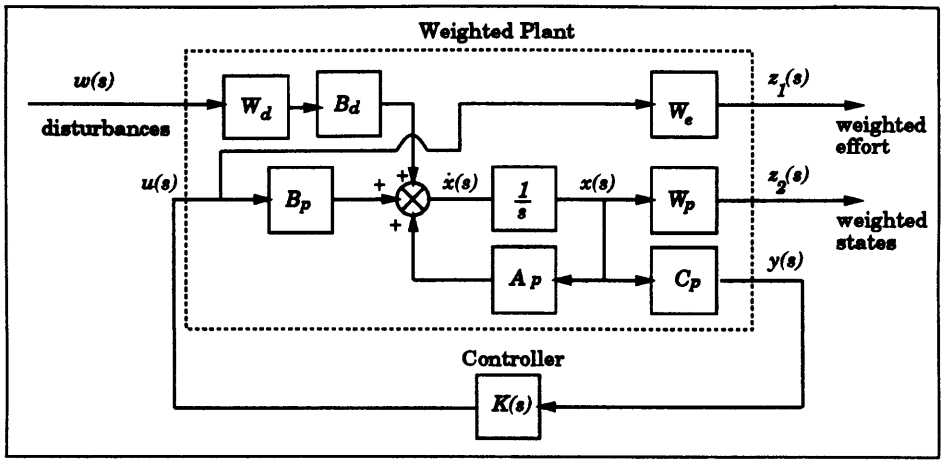

Figure 4-12: System Framework with Robust H_2 Control.

The initial compensator used for the optimization was a nonminimum phase robust controller design developed by Byun et al. [6] which met the robust stability requirements as shown in equation 4.21. Improvements in performance and stability were computed for various amounts of modal damping and values of α.

$$K(s) = \frac{0.9173(s + 0.15)(s^2 - 2s + 4)}{(s + 1.6)(s^2 + 2s + 4)} \tag{4.21}$$

The optimization toolbox in MATLAB [27] was used to perform the optimization process. The function CONSTR was used which was based on Sequential Quadratic Programming to minimize a nonlinear function given constraints.

Results

If robust control techniques can be used to provide reasonable performance with desired robustness characteristics, then why apply passive damping to a structure? The results presented indicate that improvements in performance characteristics as well as a drop in control effort result due to increased passive damping. This allows for lighter and higher performing control-structure systems than systems with only active vibration suppression. Furthermore, these results show further improvements on stability and performance robustness over the cases without passive damping.

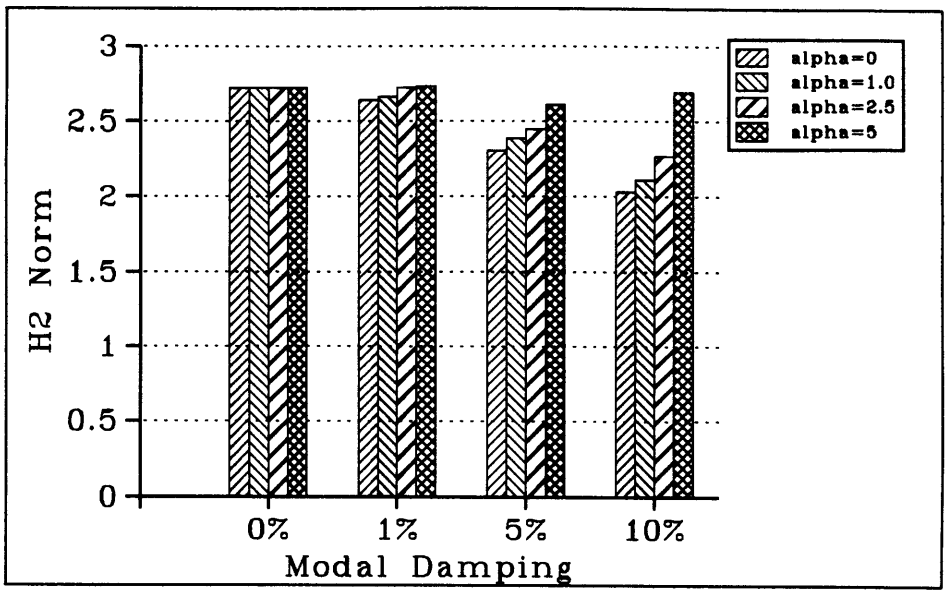

Figure 4-13: H_2 Norm of Nominal System for Various Amounts of Passive Damping.

Four structural designs were examined using 0%, 1% 5% and 10% modal damping as well as for different stiffness to damping trade-off ratios; $\alpha = 0$, $\alpha = 1$, $\alpha = 2.5$, and $\alpha = 5$. Performance measures included the H_2 norm of the weighted closed-loop system, settling time due to an impulse disturbance on the second mass, and effort variance due to white noise disturbance on the second mass. All the optimal systems hit the hard constraint of 50% downward stiffness uncertainty. Upper bounds on stiffness uncertainty were above the +100% constraint for all the cases.

Figure 4-13 shows the changes in the nominal performance index (H_2 norm) for increased passive damping. As damping increases, the H_2 norm dropped for all the cases. For the case $\alpha = 0$, there was a 25% drop in the nominal performance index using 10% damping, resulting in better vibration suppression. For the case with $\alpha = 5$, the performance index remained relatively the same due to the large drop in stiffness needed to maintain a constant mass design.

More realistic performance measures such as the settling time due to an impulse disturbance on the second mass are shown in figure 4-14. It shows no consistent change in performance was observed for increased modal damping. For the case of $\alpha = 0$, there was a 25% drop in settling time using 10% modal damping, but for

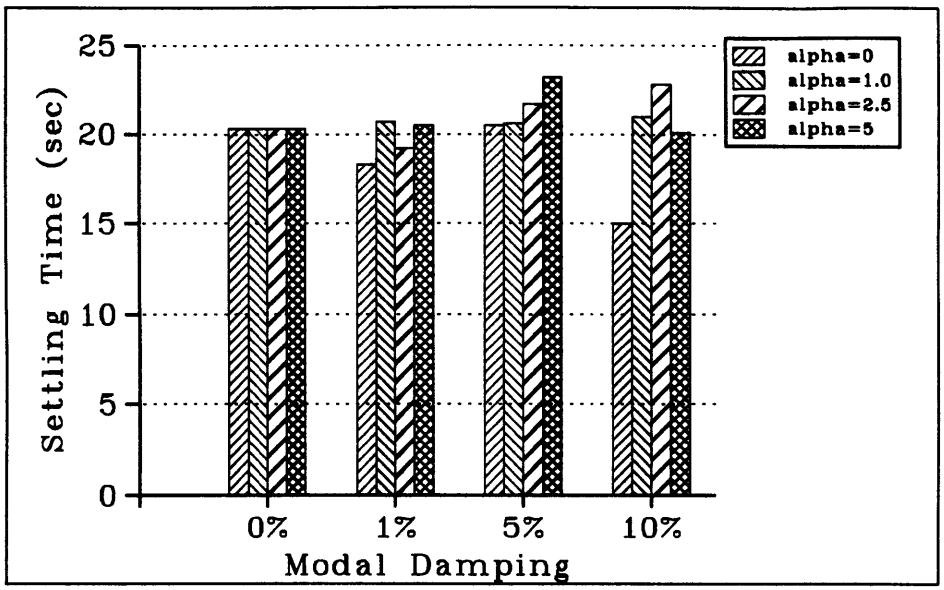

Figure 4-14: Settling Time due to Impulse Disturbance on Second Mass of Nominal System for Various Amounts of Passive Damping.

other values, the settling time increased slightly for increased modal damping. For the most part, the settling time remained about the same for all the cases.

On the other hand, there was an appreciable drop in variance of the effort due to white noise disturbances on the second mass as shown in figure 4-15. As much as a 50% drop in effort was experienced given 10% modal damping and $\alpha = 0$. For $\alpha \leq 2.5$, all the cases experienced a great drop in effort. For the case of $\alpha = 5$, effort remained relatively the same. Again, this is due to the large decrease in stiffness to maintain a constant mass design.

For all the cases investigated, the optimal designs hit the stability limit of 50% lower uncertainty bound on stiffness, but resulted in much higher than the 100% upper stiffness uncertainty bound as shown in figure 4-16. Almost all the cases showed improved upper stiffness uncertainty bounds for increased passive damping. For all the cases, uncertainty in stiffness beyond 1000% was experienced with 10% modal damping. The cases with $\alpha = 5$ tended to have smaller upper uncertainty bounds than the rest of the cases.

The performance robustness characteristics for increased damping and $\alpha = 1$ are

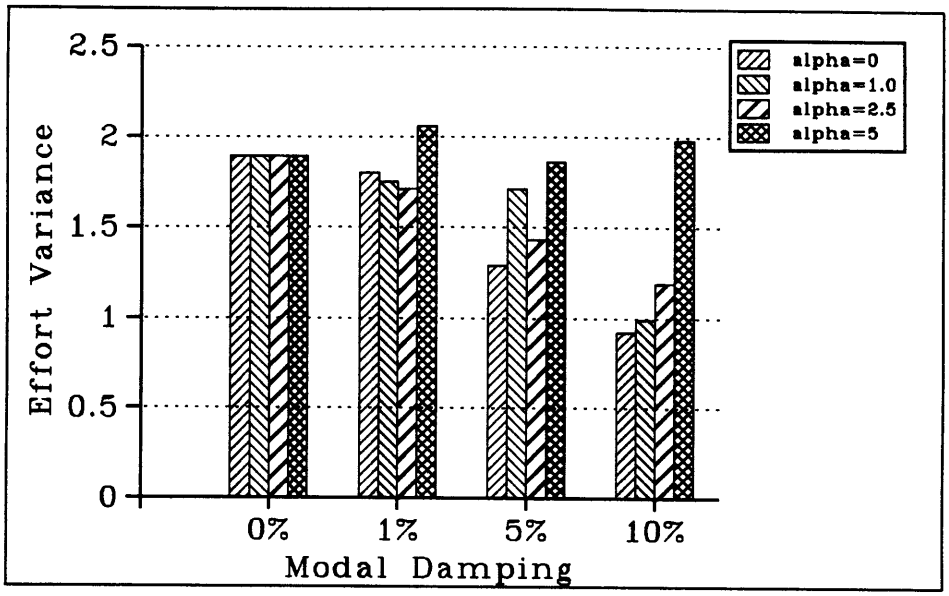

Figure 4-15: Variance of Effort of Nominal System for Various Amounts of Passive Damping.

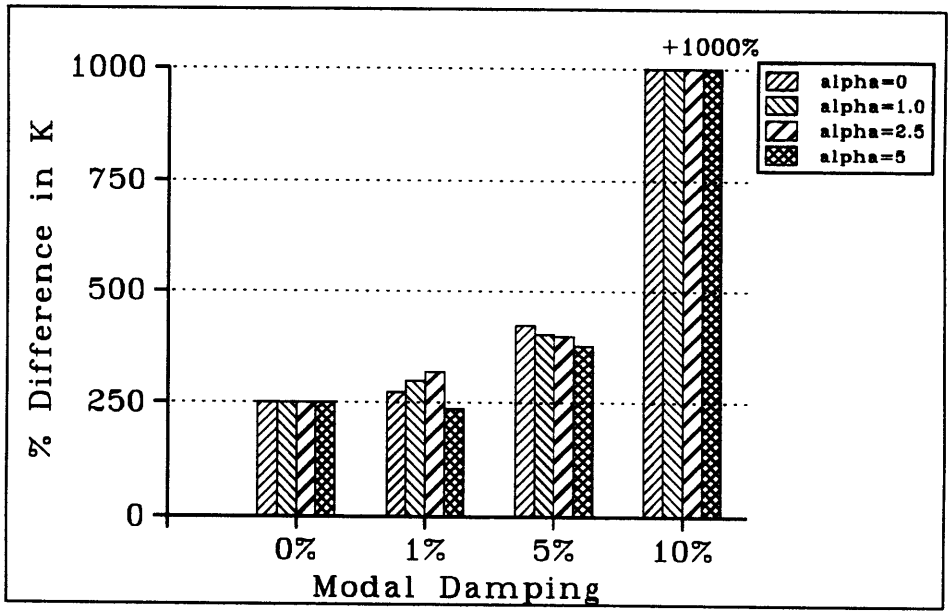

Figure 4-16: Upper Stiffness Uncertainty Bound of System for Various Amounts of Passive Damping.

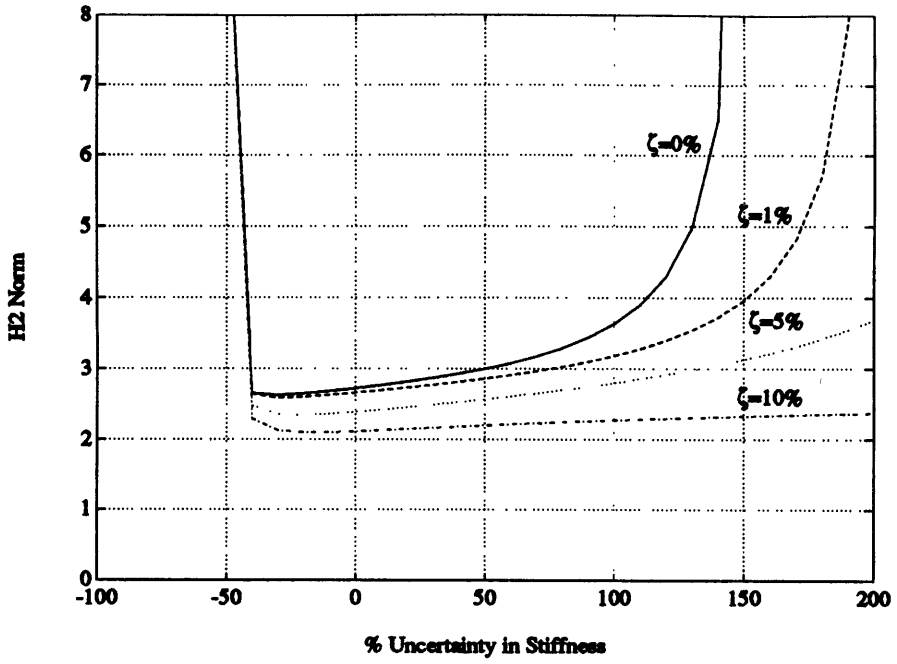

Figure 4-17: H_2 Norm Given an Error in Stiffness k ($\alpha = 1$).

shown in figures 4-17 and 4-18. As damping increases, the deviation of performance levels from the nominal case decreased given higher stiffness uncertainty. Because all the designs allowed up to a 50% decrease in stiffness, good performance was unachievable beyond that amount. But for increased stiffness uncertainty, stability and performance levels improved greatly for increased damping. With 10% modal damping, the performance level did not deviate much from the nominal design level with stiffness uncertainty values ranging from –40% to 200%.

The previous results used very high uncertainty levels in the plant model. For most designs, model uncertainty around $\pm 10\%$ is more realistic. The next few examples examine the results of decreasing the stiffness uncertainty bounds to $\pm 10\%$ compared to the first example with $+100\%$ & -50% uncertainty in stiffness. The particular case of $\alpha = 1$ was examined.

Figure 4-19 shows the difference in the H_2 norm of the two examples for different amounts of modal damping. Obviously, the case with $\pm 10\%$ uncertainty had much improved performance measure than the case with higher uncertainty. But as modal damping increased, the difference between the two decreased.

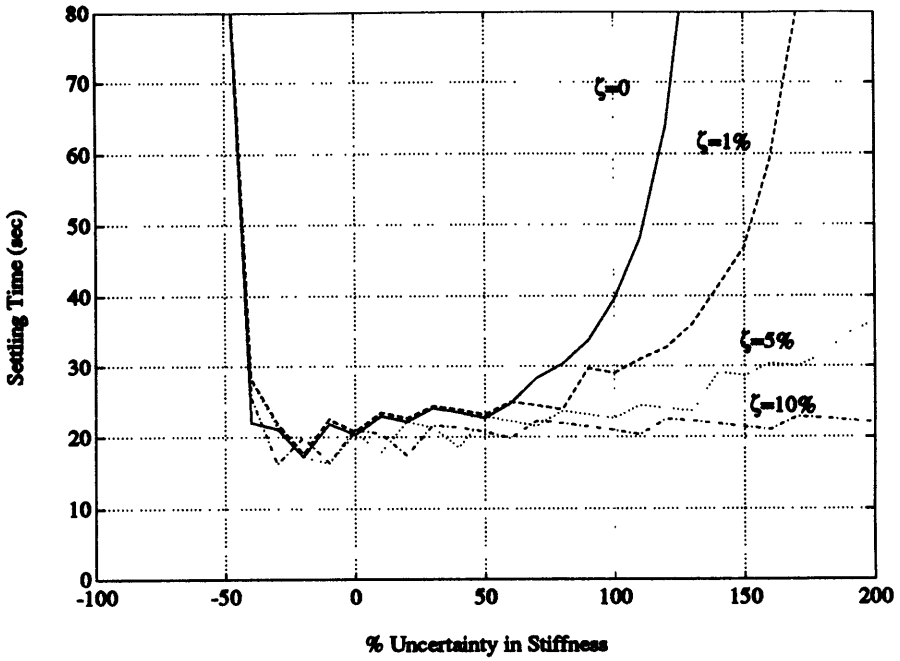

Figure 4-18: Settling Time Given an Error in Stiffness k ($\alpha = 1$).

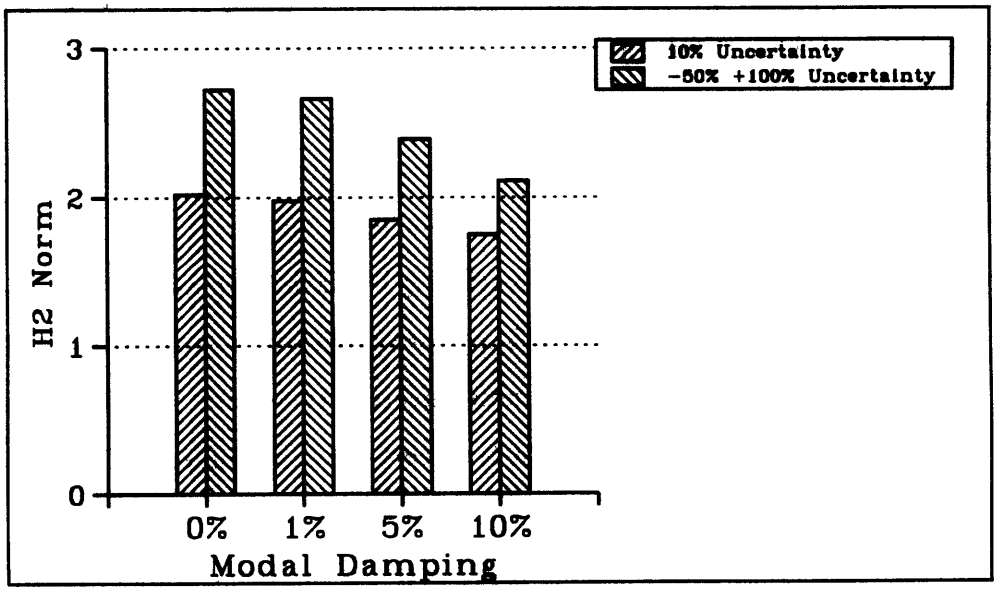

Figure 4-19: H_2 Norm of Nominal System for Various Amounts of Passive Damping and $\alpha = 1$.

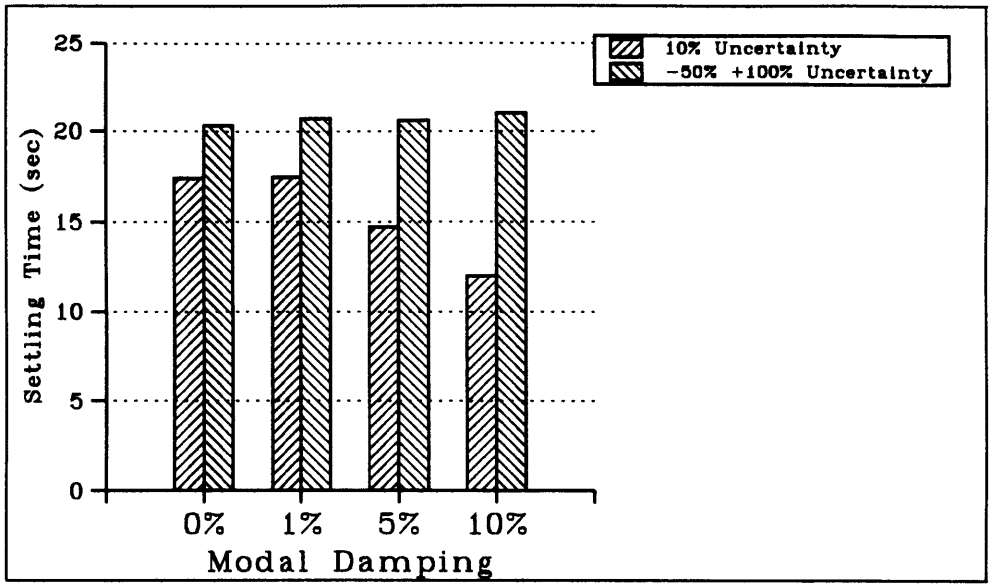

Figure 4-20: Settling Time due to Impulse Disturbances on Second Mass of Nominal System for Various Amounts of Passive Damping and $\alpha = 1$.

Using realistic performance measures such as the settling time due to an impulse disturbance on the second mass, different results than that of the H_2 norm resulted as shown is figure 4-20. As damping increased, so did the difference between the two cases. For the larger uncertainty case, the settling time remained constant, while the case with lower uncertainty bounds had a large decrease in settling time. Since the H_2 norm is composed of equal measures of both state and effort variables, the effort for the lower uncertainty case must not drop as much as compared against the case with higher uncertainty. This is observed in figure 4-21. Thus designs with large uncertainties need much effort to provide robust control. As damping increases, effort can greatly be reduced, thus lowering the H_2 norm. On the other hand, designs with smaller uncertainties, the addition of passive damping has more of an effect on reducing plant state deviation from zero, thus having a stronger effect on settling time.

Even though a lower bound of 10% stiffness uncertainty was placed on the second example, this constraint was not hit. Table 4-1 shows the percent allowable downward uncertainty in stiffness. As damping increased, so did the uncertainty bound. This is

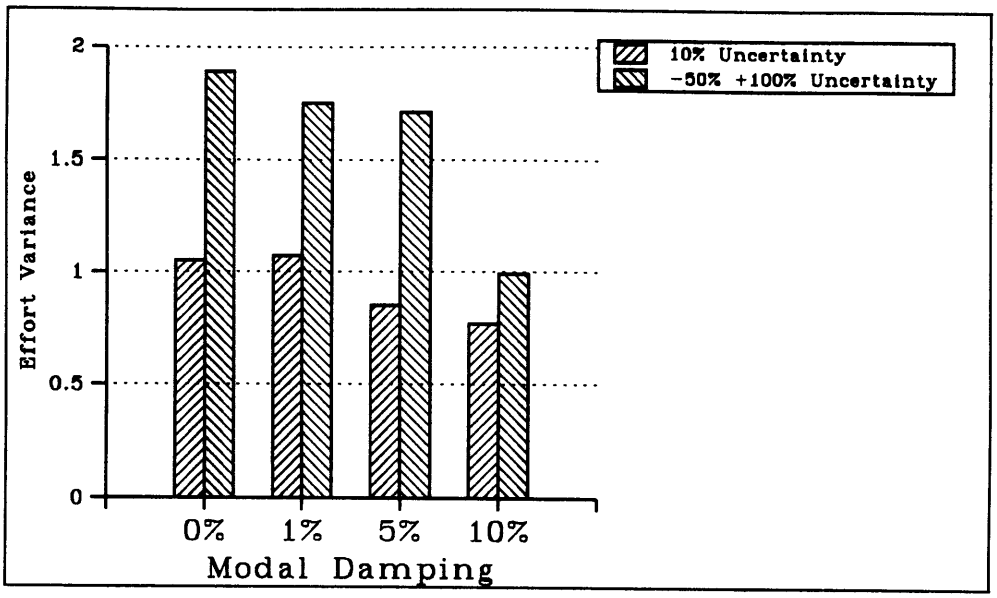

Figure 4-21: Effort Variance of Nominal Systems for Various Amounts of Passive Damping and $\alpha = 1$.

Modal Damping	Lower Stiffness Uncertainty Bound
$\zeta = 0$	12%
$\zeta = 0.01$	13%
$\zeta = 0.05$	15%
$\zeta = 0.1$	17%

Table 4-1: Lower Uncertainty Bound for Various Amounts of Passive Damping for the $\pm 10\%$ Uncertainty Case.

saying that uncertainty was not much of a design driver for this example. As damping increased, so did the upper stiffness uncertainty bound as shown in figure 4-22. At 10% modal damping, both systems had uncertainty bounds beyond 1000%.

The location of plant poles and compensator zeros for increased modal damping is shown in figures 4-23 and 4-24 for the $\pm 10\%$ and $+100\%$ & -50% stiffness uncertainty case respectively. As modal damping increased, the compensator zeros moved closer to the plant poles resulting in better plant inversion. Full plant inversion by the compensator is not achieved due to the high weighting on effort and the stability robustness constraints. For the lesser uncertainty case, the compensator zeros tended

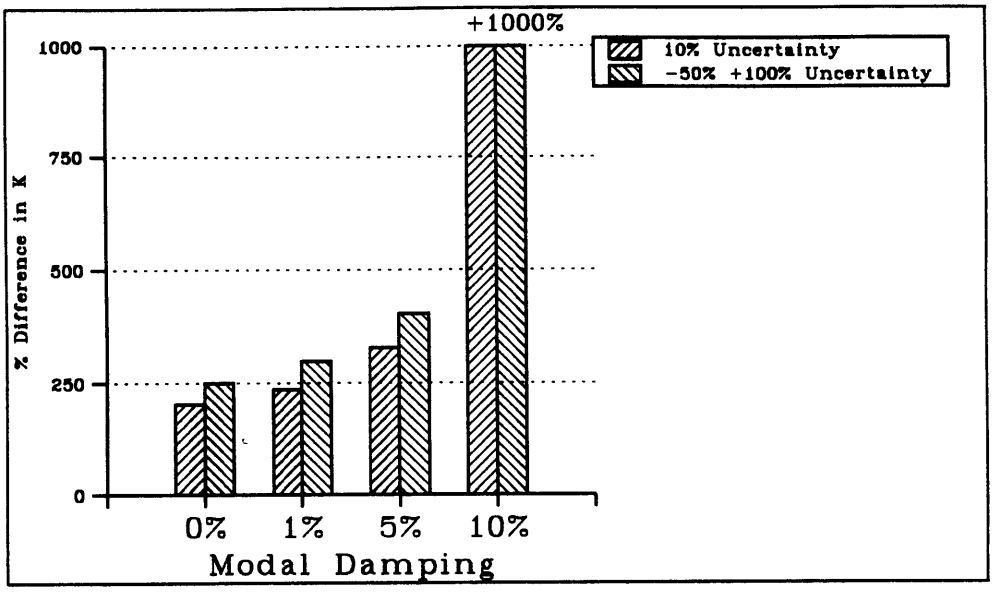

Figure 4-22: Upper Stiffness Uncertainty Stability Bound of Systems for Various Amount of Passive Damping and $\alpha = 1$.

to follow the nominal plant poles for increased damping. Note that the compensator zeros were below the plant poles preventing the root locus from crossing into the imaginary axis as discussed in section 2.2.2. For the higher uncertainty case, the zeros were far below the nominal plant poles. This shows that for robust systems, better plant inversion can be achieved by increasing the structural passive damping properties. This allows for higher bandwidth control while still maintaining desired stability robustness properties.

These results show that even for robust control synthesis, passive structural damping can be very useful. The addition of passive damping had some effect on improving performance, but greatly reduced the amount of effort necessary to control the structure. Furthermore it improved further on the stability robustness properties of the design and helped greatly in improving the performance robustness due to model uncertainty. Better plant inversion was also achieved allowing for higher bandwidth control.

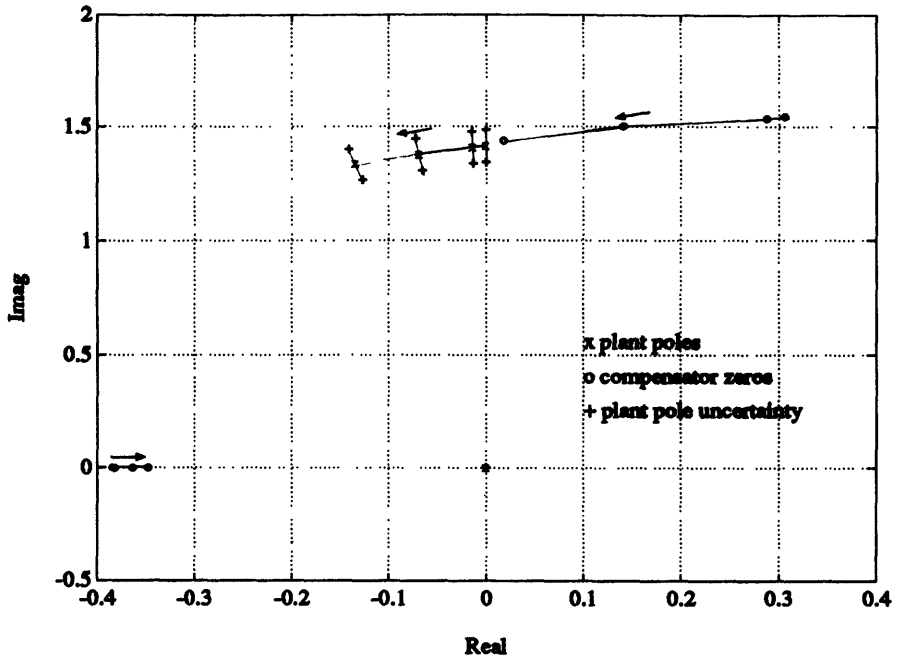

Figure 4-23: Migration of Plant Poles and Compensator Zeros for Increasing Damping ($\alpha = 1$ and $\pm 10\%$ stiffness uncertainty case).

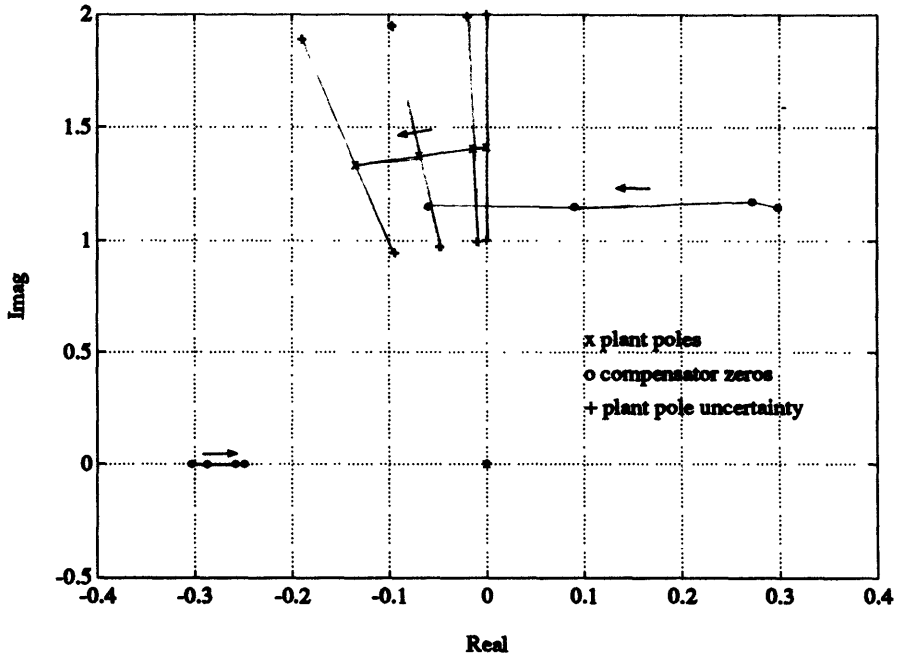

Figure 4-24: Migration of Plant Poles and Compensator Zeros for Increasing Damping ($\alpha = 1$ and $+100\%$ & -50% uncertainty case).

4.2 Four Disk Example

The next example problem investigates the virtues of passive damping on a more complicated structure consisting of four disks connected by flexible springs. The objective is to control the angular position of one of the disk by applying a force on an other disk given some uncertainty in the inertia in one of the disk. This system is based on an example problem originally examined by Rosenthal [29]. The structure uses a noncollocated pair of actuator and sensor. The structure is modeled as a fourth order system consisting of four lumped masses and three springs.

The actuator is placed such that it lies near the node of the second flexible mode. This results in a near pole-zero cancellation in the plant model. Essentially, the second mode is uncontrollable. The uncertainty in the plant model results in a pole-zero flip which makes it difficult to control near that frequency.

Improvements in control performance, stability robustness and performance robustness are investigated for various amounts of modal damping added to this system. Two examples are studied. The first example examines the advantages of passive damping on unrobust H_2 control on the four disk system. Comparisons between high bandwidth control incorporating the first structural mode and low bandwidth control with a closed-loop bandwidth ten times below the first structural mode are examined. The second example examines the advantages of passive damping with robust H_2 control.

4.2.1 Derivation of System Model

The system under investigation is a simple structure consisting of four disks connected by flexible springs with modal damping as shown in figure 4-25. The structure is made up of four disks of equal inertia J except for the first disk which is some fraction e of the inertia J. All springs are of equal stiffness k. Control torques $u(t)$ act on the second disk and the angular position $y(t)$ of the fourth disk is measured, resulting in a noncollocated sensor-actuator problem. Disturbances $\xi(t)$ act only on the second disk.

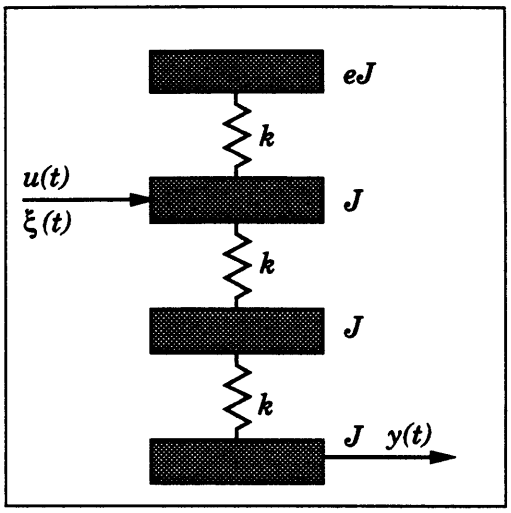

Figure 4-25: Four Disk System.

The equations of motion for the undamped structure are given by the following matrix equation

$$M\ddot{q}(t) + Kq(t) = F_e u(t) + F_d \xi(t) \tag{4.22}$$

where the matrices are as follows.

$$M = \begin{bmatrix} eJ & & & \\ & J & & \\ & & J & \\ & & & J \end{bmatrix} \quad K = k \begin{bmatrix} 1 & -1 & & \\ -1 & 2 & -1 & \\ & -1 & 2 & -1 \\ & & -1 & 1 \end{bmatrix} \quad F_e = F_d = \begin{bmatrix} 0 \\ 1 \\ 0 \\ 0 \end{bmatrix} \tag{4.23}$$

The vector $q(t)$ consists of the angular positions of each disk. Modal damping is added to the structure by converting it to modal space where Λ is the eigenvalue matrix and Φ is the eigenvector matrix. The eigenvectors are normalized such that $\Phi^T M \Phi = I$. A state space representation of the structure in modal space is used similar to that of the two mass problem (see equations 4.7) except for C_p which is modified to measure the angular position of the four disks.

$$C_p = \begin{bmatrix} 0 & 0 & 0 & 1 & 0 & 0 & 0 & 0 \end{bmatrix} \begin{bmatrix} \Phi & 0 \\ 0 & \Phi \end{bmatrix} \tag{4.24}$$

mode #	freq. (rad/sec)	description
1	0	rigid body mode
2	0.8999	1st flex. mode
3	1.6212	2nd flex. mode
4	2.0563	3rd flex. mode

Table 4-2: Natural Frequencies of Nominal Four Disk System

The nominal structure is composed of disks and springs with the following properties.

$$\begin{aligned} k &= 1 \ N \cdot m \\ J &= 1 \ N \cdot m^2 \\ e &= 0.375 \ \text{nominal} \\ \zeta &= 0 \ N \cdot m \cdot s \end{aligned}$$

The natural frequencies of the structure are described in table 4-2. Figure 4-26 shows the mode shapes of the nominal system. Notice that the actuator is placed at the location of a node of mode #3 resulting in a plant pole-zero cancellation.

An uncertainty exists in the inertia of the first disk which results in the actuator either being to the left or right of the node of mode #3. The uncertainty in the disk inertia is given by $0.25 \leq e \leq 0.5$. A nominal value of $e = 0.375$ is used to compute the controller. This uncertainty results in a pole-zero flip as shown in the pole-zero plots for the nominal and extreme uncertainty cases in figure 4-27. This uncertainty makes it impossible to control mode #3 because instability results due to the 180° phase difference between the modeled and unmodeled system at that natural frequency.

As shown in section 2.2.2, the addition of passive damping can greatly improve the control characteristics of the closed-loop system given a pole-zero mismatch. Given some desired phase margin $\delta\phi_m$ and a pole-zero mismatch of $\delta\omega$, equation 2.20 can be used to determine the amount of passive damping needed. The addition of passive damping pushes the plant poles to the left, allowing more margin for the root-locus

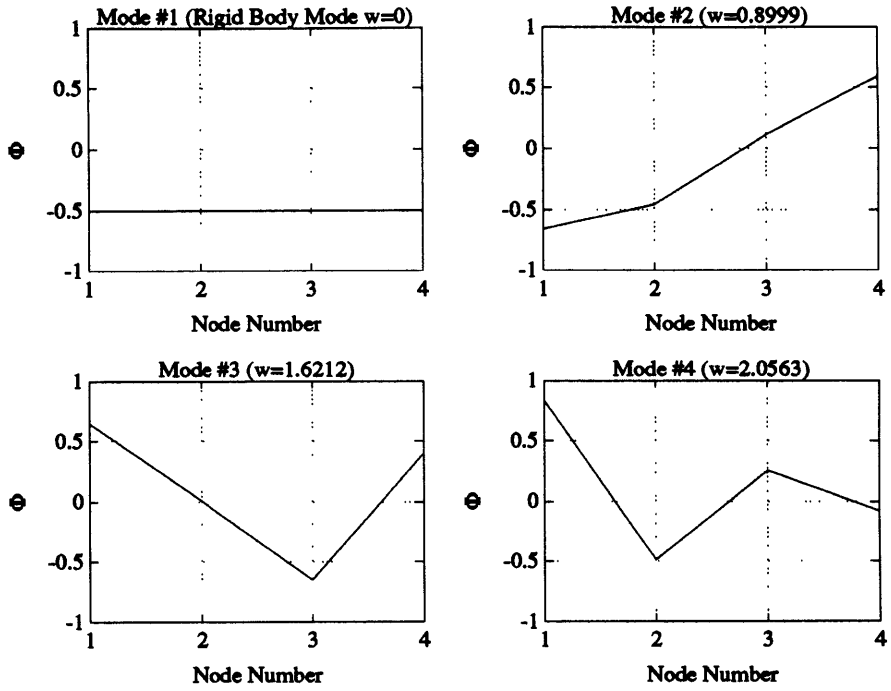

Figure 4-26: Mode Shapes of Nominal Four Disk System ($e = 0.375$).

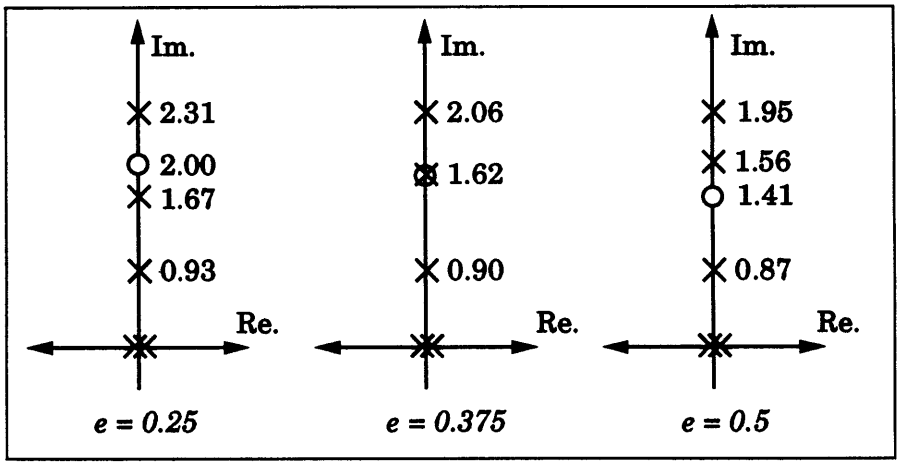

Figure 4-27: Pole-Zero Plot of Nominal and Extreme Uncertainty Cases.

of the poles to move around.

4.2.2 Unrobust H_2 Optimal Control

System Description

The advantages of adding passive damping to the four disk system with H_2 optimal control design techniques are examined. An appropriate control law is computed such that good command following of the fourth disk is achieved by applying an appropriate force on the second disk. Two control designs are examined. The first control design incorporates low bandwidth control such that it is ten times below the first structural natural frequency. This prevents large excitations of structural modes which can drive the system unstable. This example shows the advantages of passive damping on a gain stabilized system. The second control design incorporates high bandwidth control which encompasses the first structural mode and lies close to the second mode. Thus an accurate plant model is needed to assure plant dynamics do not drive the system unstable. This example shows the advantages of passive damping on a phase stabilized system. Performance and robustness characteristics for both systems are compared. Furthermore, no stiffness trade-off for added damping is performed.

The system framework is the same as that used in the two mass system (see figure 3-2). The following weights were used to derive the H_2 controller which minimized the H_2 norm of the weighted closed-loop system between disturbance and sensor noise inputs, and effort and plant state outputs. Robustness issues were ignored in the control design.

$$
\begin{aligned}
W_d &= 1 \\
W_s &= 0.1 \\
W_e &= 7 \quad \text{for low bandwidth control} \\
W_e &= 1 \quad \text{for high bandwidth control}
\end{aligned}
$$

	Closed-Loop Bandwidth (rad/sec)	Step Response Time (sec)
Low Bandwidth Control	0.08	37
High Bandwidth Control	1.2	16.7

Table 4-3: Properties of Four Disk System with Unrobust H_2 Control

$$W_p = \begin{bmatrix} 0.0001 \times I & \\ & I \end{bmatrix} \begin{bmatrix} \Phi & 0 \\ 0 & \Phi \end{bmatrix}$$

The resulting closed-loop systems had the following properties given the undamped four disk structure as described in table 4-3.

Changes in performance levels such as the H_2 norm of the weighted closed-loop system and step-response time for various amounts of damping were examined as well as effort variance due to white noise command input. An allowable uncertainty in the inertia of the first disk e to maintain stability and good performance was also computed. Good performance was based on the allowable uncertainty such that the performance measure (H_2 norm) did not change by more than 5%.

Results

Results of the investigation on the four disk system were similar to that of the two mass system. For both high and low bandwidth control, improved nominal performance as well as reduced control effort was achieved for increased modal damping. Furthermore, vast improvements in stability and performance robustness were achieved. While the lower bandwidth control system used a more conservative design, robustness issues were important for the undamped system.

The H_2 norm of the weighted closed-loop system for both low and high bandwidth control is shown in figure 4-28. Because of a lower weighting on the effort output, the high bandwidth control case was able to achieve a lower H_2 norm. As damping increased, the H_2 norm for both cases dropped. As much as a 35% decrease in

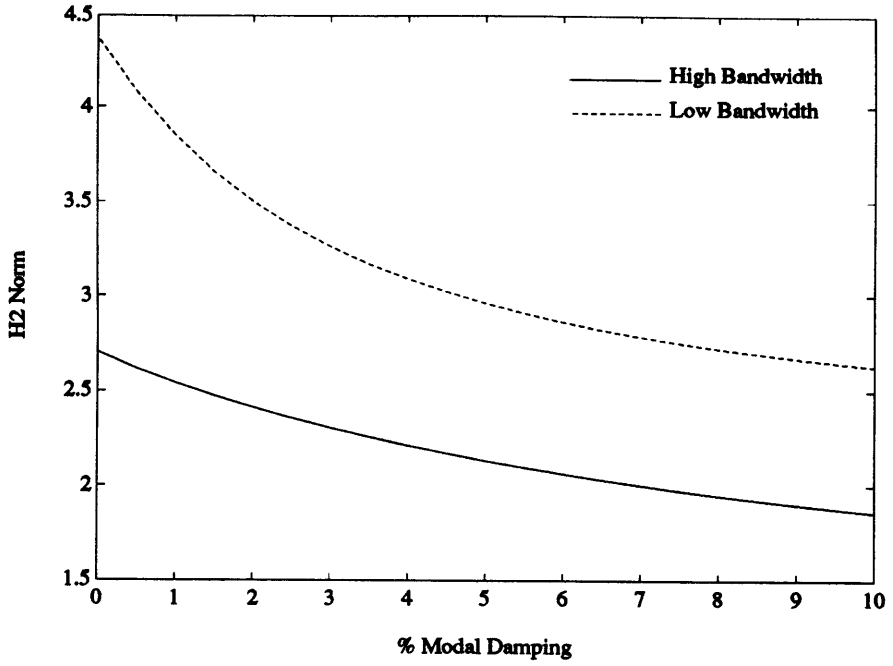

Figure 4-28: H_2 Norm of Nominal System for Various Amounts of Passive Damping.

the H_2 norm was achieved by increasing the amount of modal damping from 0% to 10%. This is due to the fact that passive damping absorbed some of the structural vibrational energy as a result of the control maneuver. Thus the need for active vibration suppression by the controller was reduced.

More realistic performance measures such as response time and maximum overshoot given a step command are shown in figures 4-29 and 4-30. While settling time decreased slightly given increased damping, a major reduction in overshoot was achieved for the high bandwidth case. For high bandwidth control, large structural vibrations occur, thus the addition of passive damping greatly helps reduce these vibrations. Since the low bandwidth case had a bandwidth ten times below the first structural mode, not much structural vibration occurred, thus the overshoot given a step command was small.

While performance characteristics showed modest improvement with increased modal damping, major reduction in effort was also achieved, especially for the high bandwidth case as shown in figure 4-31. The measurement of effort was based on the effort variance given white noise command signals. In order to achieve higher

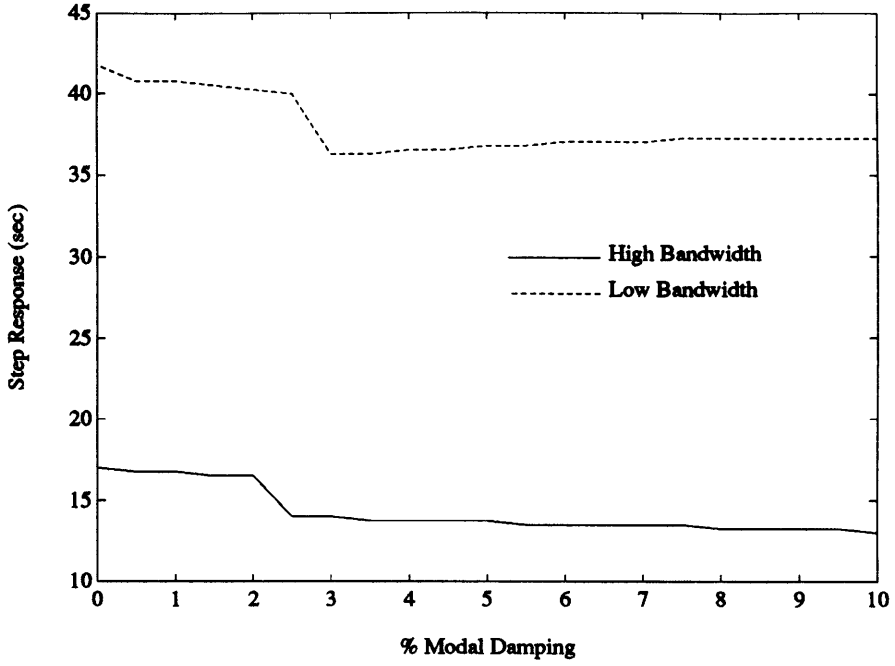

Figure 4-29: Response Time given a Step Command of Nominal System for Various Amounts of Passive Damping.

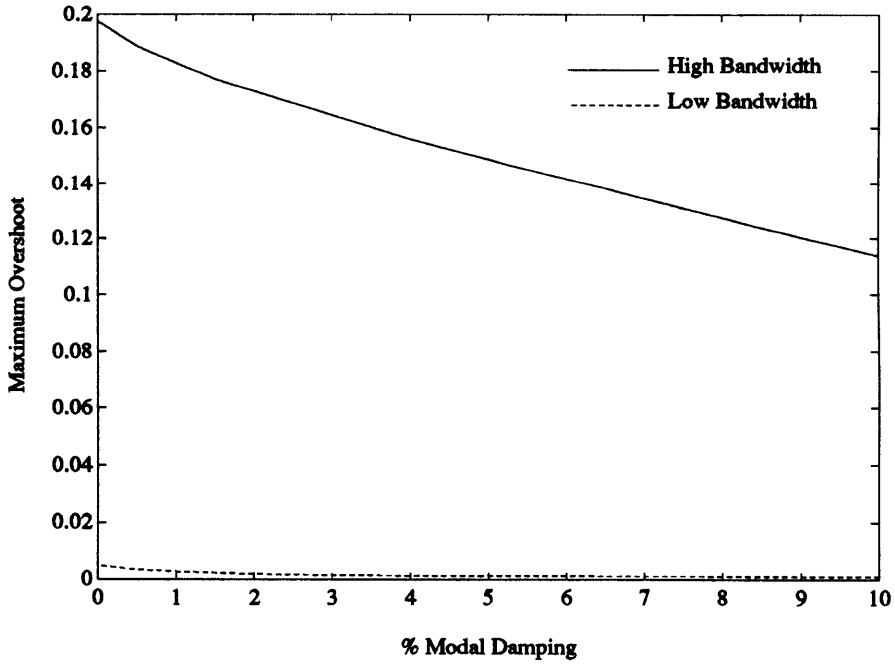

Figure 4-30: Maximum Overshoot of Nominal System given a Step Command of System for Various Amounts of Passive Damping.

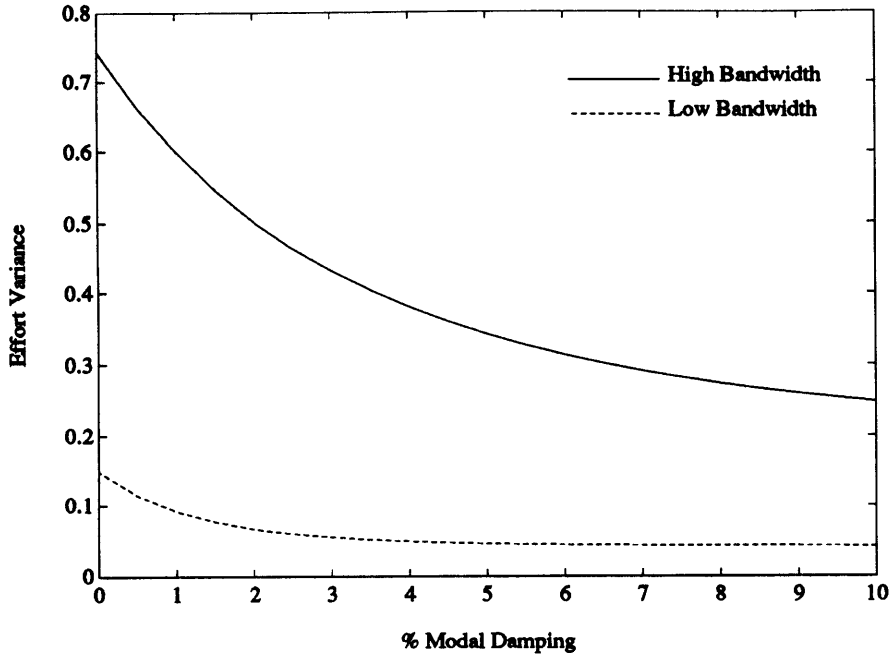

Figure 4-31: Effort Variance given White Noise Command Signal of Nominal Systems for Various Amounts of Passive Damping.

bandwidth, more effort was needed as shown in the figure. The addition of passive damping provided another source to reduce structural vibrations, reducing the burden for active vibration suppression by the control system.

The greatest benefits of the addition of passive damping came with increased performance and stability robustness properties of the structure given plant uncertainties. The allowable uncertainty in the inertia of the first disk e to maintain stability for various levels of modal damping is shown in figure 4-32. Because the low bandwidth control system was gain stabilized such as to not significantly excite the structural natural vibrations, it was more robust than the system with the high bandwidth controller. With little damping ($\zeta = 0.1\%$), the allowable uncertainty in e was about 5% for both cases. Thus model uncertainty played an important role in the stability properties of the low bandwidth control case. With just 0.7% modal damping, over a 100% uncertainty in e was allowed for the low bandwidth case. The high bandwidth case needed more damping to assure stability robustness. As much as 6% modal damping permitted 100% uncertainty in e to maintain stability.

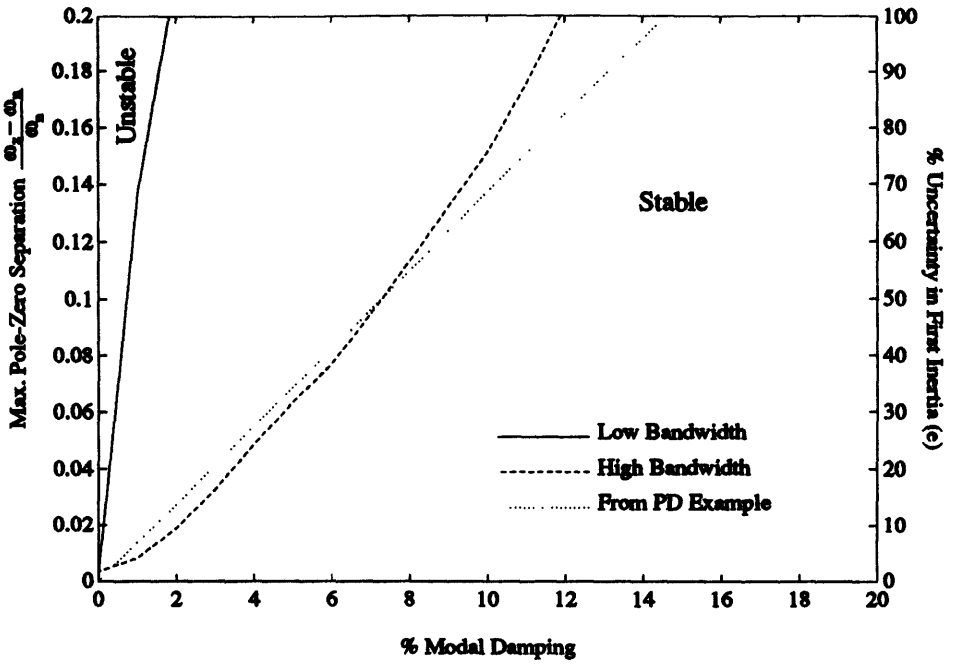

Figure 4-32: Plant Pole-Zero Mismatch and Allowable Uncertainty in Inertia of First Disk to Maintain Stability of System for Various Amounts of Passive Damping.

The results of the four disk system showed excellent correlation to the study performed on the single mode structure with PD control from section 2.2.3. The allowable uncertainty in plant pole-zero mismatch is given by

$$\frac{|\omega_z - \omega_n|}{\omega_n} = \text{ plant pole-zero mismatch} \tag{4.25}$$

where ω_z is the zero frequency and ω_n is the pole frequency match. From study on the single mode structure, a linear relationship between damping and plant pole-zero separation was established to guarantee stable control within the bandwidth of the structure (see figure 2-12). This provides evidence to the fact that there is a linear relationship between allowable uncertainty in plant pole-zero mismatch and modal damping to maintain stability.

The effects of performance robustness with increased passive damping were similar to that of the stability robustness case as shown in figure 4-33. In this example, performance robustness was based on the allowable uncertainty in e such that the

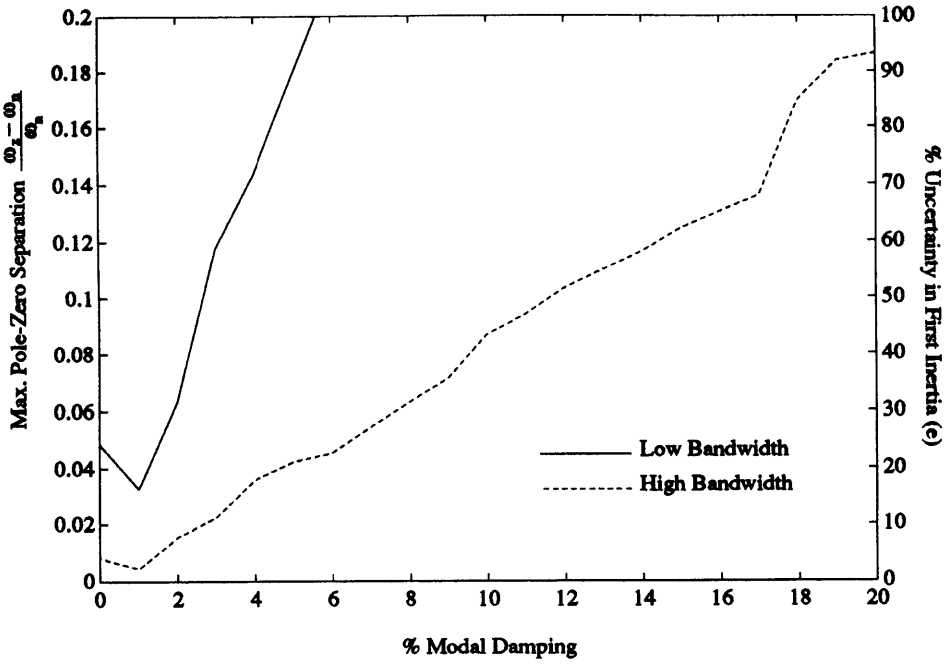

Figure 4-33: Plant Pole-Zero Mismatch and Allowable Uncertainty in Inertia of First Disk to Maintain Good Performance of System for Various Amounts of Passive Damping.

H_2 norm of the weighted system did not vary by more than 5%. To maintain good performance robustness, more damping was needed as compared with the stability robustness case. Again major gains in performance robustness was achieved with the addition of passive damping. Low bandwidth control again was less sensitive to uncertainties than high bandwidth control.

Even on more complicated systems such as the four disk example, major performance and robustness improvements were made with the addition of passive damping. This example shows that even for conservative control systems with closed-loop bandwidths ten times below the first structural mode, model uncertainty can still be destabilizing. Furthermore, uncontrollable modes resulting in a near pole-zero cancellation can be destabilizing if not modeled accurately or damped sufficiently. The uncertainty in the plant dynamics causes uncertainty in the pole-zero locations which can result in a pole-zero flip and destabilize the system. Passive damping provides an effective method to reduce the destabilizing structural vibrations and thus improve

performance, reduce effort, and improve robustness as the previous example show.

4.2.3 Robust H_2 Optimal Control

System Description

A similar investigation to that of the two mass system with robust H_2 control was performed on the four disk system. The objective was to determine the the controller $K(s)$ that minimized the H_2 norm of the system shown in figure 4-12. A fourth order compensator was used where the polynomial coefficients of its transfer function a_i were design variables.

$$K(s) = \frac{a_1 s^3 + a_2 s^2 + a_3 s + a_4}{s^4 + a_5 s^3 + a_6 s^2 + a_7 s + a_8} \tag{4.26}$$

Constraints were placed such that given an uncertainty in the inertia of the first disk, the system remained stable. Furthermore, a extra constraint was placed such that the closed-loop poles always remain to the left of $-5.4 \times 10^{-4}\ rad/sec$. This assured that closed-loop damping did not decrease from that of the initial case.

$$\text{optimization objective} \;=\; \min_{a_i} \left\| \frac{z(s)}{w(s)} \right\|_{H_2} \tag{4.27}$$

such that

$$\Re\{\lambda[A_{cl}(e)]\} \;\leq\; -5.4 \times 10^{-4} \tag{4.28}$$

$$\Re\{\lambda[A_{cl}(e + \Delta e)]\} \;\leq\; 0 \tag{4.29}$$

$$\Re\{\lambda[A_{cl}(e - \Delta e)]\} \;\leq\; 0 \tag{4.30}$$

The weighting terms and uncertainty used for this investigation were as follows.

$$W_d \;=\; 1$$

$$W_e \;=\; 1$$

$$W_p = \begin{bmatrix} 0 & & & & & & & \\ & 0 & & & & & & \\ & & 0 & & & & & \\ & & & 1 & & & & \\ & & & & 0 & & & \\ & & & & & 0 & & \\ & & & & & & 0 & \\ & & & & & & & 1 \end{bmatrix} \begin{bmatrix} \Phi & 0 \\ 0 & \Phi \end{bmatrix}$$

$$\Delta e = 0.175 \quad (\pm 47\%)$$

Since it was desired to control only the position of the first disk, weighting terms relating that state were set to one. The rest were set to zero. The initial compensator used for the optimization was the following nonminimum phase compensator which was robust given the disk inertia uncertainty.

$$K(s) = \frac{8.38s^3 - 0.955s^2 + 21.9s + 0.345}{s^4 + 37.3s^3 + 5.58s^2 + 97.6s + 5.21}$$

Again, the optimization toolbox for use with MATLAB was used to perform the constrained optimization.

Trade-offs of stiffness for passive damping were again studied where the amount of damping added resulted in a proportional drop in stiffness given by α as shown in equation 4.12. Performance and stability properties were investigated for various amounts of modal damping and stiffness to damping trade-off ratios α.

Results

Results of the investigation on the four disk system were similar to those of the two mass system. Again, the addition of modal damping showed improved nominal performance while maintaining stability given plant uncertainties. Better plant inversion by the compensator was achieved which allowed for higher bandwidth control. Furthermore, with increased damping came some improved performance robustness characteristics and a drop in effort variance. But peak effort given step commands increased greatly.

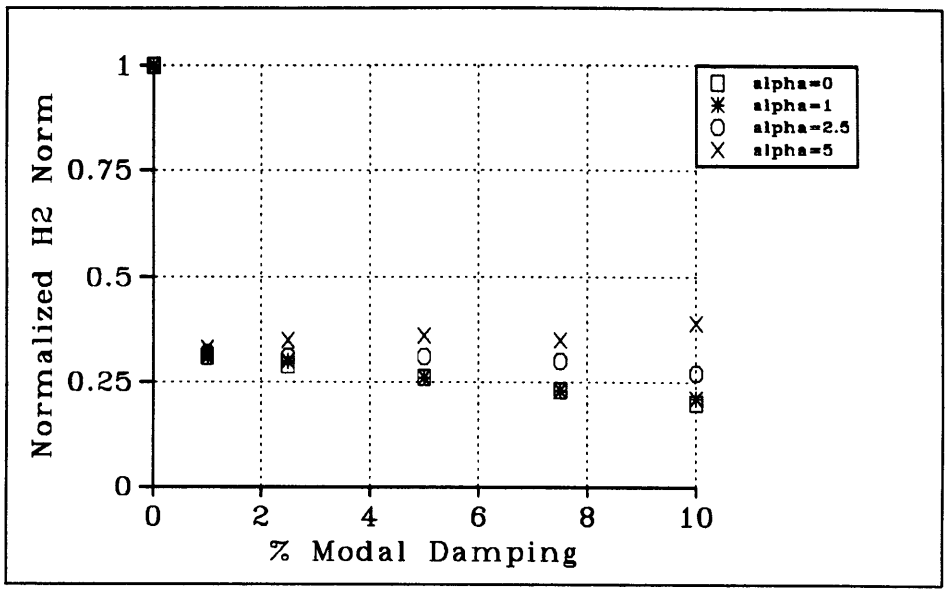

Figure 4-34: Normalized H_2 Norm of Nominal System for Various Amounts of Passive Damping.

As figure 4-34 shows, the addition of passive damping resulted in a significant drop in the nominal performance index (H_2 norm). The H_2 norm was normalized by dividing it with the value obtained for the undamped system. An almost 60% drop in the H_2 norm occurred with just the addition of 1% modal damping. The systems with low values of α showed some improved performance with increased modal damping, but not as significant as with the addition of just 1% damping.

Plots of the nominal response time given a step command also show similar results as shown in figure 4-35. An almost 90% drop in response time occurred with the addition of just 1% damping. Again, additional damping did not reduce the response time as much as compared with just 1% damping. This is due to the fact that the given weights used in the optimization resulted in a cheap control problem. Essentially, effort did not play a significant part in the H_2 norm, thus the addition of 1% passive damping was enough to allow good plant inversion by the compensator. Since only the third order compensator was used, full plant inversion was not possible. This is shown in figure 4-40 for the specific case of $\alpha = 1$.

The resulting plant inversion allowed for increased closed-loop bandwidth as shown

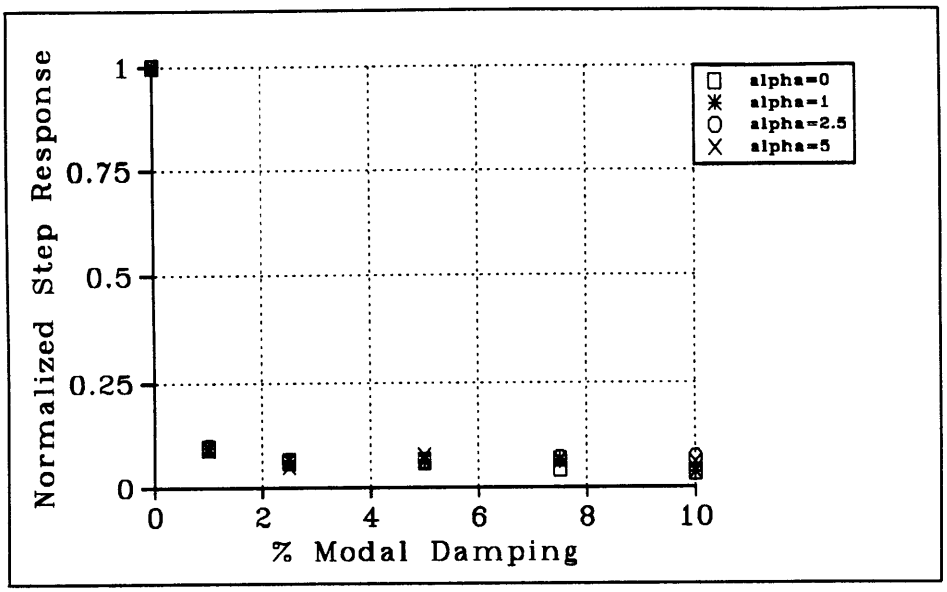

Figure 4-35: Normalized Step Response Time of Nominal System for Various Amounts of Passive Damping.

in figure 4-36. With just 1% damping, a 50% increase in bandwidth was achieved ($\omega_{bw} = 0.2121\ rad/sec$). This was 75% of the first structural natural frequency. Additional damping allowed for even higher bandwidth for low values of α. Notice that for $\alpha = 5$, more that a 300% increase in bandwidth was achieved over the nominal case with only 10% damping.

A drop in the variance of the effort due to stochastic white disturbances on the second disk was also achieved for increased modal damping as shown in figure 4-37. For most cases, the addition of damping resulted in a 75% drop in effort. Even though the variance dropped, the peak effort as a result of a step command increased greatly. Table 4-4 shows a great jump in the peak effort as a result of the addition of damping for the case of $\alpha = 1$. By adding damping, much higher nominal performance was achieved. To achieve better control, more effort was needed as shown in the table. Because cheap control weights were used, large increases in effort resulted.

For the specific case of $\alpha = 1$, improved step response occurred with the addition of passive damping which is shown in figure 4-38. Note the improved control with just the addition of 1% damping. The settling time as well as the overshoot decreased,

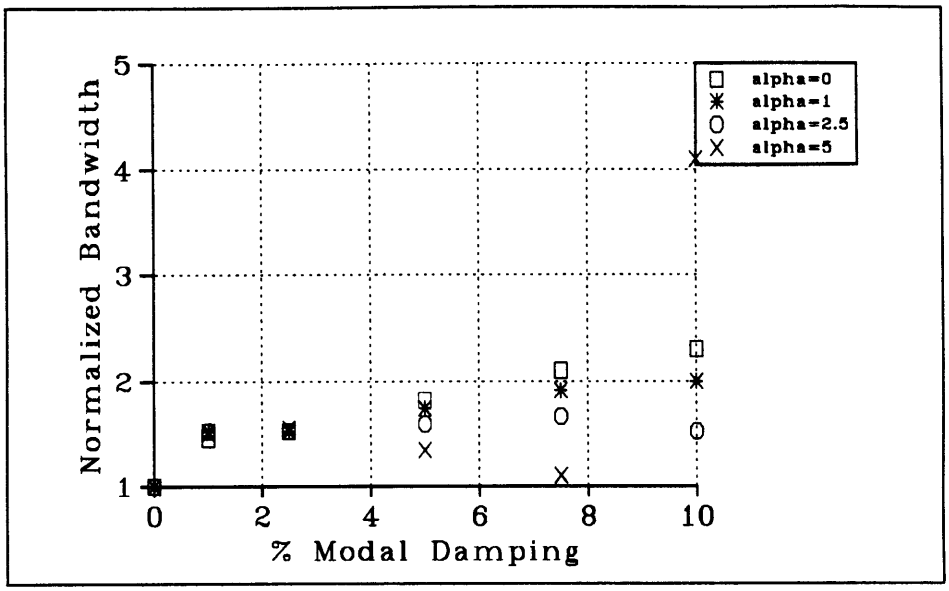

Figure 4-36: Normalized Closed-Loop Bandwidth of Nominal System for Various Amounts of Passive Damping.

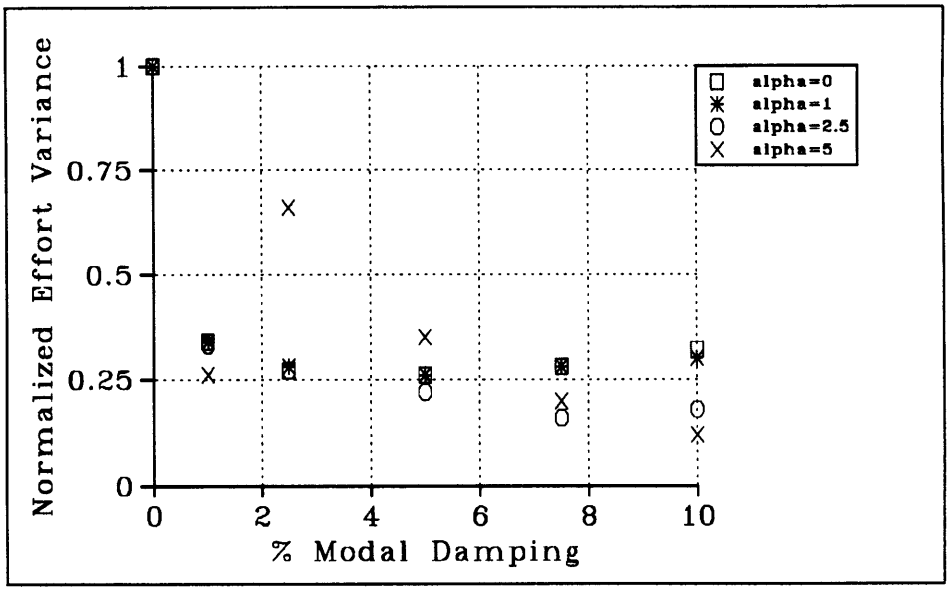

Figure 4-37: Normalized Effort Variance due to White Noise Disturbances on Second Disk of Nominal System for Various Amounts of Passive Damping.

Modal Damping	Peak Effort (N)
$\zeta = 0$	0.2180
$\zeta = 0.01$	153.2
$\zeta = 0.025$	171.0
$\zeta = 0.05$	206.8
$\zeta = 0.075$	150.3
$\zeta = 0.1$	144.5

Table 4-4: Peak Effort of Nominal System given a Step Command for Various Amounts of Passive Damping ($\alpha = 1$).

resulting in improved controlled plant. The closed-loop bode plot (figure 4-39) shows the improved frequency characteristics with the addition of passive damping. Again, increased damping showed improved bandwidth and decreases in the amplitude peaks at lower frequencies. Note that the high frequency peaks were not greatly reduced due to the fact that a third order compensator was used which did not allow full plant inversion.

The degree of plant inversion with increasing damping is shown in the pole-zero plot of the plant and compensator (see figure 4-40. The undamped case showed bad plant inversion by the compensator. The compensator zero laid near the second mode. But as damping increased to 1%, the compensator zero moved closer to the first plant pole. This resulted in better filtering of the first flexible mode achieving better control. Increased damping shows even better plant inversion.

The performance robustness characteristics of the four disk system for various levels of modal damping and a stiffness to damping trade-off ratio $\alpha = 1$ are shown in figures 4-41 and 4-42. For zero damping, very good performance robustness was achieved, but at the cost of poor performance. To remain stable given the plant uncertainty, the controller had a low cut-off frequency such that the plant looks rigid to the controller. The uncertainty in the inertia does not significantly change the rigid body dynamics of the plant, thus indicating good performance robustness characteristics for low cut off frequencies. For moderate damping values ($\zeta = 2.5\%$), good performance robustness was achieved as well as improved stability robustness. But

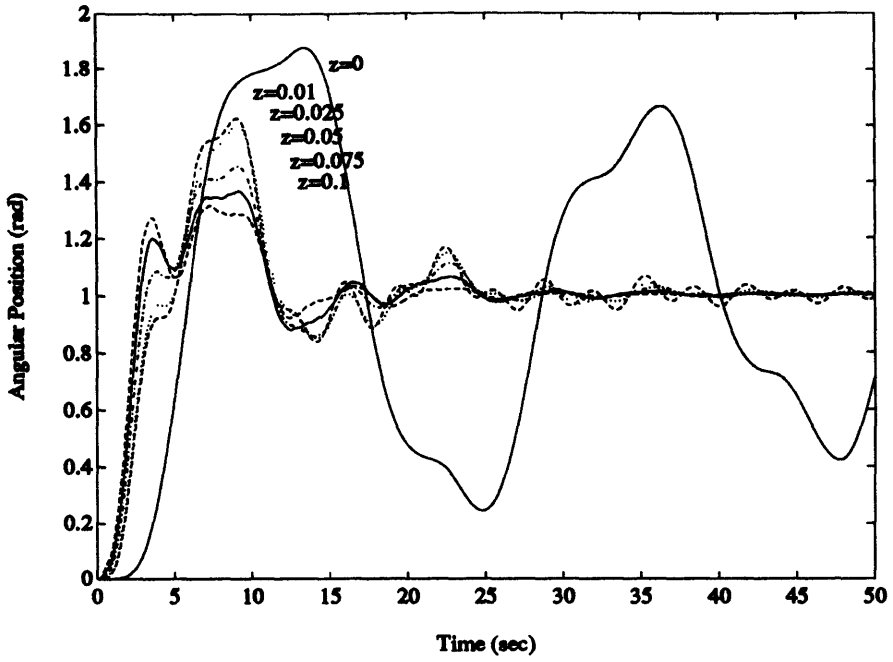

Figure 4-38: Step Response of Nominal System for Increasing Damping ($\alpha = 1$).

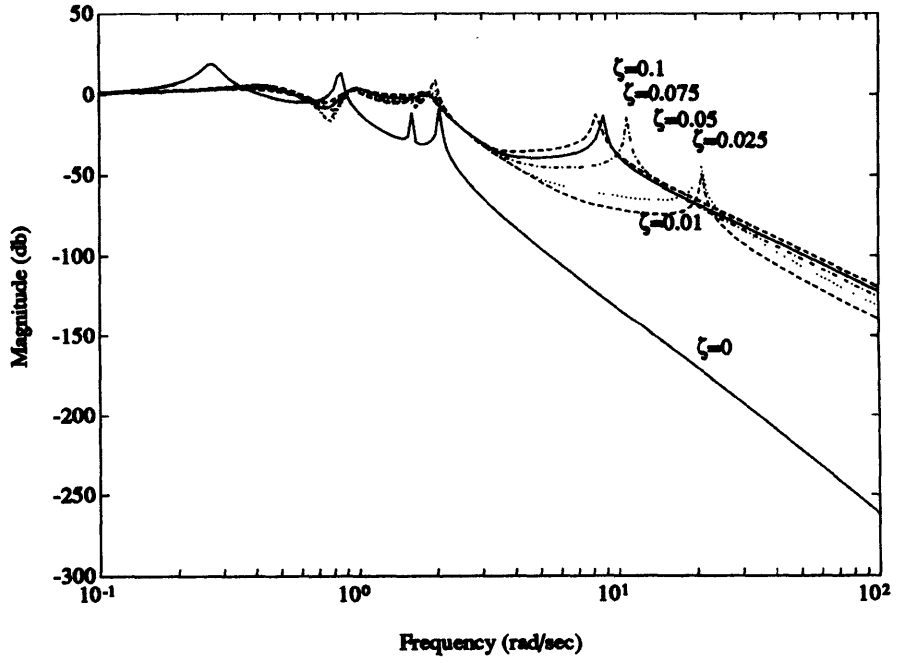

Figure 4-39: Closed-Loop Control Bode Plot of Nominal System for Increasing Damping ($\alpha = 1$).

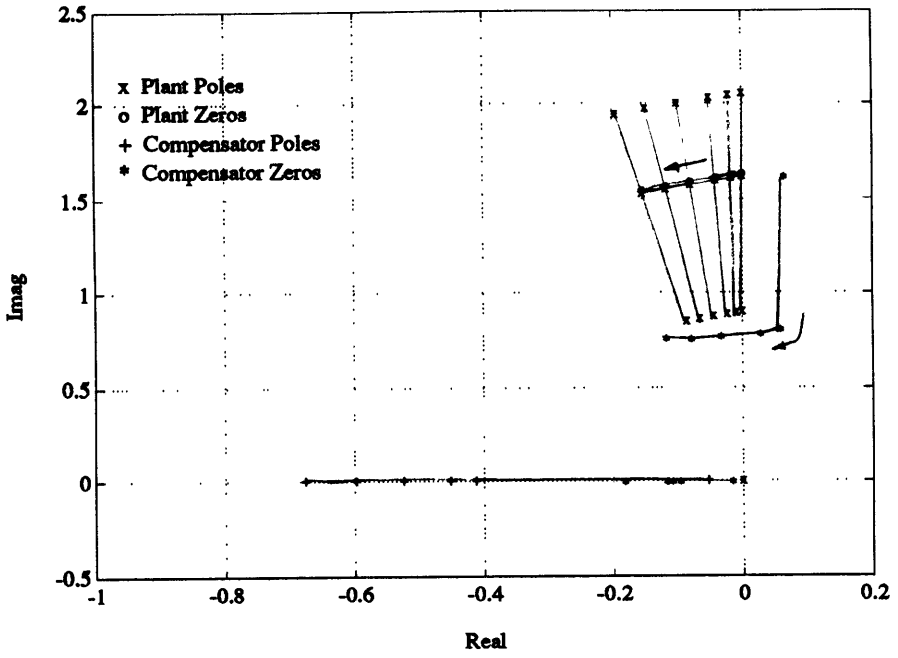

Figure 4-40: Migration of Plant Pole-Zeros and H_2 Compensator Pole-Zeros for Increasing Damping ($\alpha = 1$).

higher damping resulted in a drop-off in the performance robustness characteristics, probably due to the drop in stiffness associated with increased damping.

These results further show the virtues of passive damping for more complicated system. The addition of passive damping pushes the plant poles to the left, providing more room for the root locus of the poles to move around in a stable manner. This is especially important when a plant pole-zero flip exists due to plant uncertainty. As shown in section 2.2.2, when the pole lies below the zero, its root locus goes into the right hand plane if no damping exists, thus high bandwidth control is very difficult. The addition of just 1% modal damping allowed for the poles to migrate to the zero in a stable fashion, thus allowing better plant inversion and improved control. But at the cost of an increase in peak effort given a step command input. Furthermore, for moderate levels of modal damping, improved stability and performance robustness characteristics were achieved.

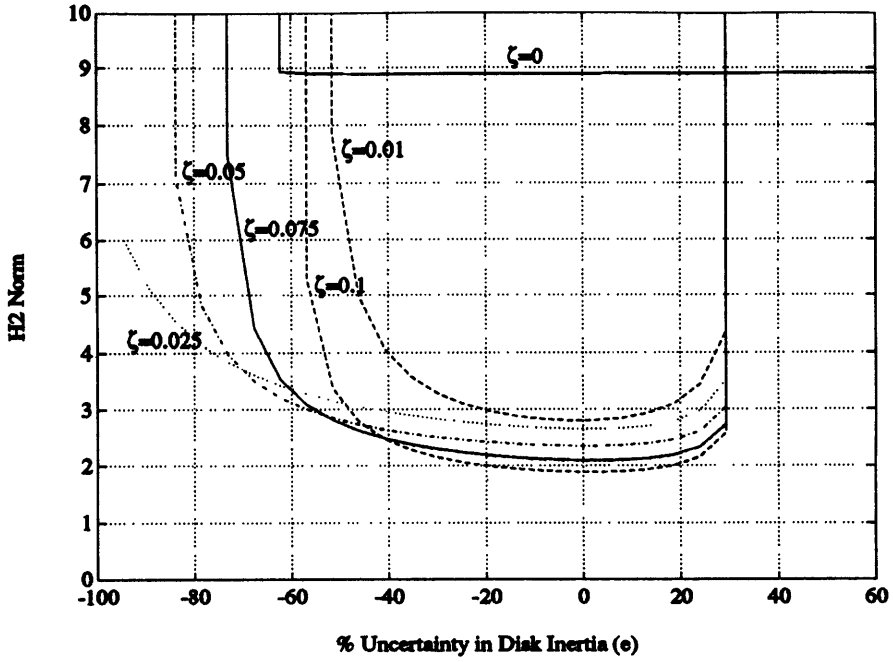

Figure 4-41: H_2 Norm Given an Uncertainty in Inertia of 1st Disk e ($\alpha = 1$).

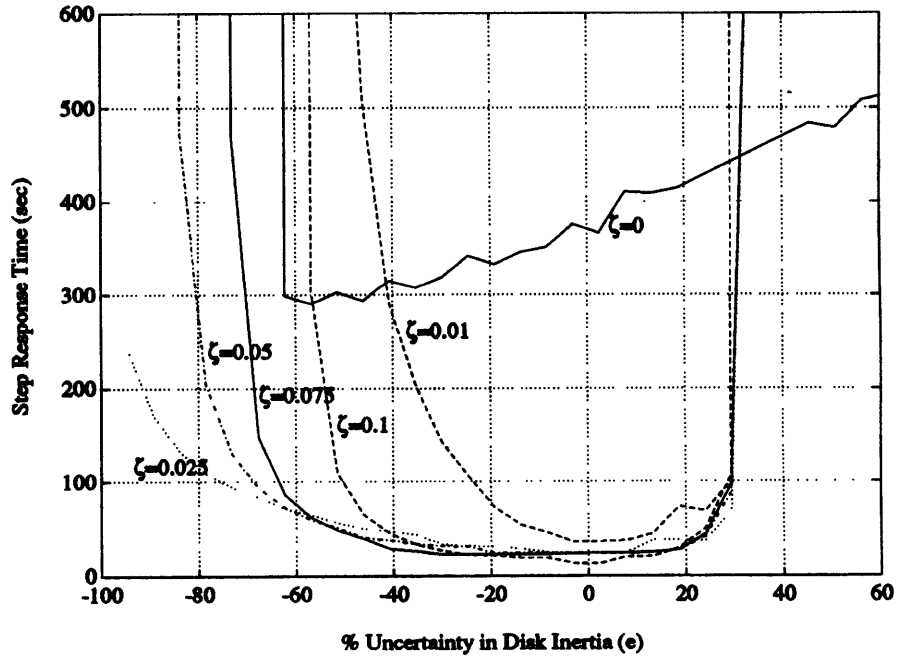

Figure 4-42: Settling Time Given an Uncertainty in Inertia of 1st Disk e ($\alpha = 1$).

Chapter 5

MIMO Design Studies

MIMO control methods such as H_2 control take advantage to the directionality of the system dynamics to improve control. Thus robustness with respect to plant directions becomes extremely important in the control of MIMO flexible structures. In this chapter, passive damping effects are examined on MIMO systems. Two controlled structures are examined. The first system is the four disk system with two noncollocated actuators and sensors. The second system is a nine disk system connected by flexible springs with two actuators and sensors. Performance and robustness characteristics are computed as a function of passive damping.

5.1 Four Disk Example

While the previous examples examined the virtues of passive damping on SISO systems, this example examines the virtues of passive damping on a flexible structure with MIMO control. The four disk structure examined in section 4.2 is used again with two noncollocated sensors and actuators.

Improvements in control performance, stability robustness, and performance robustness are investigated for various amounts of structural passive damping. H_2 optimal control is used to derive the necessary control law for good disturbance rejection on the structure. The design objective is to develop a control law to maintain a desired structural shape given disturbances on the structure.

5.1.1 Derivation of System Model

The same four disk structure examined in section 4.2 is used in this investigation. Actuators are located on the second and third disk and sensors are on the first and fourth disk as shown in figure 5-1. Only angular positions of the two disks are measured. Passive damping is added to the structure as a ratio of critical. The equations of motion of the undamped structure are the same as for the SISO example (see equation 4.22) except for the disturbance and effort distribution matrices which are as follows.

$$F_d = F_e = \begin{bmatrix} 0 & 0 \\ 1 & 0 \\ 0 & 1 \\ 0 & 0 \end{bmatrix} \tag{5.1}$$

A state space representation of the structure in modal space is used similar to the SISO example except that the output state matrix C_p is changed to compute the physical displacements of the first and fourth disk.

$$C_p = \begin{bmatrix} 1 & 0 & 0 & 0 & 0 & 0 & 0 & 0 \\ 0 & 0 & 0 & 1 & 0 & 0 & 0 & 0 \end{bmatrix} \begin{bmatrix} \Phi & 0 \\ 0 & \Phi \end{bmatrix} \tag{5.2}$$

The natural frequencies and mode shapes of the structure remain unchanged (see table 4-2 and figure 4-26) and the undamped structure has no transmission zeros. The nominal zeros of the structure from each input to each output is shown in table 5-1. These zeros play a crucial role in determining the plant directions. MIMO optimal control design uses the directional information of the plant to achieve good control. The phase difference of the two outputs as described in section 2.2.4 is shown in figure 5-2. Note that the phase changes occur at the location of the individual input-output zeros as shown in the table. As damping increases, the severity of change in phase difference reduces, thus allowing for greater uncertainty in the plant model.

Figures 5-3 and 5-4 show the difference in magnitude and phase between two most uncertain plants ($e_{min} = 0.25$ & $e_{max} = 0.5$) for each input to output relation.

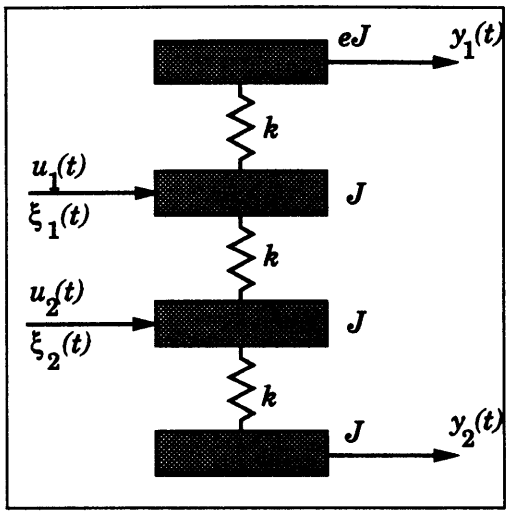

Figure 5-1: Four Disk MIMO Structure.

	Input #1 u_1	Input #2 u_2
Output #1 y_1	$\pm 0.6180j$ $\pm 1.6180j$	$\pm j$
Output #2 y_2	$\pm 1.6330j$	$\pm 2j$ $\pm 0.8165j$

Table 5-1: Location of Individual Input-Output Zeros of Undamped Four Disk System

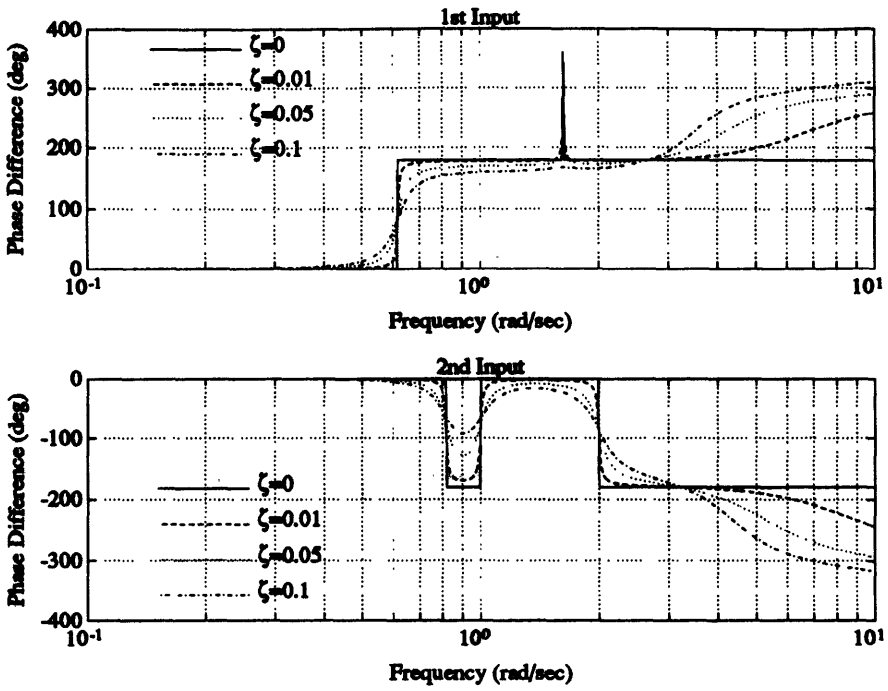

Figure 5-2: Phase Difference between Outputs of Four Disk System.

A comparison is made between the undamped structure and the structure with 5% modal damping. The peaks and valleys in the magnitude difference occur at the pole and zero locations respectively. For the undamped system, the magnitude differences at resonance are infinite and phase differences are $\pm 180°$. The addition of 5% damping greatly reduced the difference in magnitude and phase between resulting from the differences in plant uncertainty indicating a more robust plant.

As with the SISO example, the stability and performance robustness properties of the system are investigated given an uncertainty in the inertia of the first disk. Because the structure is MIMO, the actuators can compensate for the fact that the first actuator lies on the node of the third mode. Thus this MIMO system tends to be more robust than the SISO system. The allowable uncertainty in the inertia of the first disk to maintain stability and good performance are computed for various levels of modal damping. Good performance is computed such that given an uncertainty in the first disk, the performance measure (H_2 norm) does not deviate by more than $\pm 5\%$ from nominal.

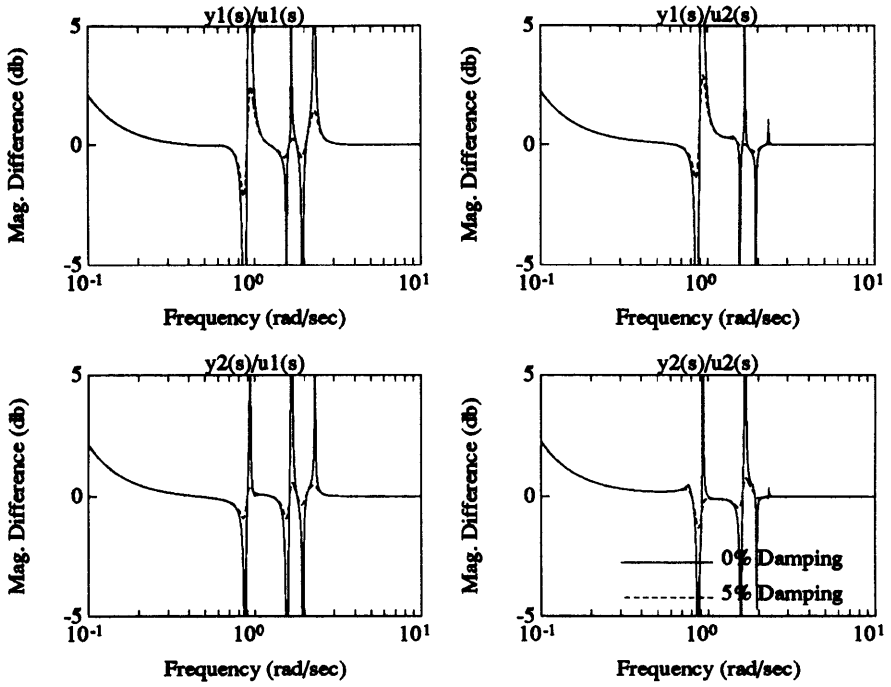

Figure 5-3: Magnitude Difference between the Two Most Uncertain Structures.

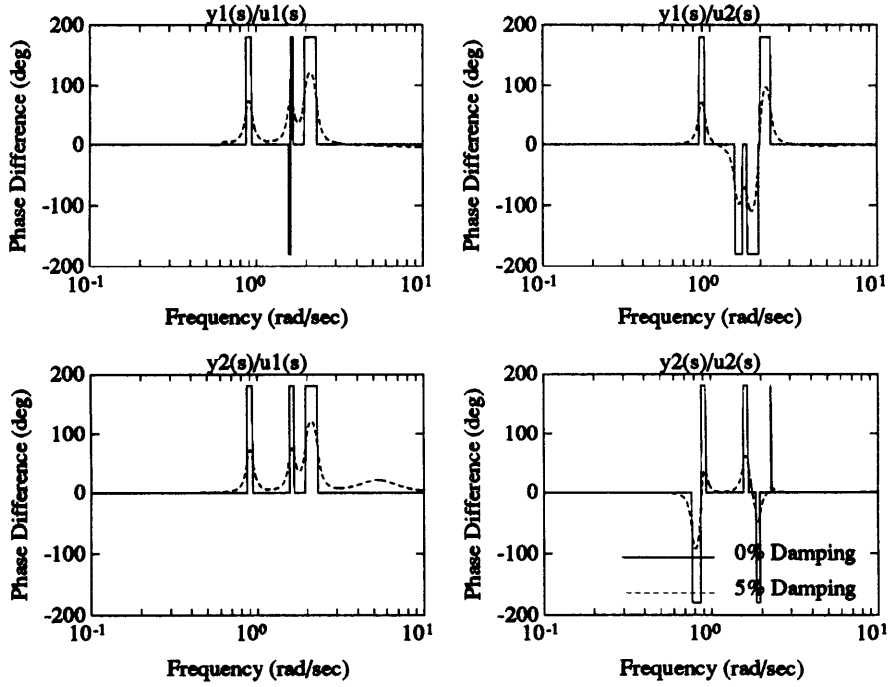

Figure 5-4: Phase Difference between the Two Most Uncertain Structures.

5.1.2 Derivation of Control Model

This example investigates the advantages of passive damping on the four disk system with MIMO control for active vibration suppression. The system makes use of H_2 optimal control design to derive the necessary control law. Robustness issues are ignored in the control design. An appropriate control law is derived to maintain the original shape of the structure given an impulse disturbance on the first disk.

The system framework is again the same as used in the SISO example (see figure 3-2). The following weights were used to derive the H_2 controller that minimized the weighted closed-loop system between disturbance and sensor noise inputs, and effort and plant outputs.

$$
\begin{aligned}
W_d &= I \\
W_s &= 1 \times 10^{-6}\, I \\
W_e &= 1 \times 10^{-6}\, I \\
W_p &= \begin{bmatrix} I & \\ & 0.01 \times I \end{bmatrix} \begin{bmatrix} \Phi & 0 \\ 0 & \Phi \end{bmatrix}
\end{aligned}
$$

As much as a -34 db attenuation of disturbances was achieved with this control design. This included attenuation of disturbances within the structural natural frequency.

5.1.3 Results

Results of the investigation on the four disk system with MIMO control were similar to the results using SISO control. Again, improved performance as well as a reduction in control effort was achieved with increased modal damping. While the undamped system tended to be more robust than in the SISO example, further gains were achieved in stability and performance robustness through the addition of passive damping.

The H_2 norm of the weighted closed-loop system for various amounts of modal

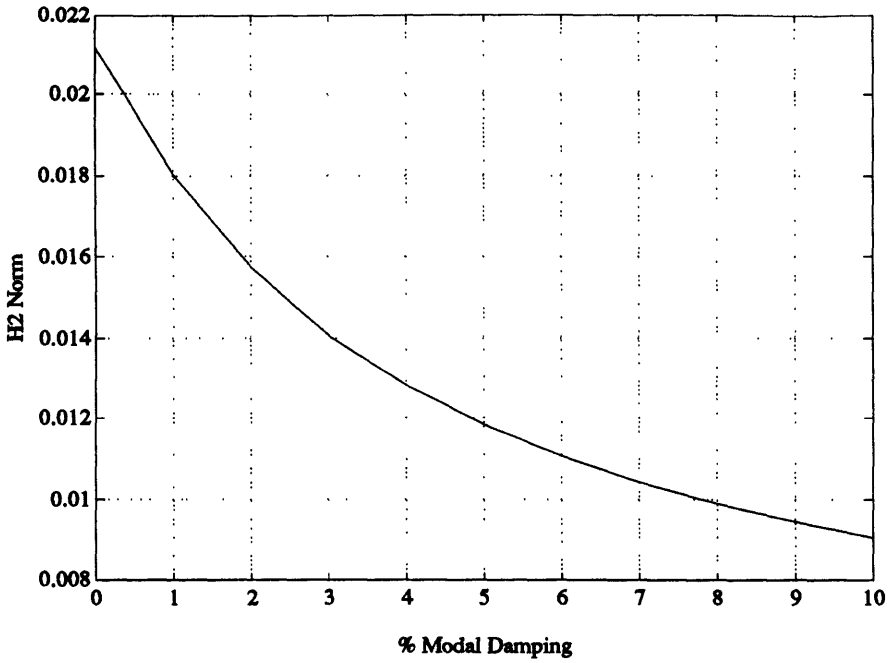

Figure 5-5: H_2 Norm of Nominal System for Various Amounts of Passive Damping.

damping is shown in figure 5-5. As the figure shows, the addition of modal damping resulted in a drop in the nominal H_2 norm indicating improved performance. More than a 50% drop in the performance measure was achieved with the addition of 10% modal damping. Passive damping provided another source for the removal of vibrational energy reducing the need of active vibration suppression.

Since the need for active control to suppress structural vibrations was reduced with increased modal damping, a decrease in control effort also resulted. Figure 5-6 shows the variance of both outputs as a result of white noise disturbance inputs on all disks. As much as an 80% drop in the variance was achieve through the addition of 10% modal damping. Due to the small inertia of the first disk, disturbances tend to affect it more requiring more effort to remove the resulting vibrations.

By observing the singular values across frequency between the disturbance input and sensor outputs, the effectiveness of vibration suppression across frequency is made evident. Figure 5-7 shows the singular values for an undamped and a 10% modally damped structure. With no damping, the amount of vibration suppression was about -34 *db* for the worst case. Notice that through the addition of passive damping, the

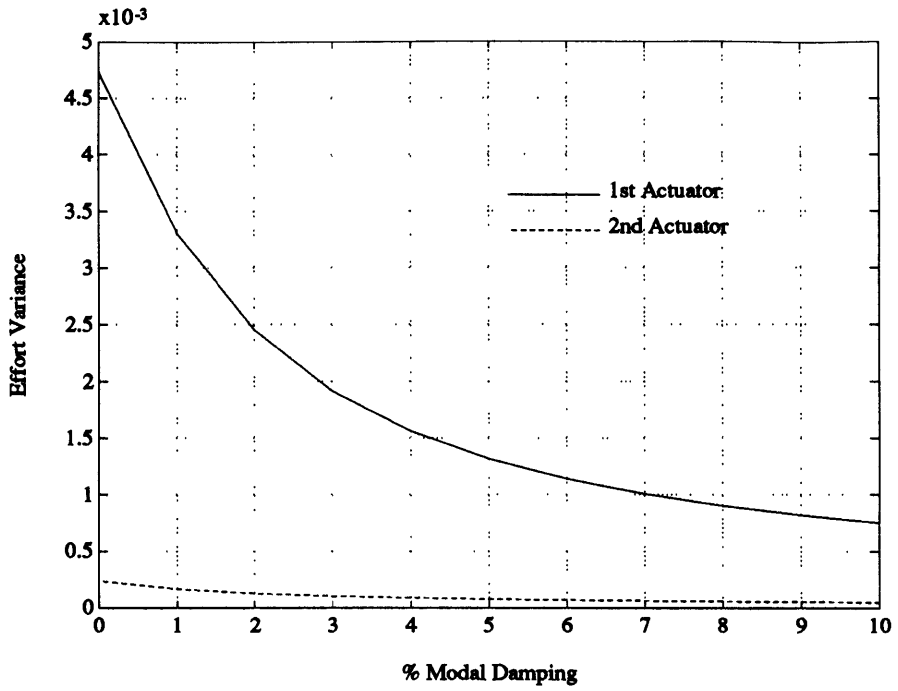

Figure 5-6: Effort Variance of Nominal System for Various Amounts of Passive Damping.

singular values shifted downward indicating more effective vibration suppression. As much as an 80% drop in the peak singular value was achieve with just 10% modal damping.

By observing more realistic measures of performance such as the response given an impulse disturbance, the true advantages of passive damping are evaluated. Figure 5-8 shows the response on the first disk as a result of an unit impulse disturbance on it. Plots are shown for both an undamped and a 10% modally damped structure. A reduction in overshoot as well as improved settling time was achieved with the addition of passive damping.

A major difference between the MIMO and SISO system was in the inherent robustness of the undamped system. This appears due to the fact that one actuator can compensate for a deficiency in the other. Figures 5-9 and 5-5 show the stability and performance robustness characteristics of the closed-loop system given an uncertainty in the inertia of the first mass. Stability robustness was based on the allowable uncertainty in the first inertia e to maintain stability. Performance robustness was based

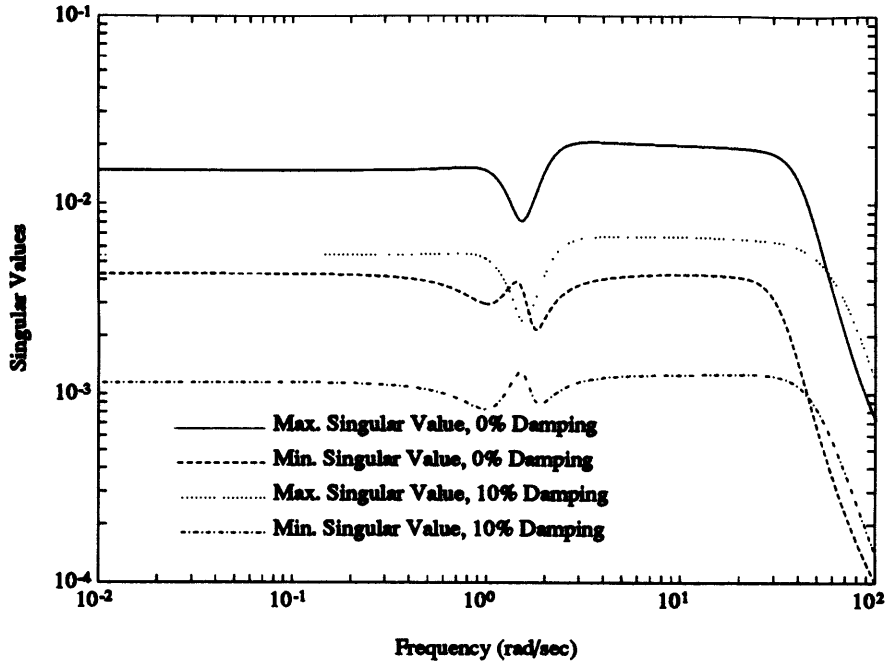

Figure 5-7: Singular Values of Nominal Closed-Loop System from Disturbance Inputs to Sensor Outputs.

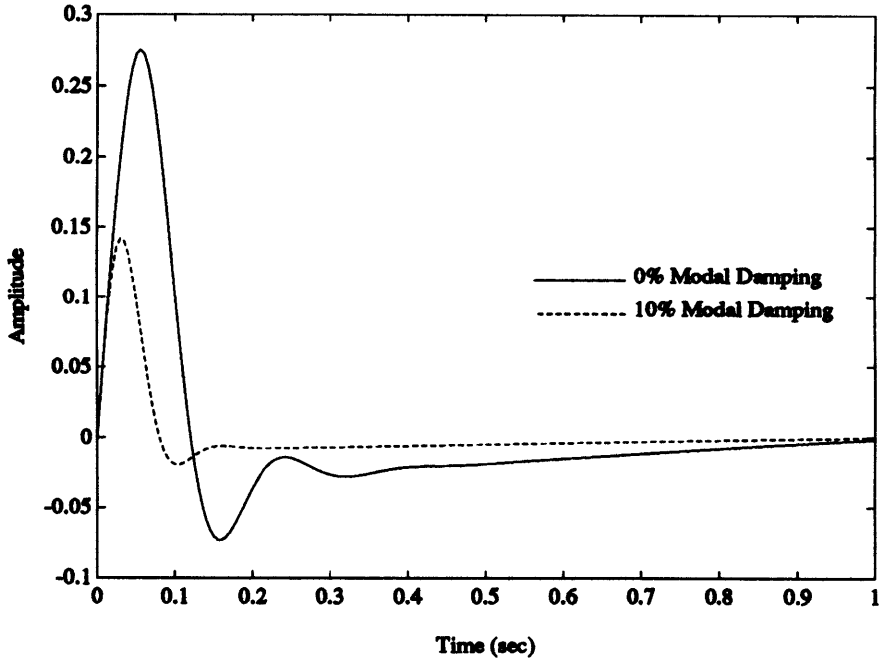

Figure 5-8: Response of First Disk of the Nominal System given a Unit Impulse Disturbance.

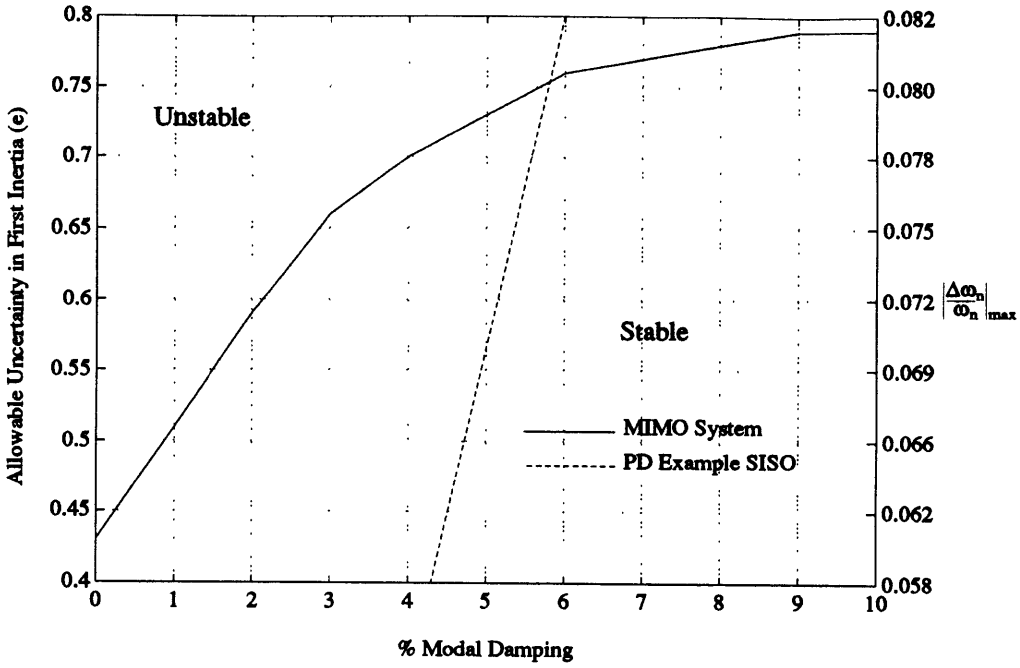

Figure 5-9: Allowable Uncertainty in Inertia of First Disk to Maintain Stability of System for Various Amounts of Passive Damping.

on the allowable uncertainty in e to maintain no greater than a 5% change in the H_2 norm. As much as a 29% uncertainty in e was allowed to maintain good performance of the undamped system. Furthermore, a 43% uncertainty in e was allowed to maintain stability of the undamped system. The addition of passive damping showed additional performance and stability robustness, but this example experienced fairly good robustness characteristics even in the undamped system.

The addition of passive damping to MIMO controlled structures has also been shown to be beneficial using the four disk structure example. As with SISO plants, major performance improvements as well as reduction in control effort was achieved with the addition of passive damping. While this particular example tended to be very robust even for undamped dynamics, further improvement in its robustness characteristics were achieved with added passive damping.

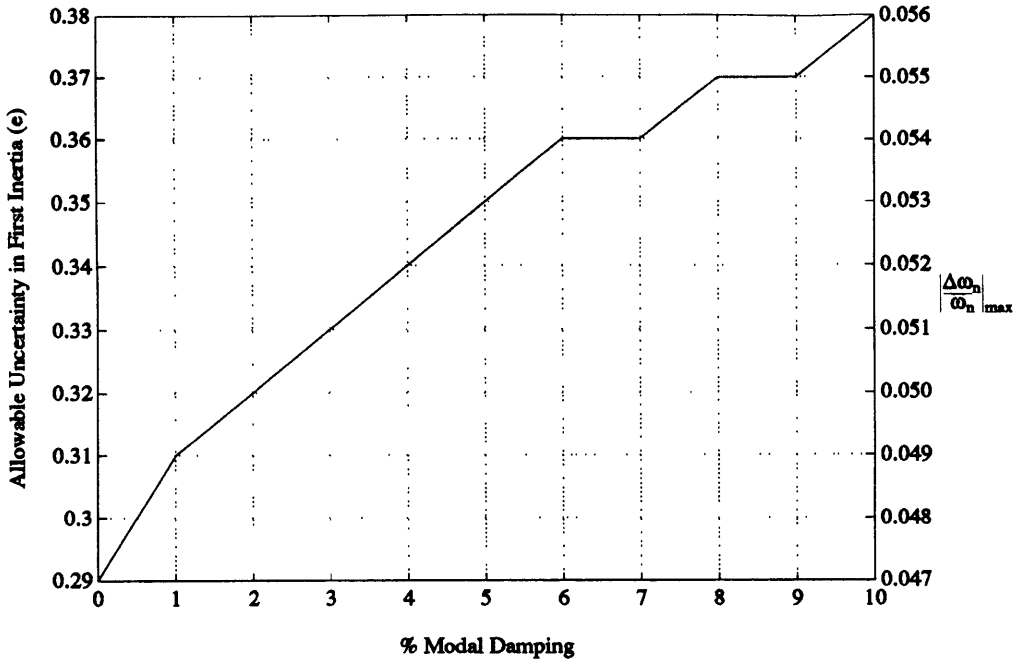

Figure 5-10: Allowable Uncertainty in Inertia of First Disk to Maintain Good Performance of Nominal System for Various Amounts of Passive Damping.

5.2 Nine Disk Example

The previous example showed performance and robustness improvements with the addition of passive damping to a simple MIMO structure. While improvements were shown, stability and performance robustness properties were good for the undamped system. As much as a 29% uncertainty in the inertia of the first disk was tolerable to maintain good control. Because of the low order of the problem, robust estimation of the plant was achieved allowing for good control characteristics. This example examines the benefits of passive damping on a similar, but more complicated structure which is unrobust with no modal damping. The structure consists of nine disks connected by flexible springs. Two sensors and two actuators are used to eliminate disturbances on the system. Again H_2 optimal control design is used to derive the necessary control law. Performance and robustness properties are investigated for various amounts of modal damping.

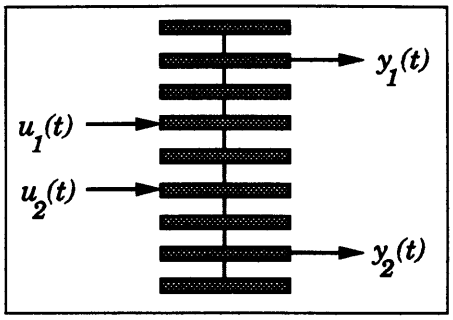

Figure 5-11: Nine Disk MIMO Structure.

5.2.1 Derivation of System Model

A similar structure to that of the four disk system (section 5.1) is used except that it has nine disks connected by flexible springs as shown in figure 5-11. The system has the following stiffness and mass properties.

$$\begin{aligned} k &= 1\ N \cdot m \\ J &= 1\ kg \cdot m^2 \end{aligned}$$

The actuators are located on the fourth and sixth disk, while the sensors are on the second and eighth disk. Similar equation of motion to the previous section are derived (see equation 4.22), except that the system of ninth order.

The structure has nine modes given by table 5-2. This first four mode shapes are shown in figure 5-12. Note that the sensors are located at the nodes of the fourth mode, thus making it unobservable. Active control at the frequency of the fourth mode is impossible. Thus a transmission zero lies at the frequency of the fourth mode resulting in a plant pole-zero cancellation. Any uncertainty in the model can result in a pole/zero flip which can cause instability. The structure also has a transmission zero at 1.4121 rad/sec.

Figures 5-13 and 5-14 show the difference in magnitude and phase between two most uncertain plants where uncertainty lies in the inertia of the first (top) disk ($J_{min} = 1.8$ & $J_{max} = 0.8$) for each input to output relation. A comparison is made

Poles	
Mode #	Frequency rad/sec
1	0
2	± 0.3473
3	± 0.6840
4	± 1.0
5	± 1.2856
6	± 1.5321
7	± 1.7321
8	± 1.8794
9	± 1.9696
Zeros	
1	± 1.0
2	± 1.4142

Table 5-2: Poles and Zeros of Nine Disk Structure.

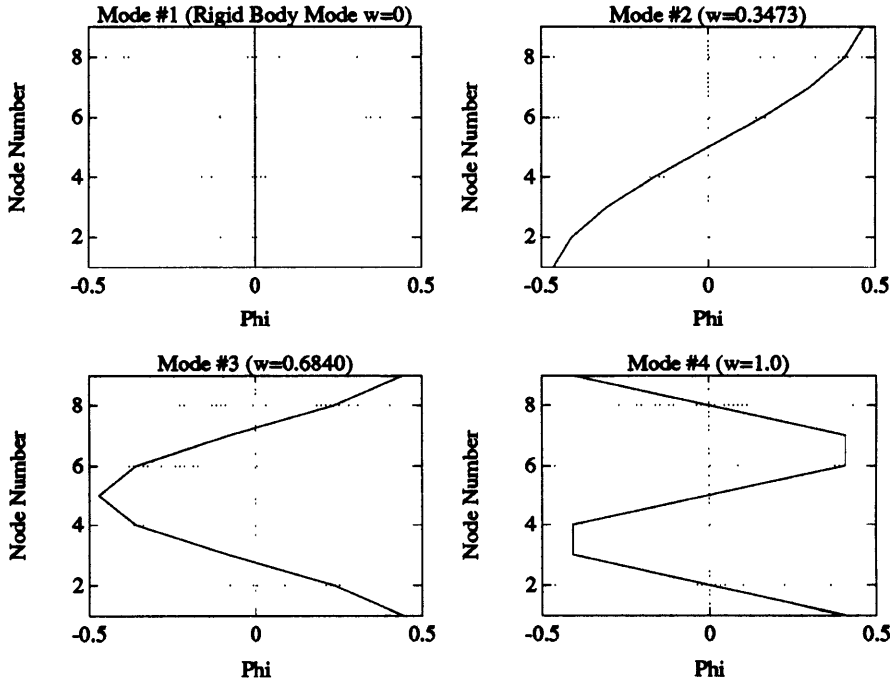

Figure 5-12: First Four Mode Shapes of Nominal Nine Disk System.

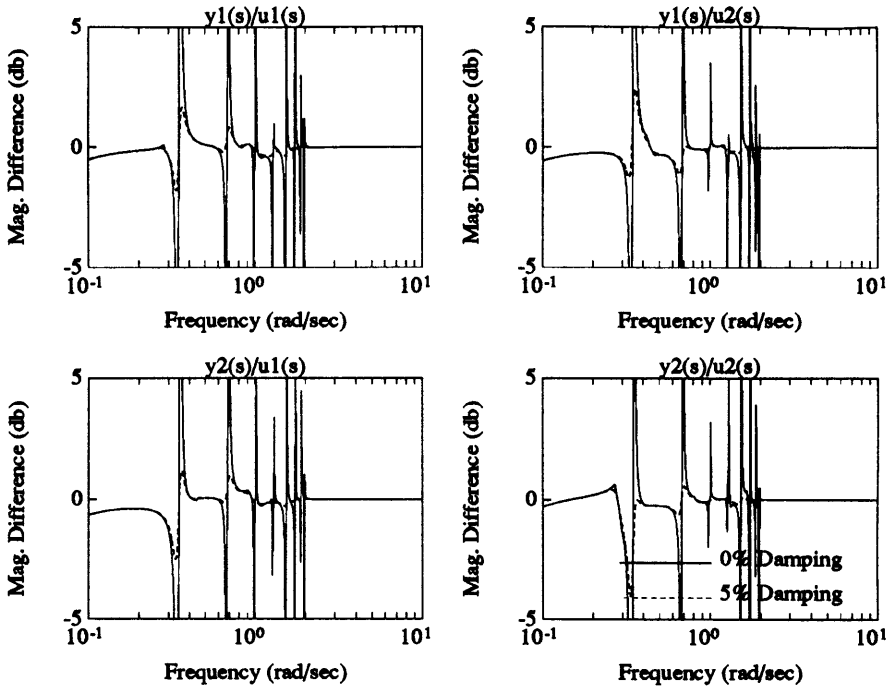

Figure 5-13: Magnitude Difference between the Two Most Uncertain Structures.

between the undamped structure and the structure with 5% modal damping. The peaks and valleys in the magnitude difference occur at the pole and zero locations respectively of each input/output transfer function. For the undamped system, the magnitude differences at resonance are infinite and phase differences are $\pm 180^{o}$. The addition of 5% damping greatly reduced the difference in magnitude and phase between resulting from the differences in plant uncertainty indicating a more robust plant.

As with the previous example, this investigation examines the virtues of passive damping on the nine disk system with MIMO control for active vibration suppression. The system makes use of H_2 optimal control design to derive the necessary control law. Robustness issues are ignored in the control design. An appropriate control law is derived to maintain the unforced structural shape given an impulse disturbance on the first disk.

The system framework is the same as in the previous section (see figure 3-2). The following weights were used to derive the H_2 controller that minimized the weighted closed-loop system between disturbances and sensor noise inputs, and effort and plant

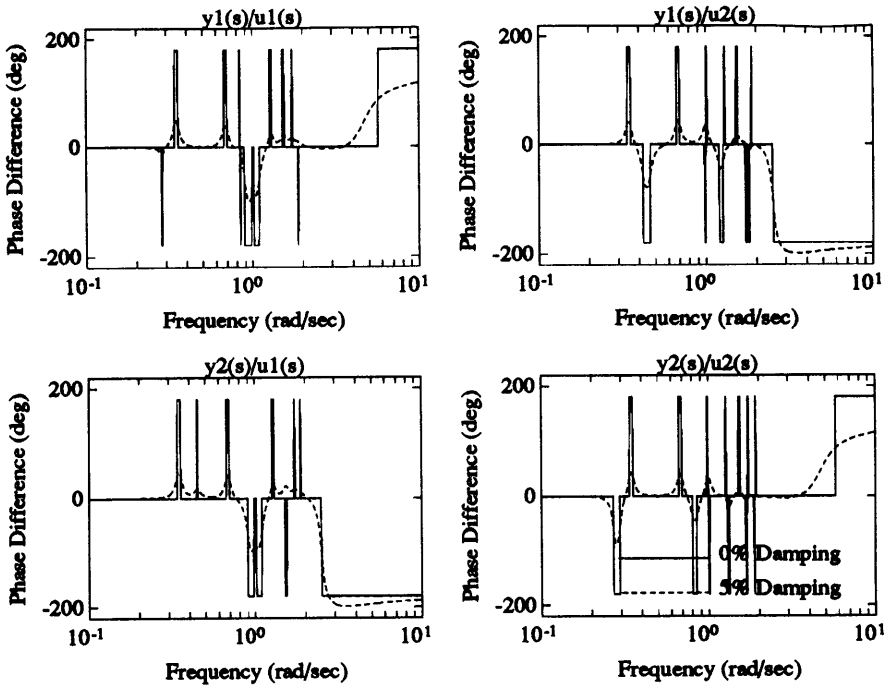

Figure 5-14: Phase Difference between Actual the Two Most Uncertain Structures.

outputs.

$$
\begin{aligned}
W_d &= I \\
W_s &= 1 \times 10^{-6} I \\
W_e &= 1 \times 10^{-6} I \\
W_p &= \begin{bmatrix} I & \\ & 0.01 \times I \end{bmatrix} \begin{bmatrix} \Phi & 0 \\ 0 & \Phi \end{bmatrix}
\end{aligned}
$$

The response of the first disk given an impulse is shown in figure 5-17. Note that the undamped case continued to resonate at about 6 Hz (1 rad/sec) due to the unobservable fourth mode.

As with the previous example, the stability and performance robustness properties of the system are investigated given an uncertainty in the inertia of the first disk. Because of the higher complexity and pole-zero cancellation in the system, the control system is very sensitive to changes in the undamped structure. Again good

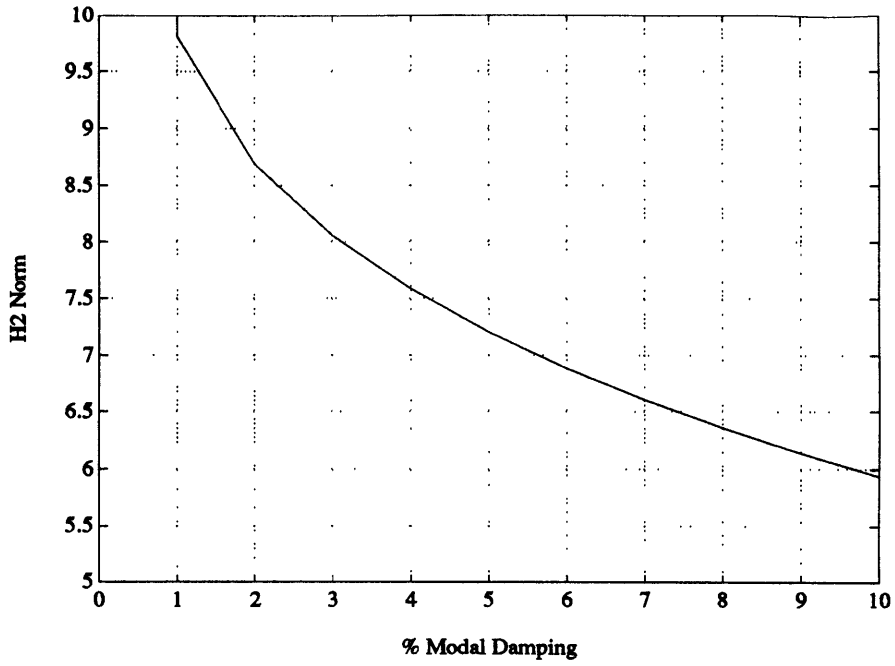

Figure 5-15: H_2 Norm of Nominal System for Various Amounts of Passive Damping.

performance is based on the H_2 norm not deviating by $\pm 5\%$ from the nominal value given an uncertainty in the inertia of the first disk.

5.2.2 Results

Results of this investigation using MIMO control on the nine disk system were similar to that of the four disk system. Again, improved performance as well as a reduction in control effort was achieved with increased modal damping. Gains in stability and performance were also achieved.

The nominal H_2 norm of the weighted closed-loop system for various amounts of modal damping is shown in figure 5-15. As the figure shows, the addition of modal damping results in a drop in the H_2 norm indicating improved performance. For the undamped case, the H_2 norm was infinite due to the unobservable fourth mode. Vibrations at the frequency of the fourth mode (1 rad/sec) cannot be removed due to the sensors being at the location of the nodes of that mode.

Since the need for active control to suppress structural vibrations is reduced with

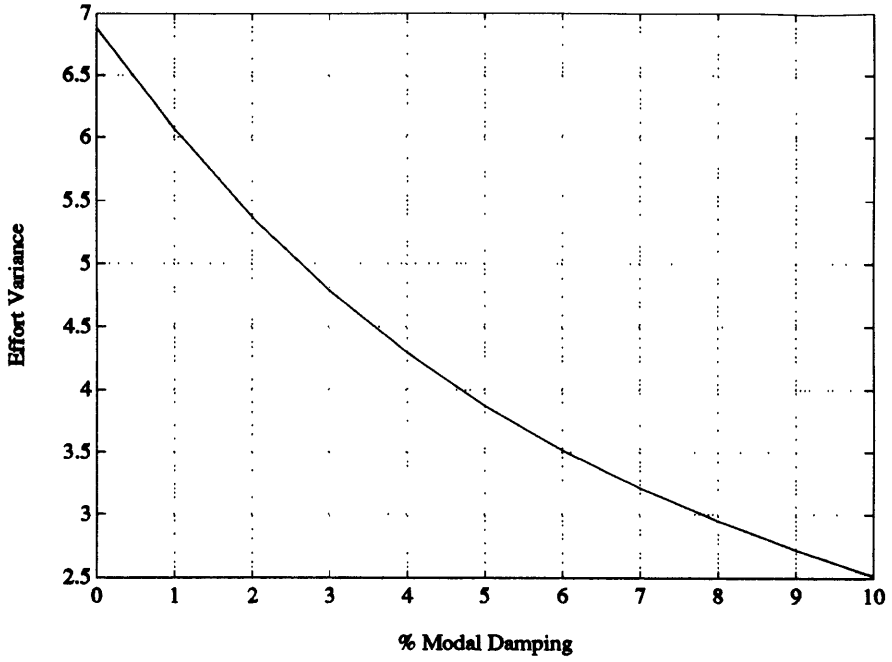

Figure 5-16: Effort Variance of Nominal System for Various Amounts of Passive Damping.

increased modal damping, a decrease in control effort also results. Figure 5-16 shows the nominal effort variance of the outputs as a result of white noise disturbance inputs on all disks. Due to the symmetry of the structure, the variance of the effort is equal for both actuators. As much as a 60% drop in effort was achieved by increasing damping to 10%.

Realistic performance improvements by increasing passive damping of the nine disk system are shown in figures 5-17 and 5-18. The first figure is the response of the first disk of the system as a result of a unit impulse applied on it. Note that for the undamped system, the resonance at 1 rad/sec does not decay due to the unobservable mode. The addition of passive damping reduces the maximum displacement and settling time as a result of the impulse as shown in the figure. The second figure is of the effort applied on the structure as a result of the disturbance. Note that the effort is reduced for the damped case. The maximum effort needed and settling time is reduced for the damped case.

The major difference with the nine disk system as compared to the four disk

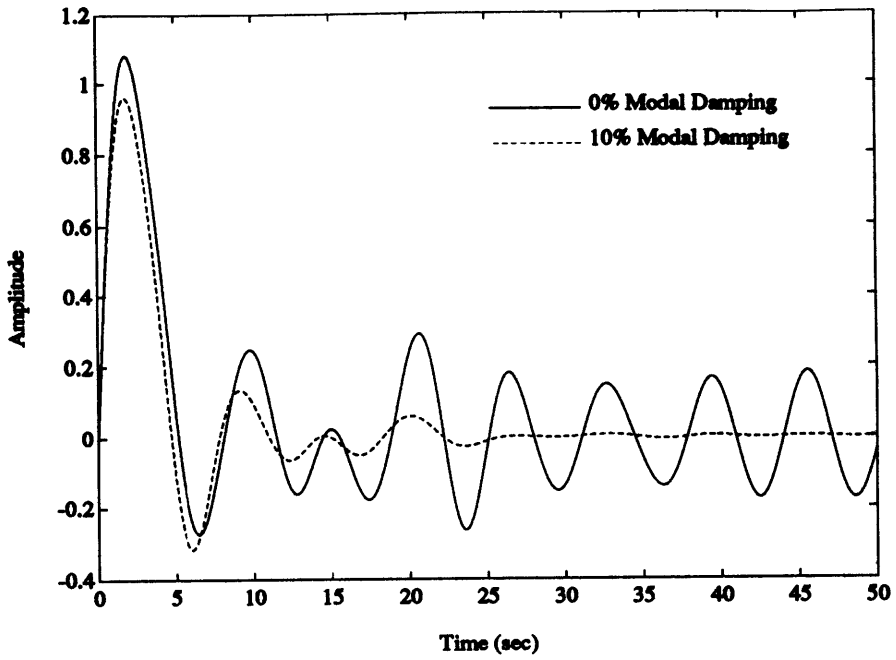

Figure 5-17: Response of First Disk of Nominal System given a Unit Impulse Disturbance.

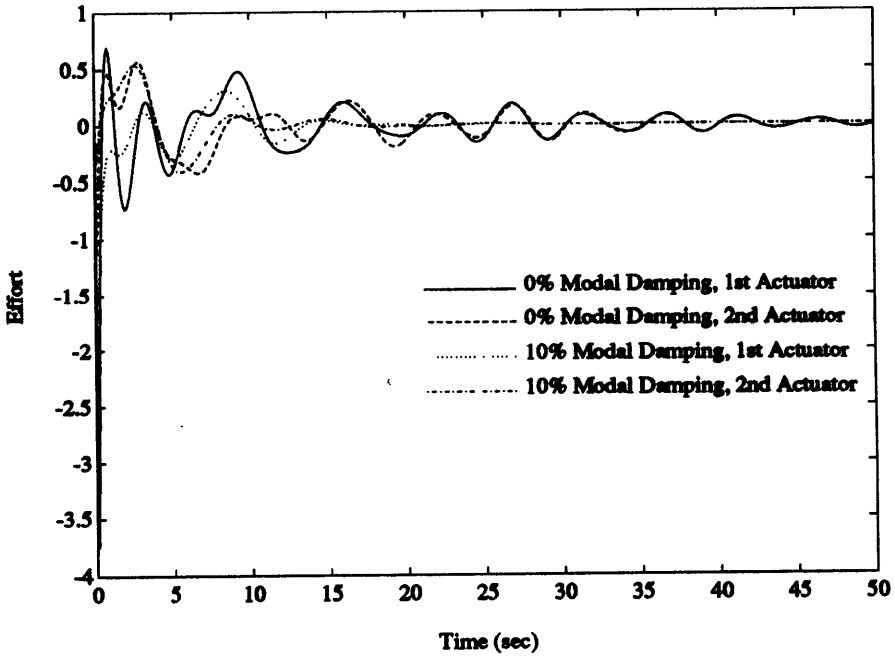

Figure 5-18: Effort Applied on Nominal Structure given a Unit Impulse Disturbance on the First Disk.

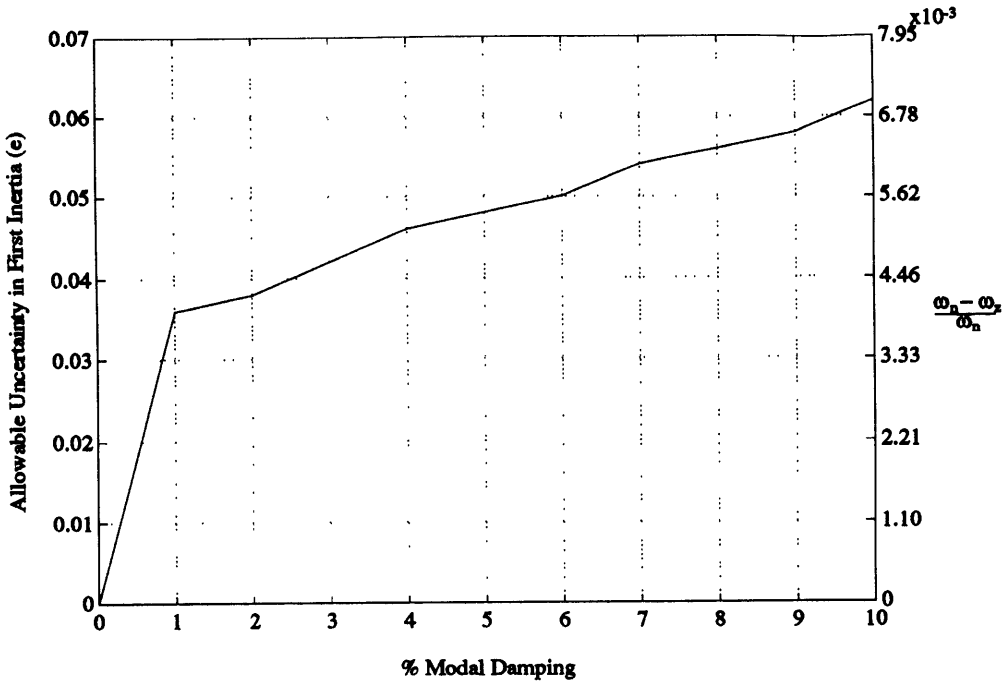

Figure 5-19: Allowable Uncertainty in Inertia of First Disk to Maintain Stability of Optimal System for Various Amounts of Passive Damping.

system was in the inherent robustness. The undamped nine disk system was very sensitive to model uncertainty as shown in figures 5-19 and 5-20. They show the stability and performance robustness characteristics given an uncertainty in the inertia of the first disk. The undamped case could not tolerate any uncertainty. This corresponds to the results in chapter 2 where no uncertainty was tolerable for control of simple undamped structures with pole-zero cancellation. But for both stability and performance robustness, as much as a 6% uncertainty was allowed in the inertia of the first disk given 10% modal damping. With just 1% modal damping, a 3.5% uncertainty was tolerable.

This investigation has shown that passive damping is effective on even more complicated structures such as the nine disk example. This system suffered from a pole-zero cancellation which made the fourth mode unobservable, thus unrobust. This also resulted in undamped vibrations at the frequency of the unobserved mode. Passive damping allowed for removal of the unobserved vibrations as well as improving the overall performance and reducing the necessary effort for control of the structure.

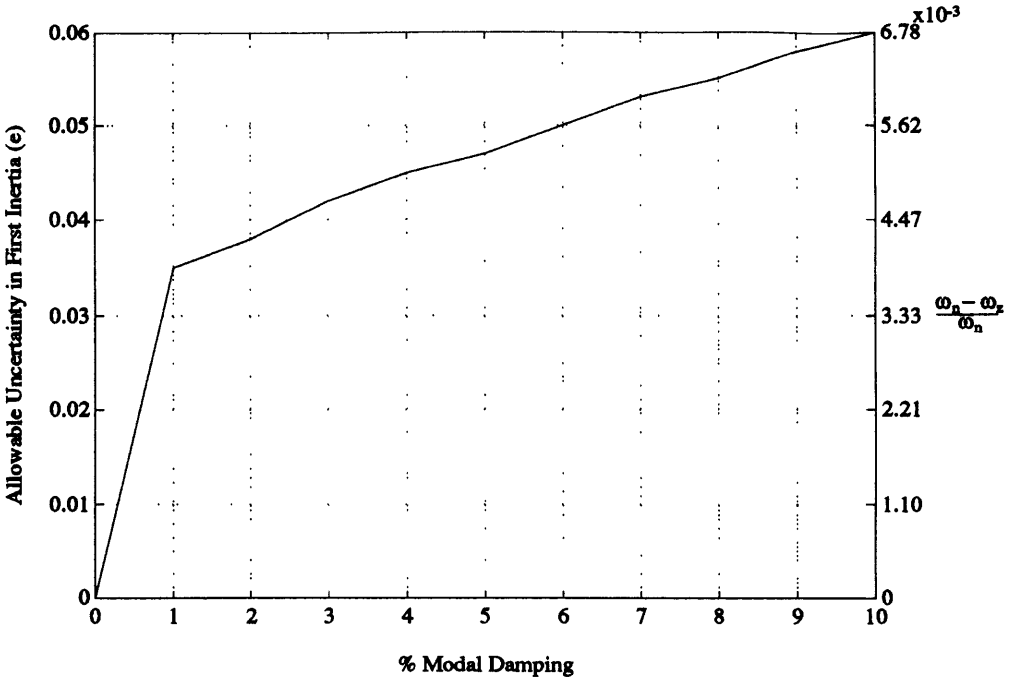

Figure 5-20: Allowable Uncertainty in Inertia of First Disk to Maintain Good Performance of Optimal System for Various Amounts of Passive Damping.

Furthermore, improvements in stability and performance robustness were achieved with increased damping.

Chapter 6

Conclusion and Suggestions for Further Research

The need for high performing, yet robust and light weight controlled structures is critical in achieving the goals of future space missions. The evidence presented clearly points to the advantage of passive damping in achieving these goals. Robust control techniques with closed-loop bandwidths incorporating the structural natural frequencies are extremely difficult to implement without passive damping. Passive damping provides a reliable and light weight method to reduce structural vibrations allowing for increased robustness and improved control. Structural design for robust control allows for reduced controller complexity and a reduction in the size and number actuators and power sources needed for active control. Thus passive damping is an important design variable in the structural design of future spacecraft.

The design studies provided evidence supporting performance and robustness improvements in SISO and MIMO controlled structures. Not only were performance variables such as the H_2 norm, settling time, and maximum overshoot reduced, but control effort was also reduced. In addition, by examining passively damped controlled structures, improved stability and performance robustness characteristics were quantified. Most undamped systems studied allowed for no model uncertainty to achieve high bandwidth control objectives. By raising the amount of passive damping to 10%, as much as a 6% uncertainty in natural frequency was allowed for the two mass sys-

tem to remain stable. More than a 10% allowable uncertainty in natural frequency of the four disk system was shown. Even with robust control techniques, nominal performance was improved as well as performance robustness improvement achieved by increasing passive damping.

The results from the design studies showed much similarity to the those predicted theoretically in chapter 2. Three formulations for predicting required amounts of passive damping were derived for plants with pole and zero uncertainties. The first formulation examined simple root locus of structures controlled with plant inversion techniques involving pole-zero cancellation. The amount of damping needed was based on the size of the semicircle the root locus made by uncertain plant poles or compensator zeros migrating to compensator zeros or plant poles (see equation 2.13). The second formulation was based on phase uncertainty and desired phase margins in the frequency domain (see equation 2.18). The third formulation was based on stability bounds derived for a simple two degree of freedom structure with PD control (see figure 2-12). All derivations showed linear increases in stability bounds with increased passive damping, with minor differences in the slope.

The SISO four disk system showed excellent correspondence with the third formulation as shown in figure 4-32. The four disk system contained an actuator at the node of the third mode resulting in a plant pole-zero cancellation, thus making the third mode uncontrollable. Passive damping reduced the effects of the vibrations at that frequency allowing for improved performance and robustness. The two mass system required more damping to maintain stability given plant uncertainty as compared with the formulations in chapter 2 as shown in figure 4-7. The allowable uncertainty did increase linearly with passive damping. Because perfect pole-zero cancellation was not exhibited for the two mass system, good correlation to the theoretical formulations did not occur. But based on these examples, a one-to-one relationship between passive damping and plant eigenvalue uncertainty is shown to be sufficient to assure a robust plant design.

$$\zeta = \frac{\Delta\omega_n}{\omega_n} \tag{6.1}$$

While each plant will exhibit different robustness characteristics, passive damping greatly improves the allowable uncertainty to maintain stability and good performance.

While this thesis made a first attempt in addressing required amounts of passive damping for controlled structures, much work still needs to be continued. Damping was treated as a percentage critical (modal). Real damping treatments such as tuned mass dampers or damping elements need to be modeled directly as elements in a finite element model. Methodologies to determine appropriate amounts of damping based on actual treatments need to be developed. McLoughlin thesis [21] developed a required amount of passive structural damping based on open loop dynamics of the plant. This method determined optimal damper locations and amounts of damping needed to minimize an open loop performance measure. In the PACOSS study [24], passive damping treatments were applied based on modal strain energy of the plant. The control design played little role in the application of the damping treatments. Design methods incorporating passive damping must be expanded to include the control design and system objectives.

While damping treatments helped improve robustness characteristics with respect to stiffness and mass uncertainty, these systems are very sensitive to uncertainty damping values. A conservative approach might include modeling damping levels below actual values assuring that the root locus of the system does not cross the imaginary axis. For high performing system, accurate representation of passive damping might be essential to assure stability and good performance.

While many damping treatments exist, applying them in the engineering community is slow. Robust design is essential to any system, especially in the control of flexible structures where plant inversion techniques are necessary for good control. Success of any space mission where precision pointing of large structures is needed can greatly be improved by the addition of passive damping techniques. Development of structural design tools incorporating passive damping would greatly help in improving the success of future space missions.

Appendix A

Mathematical Necessities

A.1 Singular Value Properties

$$\begin{aligned} \sigma_{max}[A^{-1}] &= \frac{1}{\sigma_{min}[A]} \\ \sigma_{min}[A^{-1}] &= \frac{1}{\sigma_{max}[A]} \end{aligned}$$

$$\sigma_{max}[A] - 1 \leq \sigma_{max}[I + A] \leq \sigma_{max}[A] + 1$$

$$\sigma_{min}[A] - 1 \leq \sigma_{min}[I + A] \leq \sigma_{min}[A] + 1$$

$$\begin{aligned} \sigma_{max}[A + B] &\leq \sigma_{max}[A] + \sigma_{max}[B] \\ \sigma_{max}[AB] &\leq \sigma_{max}[A] \cdot \sigma_{max}[B] \end{aligned}$$

A.2 Stochastic MIMO LTI Systems

Taken from Athans [4].

- $\xi(t)$ is a white noise vector.

$$\begin{aligned} E[\xi(t)] &= 0 \\ \Psi_{\xi\xi}(\tau) &= I \cdot \delta(\tau) \end{aligned}$$

$$\Phi_{\xi\xi}(\omega) = I$$

The operators $E[\cdot]$, $\Psi(\tau)$, and $\Phi(\omega)$ are the expectation, autocorrelation, and power spectral density functions respectively.

- LTI Dynamic System is stable (i.e. $\lambda_i[A] < 0$).

$$\begin{aligned} \dot{x}(t) &= Ax(t) + L\xi(t) \\ y(t) &= Cx(t) \end{aligned}$$

- In statistical steady-state, both $x(t)$ and $y(t)$ are stationary vector valued random processes.

- Mean

$$\begin{aligned} E[x(t)] &= 0 \\ E[y(t)] &= 0 \end{aligned}$$

- State Covariances Σ_x.

$$\Sigma_x \equiv E[x(t)x^T(t)]$$

where Σ_x is the solution of the following Lyapunov Equation.

$$A\Sigma_x + \Sigma_x A^T + LL^T = 0$$

- Output Covariance Σ_y.

$$\Sigma_y \equiv E[y(t)y^T(t)]$$

which is a function of Σ_x.

$$\Sigma_y = C\Sigma_x C^T$$

- For SISO, the covariance is the same as the variance of the system.

$$\sigma_{yy}^2 = \Sigma_y$$

Bibliography

[1] Anderson, E., Trubert, M., Fanson, J., and Davis, P., "Testing and Application of a Viscous Passive Damper for use in Precision Truss Structures," AIAA, 1991, to be published.

[2] Athans, Michael, *Lecture Notes for Multivariable Control Systems, II*, MIT, Cambridge, MA, Spring 1990.

[3] Athans, Michael, *Viewgraphs for Multivariable Control Systems, I 6.233J*, MIT, Cambridge, MA, Fall 1989.

[4] Athans, Michael, *Viewgraphs for Multivariable Control Systems, II 6.234J*, MIT, Cambridge, MA, Spring 1990.

[5] Belvin, W. Keith and Park, K. C., "Structural Tailoring and Feedback Control Synthesis: An Interdisciplinary Approach," *Journal of Guidance, Control, and Dynamics*, Vol. 13, No. 3, May–June 1990, pages 424–429.

[6] Byun, K., Wie, B., and Sunkel, J., "Robust Control Synthesis for Uncertain Dynamical Systems," , Conference Paper No. 89-3516-CP, AIAA, 1989.

[7] Doyle, J. C., Glover, K., Khargonekar, P. P., and Francis, B. A., "State-Space Solutions to the Standard H_2 and H_∞ Control Problem," *IEEE Transaction of Automatic Control*, Vol. 34, No. 8, Aug. 1989, pages 831–846.

[8] Friedland, Bernard, *Control System Design, An Introduction to State-Space Methods*, McGraw-Hill, New York, 1986.

[9] Gehling, R. N., Harcrow, H. W., and Morosow, G., "Benefits of Passive Damping as Applied to Active Control of Large Space Structures," *Mechanical Qualification of Large Flexible Space Structures,* AGARD CP-397, July 1986, pages 21-1–21-8.

[10] Gilbert, Michael G. and Schmidt, David K., "Integrated Structure/Control Law Design by Multilevel Optimization," AIAA, No. 89-3470-CP, 1989, pages 376–385.

[11] Grandhi, Ramana V., "Optimum Design of Space Structures with Active and Passive Damping," *Engineering with Computers*, Vol. 6, No. 3, Summer 1990, pages 177–183.

[12] Hagood, Nesbit W., *Cost Averaging Techniques for Robust Control of Parametrically Uncertain Systems,* PhD thesis, Massachusetts Institute of Technology, Dept. of Aeronautics and Astronautics, June 1991.

[13] Hughes, Peter C. and Abdel-Rahman, Tarek M., "Stability of Proportional-Plus-Derivative-Plus-Integral Control of Flexible Space Craft," *Journal of Guidance, Control, and Dynamics,* Vol. 2, No. 6, Nov.–Dec. 1979, pages 499–503.

[14] Junkins, J. L. and Rew, D. W., "Unified Optimization of Structures and Controllers," *Springer Series in Computational Mechanics*, Springer-Verlag, Berlin, 1988, pages 324–353.

[15] Khot, N. S., "An Integrated Approach to the Minimum Weight and Optimal Control Design of Space Structures," *Springer Series in Computational Mechanics*, Springer-Verlag, Berlin, 1988, pages 355–363.

[16] Khot, N. S., "Optimization of the Structural and Control System for LSS with Reduced-Order Model," *Third NASA/DOD Controls-Structures Interaction (CSI) Technology Conference*, NASA/DOD, Jan.–Feb. 1989, pages 229–239.

[17] Khot, N. S., Grandhi, R. V., and Venkayya, V. B., "Structural and Control Optimization for Space Structures," Technical Report 87-0939, NASA, 1987.

[18] Khot, N. S., Venkayya, V. B., and Eastep, F. E., "Optimal Structural Modifications to Enhance the Active Vibration Control of Flexible Structures," *AIAA Journal*, Vol. 24, No. 8, August 1986, pages 1368–1374.

[19] Kwakernaak, H. and Sivan, R., *Linear Optimal Control Systems*, John Wiley & Sons, Inc., New York, 1972.

[20] Lim, K. B., and Junkins, J. L., "Robustness Optimization of Structural and Control Parameters," *Journal of Guidance, Control, and Dynamics*, Vol. 12, No. 1, Jan.–Feb. 1989, pages 89–96.

[21] McLoughlin, Frank A., *Integrated Structural Damping and Control System Design for High-Order Flexible Systems,* PhD thesis, Stanford University, Dept. of Aeronautics and Astronautics, December 1990, #SADAAR 601.

[22] Maciejowski, J. M., *Multivariable Feedback Design*, Addison-Wesley, Wokingham, England, 1989.

[23] Milman, M., Salama, M., Scheid, R., Bruno, R., and Gibson, J. S., "Integrated Control-Structure Design: A Multiobjective Approach," Jet Propulsion Laboratory, Pasadena, CA, Technical Report JPL D-6767, January 1990.

[24] Morgenthaler, Daniel R., and Gehling, Russell N., *Passive and Active Control of Space Structures,* Vol. 1–3, Flight Dynamics Laboratory, Wright Research and Development Center, #WRDC-TR-90-3044, September 1990.

[25] Onoda, Junjiro and Haftka, Raphael T., "An Approach to Structure/Control Simultaneous Optimization for Large Flexible Spacecraft," *AIAA Journal*, Vol 24, No. 8, August 1987, pages 1133–1138.

[26] Onoda, Junjiro and Wantabe, Naoyuki, "Integrated Direct Optimization of Structure/Regulator/Observer for Large Flexible Spacecraft," *AIAA Journal*, Vol. 28, No. 9, September 1990, pages 1677–1685.

[27] Grace, Andrew, *The Optimization Toolbox for uses with MATLAB, User's Guide*, The MathWorks, Inc., South Natick, MA, November 1990.

[28] Rao, S. S., Pan, T., and Venkayya, V. B., "Robustness Improvements of Actively Controller Structures through Structural Modifications," *AIAA Journal*, Vol. 28, No. 2, February 1990, pages 353–361.

[29] Rosenthal, Dan E., *Experiments in Control of Flexible Structures with Uncertain Parameters,* PhD thesis, Stanford University, Dept. of Aeronautics and Astronautics, March 8, 1984.

[30] Spanos, John T., "Control-Structure Interaction in Precision Pointing Servo Loops," *Journal of Guidance, Control, and Dynamics,* Vol. 12, No. 2, March–April 1989, pages 256–263.

[31] von Flotow, A. H. and Vos D. W., "The Need of Passive Damping in Feedback Controlled Structures," *Damping '91 Conference*, San Diego, Ca, February 1991.

[32] Wie, Bong and Bernstein, Dennis S., "A Benchmark Problem for Robust Control Design," for 1990 ACC.

2977-46